

**LIPOPROTEIN-ASSOCIATED PHOSPHOLIPASE A2:
UTILIZING POTENT AND SPECIFIC INHIBITORS
TO PROBE THE STRUCTURE FUNCTION RELATIONSHIP**

by

Tara Drake Gonzalez

A dissertation submitted to the Faculty of the University of Delaware in partial fulfillment of the requirements for the degree of Doctor of Philosophy in Chemistry and Biochemistry

Summer 2015

© 2015 Tara Drake Gonzalez
All Rights Reserved

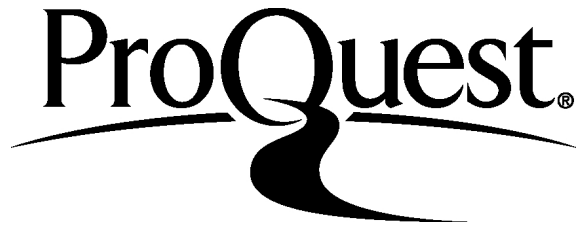
ProQuest Number: 3730235

All rights reserved

INFORMATION TO ALL USERS

The quality of this reproduction is dependent upon the quality of the copy submitted.

In the unlikely event that the author did not send a complete manuscript and there are missing pages, these will be noted. Also, if material had to be removed, a note will indicate the deletion.



ProQuest 3730235

Published by ProQuest LLC (2015). Copyright of the Dissertation is held by the Author.

All rights reserved.

This work is protected against unauthorized copying under Title 17, United States Code
Microform Edition © ProQuest LLC.

ProQuest LLC.
789 East Eisenhower Parkway
P.O. Box 1346
Ann Arbor, MI 48106 - 1346

**LIPOPROTEIN-ASSOCIATED PHOSPHOLIPASE A2:
UTILIZING POTENT AND SPECIFIC INHIBITORS
TO PROBE THE STRUCTURE FUNCTION RELATIONSHIP**

by

Tara Drake Gonzalez

Approved: _____

Murray V. Johnston, Ph.D.
Chair of the Department of Chemistry and Biochemistry

Approved: _____

George H. Watson, Ph.D.
Dean of the College of Arts and Sciences

Approved: _____

James G. Richards, Ph.D.
Vice Provost for Graduate and Professional Education

I certify that I have read this dissertation and that in my opinion it meets the academic and professional standard required by the University as a dissertation for the degree of Doctor of Philosophy.

Signed:

Brian J. Bahnson, Ph.D.
Professor in charge of dissertation

I certify that I have read this dissertation and that in my opinion it meets the academic and professional standard required by the University as a dissertation for the degree of Doctor of Philosophy.

Signed:

Tatyana Polenova, Ph.D.
Member of dissertation committee

I certify that I have read this dissertation and that in my opinion it meets the academic and professional standard required by the University as a dissertation for the degree of Doctor of Philosophy.

Signed:

Donna S. Woulfe, Ph.D.
Member of dissertation committee

I certify that I have read this dissertation and that in my opinion it meets the academic and professional standard required by the University as a dissertation for the degree of Doctor of Philosophy.

Signed:

Zhihao Zhuang, Ph.D.
Member of dissertation committee

ACKNOWLEDGMENTS

“Surround yourself with the dreamers and the doers, the believers and thinkers, but most of all, surround yourself with those who see the greatness within you, even when you don’t see it yourself.” – Edmund Lee

First and foremost, I would like to thank my advisor, Dr. Brian Bahnson, for giving me the opportunity to perform this research in your lab. I appreciate your support, particularly in the unpleasant times when science felt more like magic. Under your guidance I was able to share my work at conferences around the country as well become and advocate for biomedical research. You have taught me that my future is what I put into it, and for that I will be forever grateful.

There are a number of faculty members at the University of Delaware that were exceptionally helpful to me during my doctoral studies. I have benefitted immensely from the insight of my committee members, Dr. Zhihao Zhuang, Dr. Tatyana Polenova, Dr. Donna Woulfe and former committee member Dr. Uhlas Naik. In addition to serving on my committee, Drs. Woulfe and Naik allowed me access of their lab and provided guidance in platelet preparation.

This whole experience would have been vastly different if not for my lab mates, both past and present. Thank you to my predecessor, Dr. Prabha Srinivasan, who answered my emails even after she had graduated, as well as Drs. Ming Dong, Benjamin Israel, Elizabeth Monillas, Stephanie Scott, Anastasia Thévenin and Jessica Wallick for their guidance and advice. Thank you to the current lab members, Walter Drake, Meghan Klems, Mackenzie Lauro, and Michael Willburn, as well as Kaitlyn

Woerner and the two undergraduates I had the privilege of training, Elizabeth Glinka and Thomas Rivas. While our office occasionally had relevant scientific discussions, the times I cherish most were significantly more fun.

I am lucky to have friends who were always a phone call away. Thank you to Nicole, Liz, Sara, Dana, Kelly, Stephanie, Ally, Kat, Kim, Jeff, Seamus and my bee's Andrea, Bethany, Emily, Jaime, Jeannine, Jess, Meaghan, Sarah, and Shannon. All of your support, and especially your distractions, are more appreciated than you realize.

The support and love I have received from my family is overwhelming. Thank for always asking me how "science" is going, and trying your best to understand what I was talking about. I would like to specifically acknowledge the Goldsteins, my in-laws, Joey and Stephanie, as well as my aunts, uncles and cousins for their unwavering support. Thank you to my grandparents, I hope that I have made you proud.

Thank you to my brother, Wally, for correcting my grammar and allowing me to use your blood for the platelet experiments. I never imagined how parallel our lives would be, and I am so lucky to have you as my brother.

Of course, thank you to my parents, Walter and Susan Drake, for the constant guidance, continued support, never-ending encouragement and for loving me even when I was unlikable. Without your help I would never have made it this far, and I know that everything I achieve is a direct result of your amazing work as parents.

Finally, I would like to thank my wonderful husband, Lou. You never waived in your dedication, and I would not have been able to make it this far without your love and sacrifice. Thank you for never making me feel guilty for the decision that I made, putting our lives on hold, and for being up for whatever our next adventure is.

TABLE OF CONTENTS

LIST OF TABLES	xi
LIST OF FIGURES	xii
LIST OF ABBREVIATIONS	xiv
ABSTRACT	xvi

Chapter

1	INTRODUCTION	1
1.1	Atherosclerosis	1
1.2	Platelet-Activating Factor Acetylhydrolase (PAF-AH)	3
1.2.1	Types of PAF-AH.....	5
1.2.2	Lipoprotein-associated phospholipase A ₂ (Lp-PLA ₂)	6
1.2.2.1	Active site	7
1.2.2.2	Lp-PLA ₂ terminal flexibility and disordered regions	9
1.2.2.3	Polymorphisms	10
1.3	Lipoprotein Association of Lp-PLA ₂	10
1.3.1	Lp-PLA ₂ molecular interactions with LDL	12
1.3.2	Lp-PLA ₂ interactions with HDL	15
1.4	Role of Lp-PLA ₂ in Atherosclerosis	16
1.5	Lp-PLA ₂ Complexes with Organophosphorus Compounds	18
	REFERENCES	23
2	EXPRESSION AND PURIFICATION OF LP-PLA ₂	31
2.1	Introduction	31
2.2	Materials and Methods	32
2.2.1	Materials	32
2.2.2	Subcloning	33
2.2.3	Mutations of Lp-PLA ₂	33

2.2.3.1	Insertion of TEV recognition site	33
2.2.3.2	Lipoprotein binding mutations	34
2.2.4	Expression of recombinant Lp-PLA ₂ in <i>E. coli</i>	36
2.2.5	Purification of recombinant Lp-PLA ₂	37
2.2.6	PNPA Assay	39
2.3	Results and Discussion	40
2.3.1	Lp-PLA ₂ constructs	40
2.3.1.1	Lp-PLA ₂ in pGEX-4T-3	40
2.3.1.2	Lp-PLA ₂ in pGEX-6P-1	43
2.3.1.3	Lipoprotein binding mutants	43
2.3.2	Expression of recombinant Lp-PLA ₂	44
2.3.3	Purification of recombinant Lp-PLA ₂	46
2.3.4	Characterization of purified Lp-PLA ₂ constructs	48
2.4	Conclusions	52
	REFERENCES	54
3	SELECTIVE INHIBITOR DISCOVERY OF LP-PLA ₂	56
3.1	Introduction	56
3.2	Materials and Methods	58
3.2.1	Materials	58
3.2.2	Scripps BioAssay	58
3.2.3	Circular dichroism	59
3.3	Results and Discussion	60
3.3.1	Scripps BioAssay results and inhibitor optimization	60
3.3.2	Inhibitor characterization	62
3.3.2.1	Potency	64
3.3.2.2	Selectivity	65
3.3.2.2.1	Comparison of lead inhibitors and JMN4 ..	65
3.3.2.2.2	Comparison of JMN4 and darapladib	66
3.3.3	Kinetic and biophysical characterization of Lp-PLA ₂ inhibitor complexes	73

3.3.3.1	Kinetic analysis of inhibited complexes	74
3.3.3.2	Circular dichroism analysis	74
3.4	Conclusions	78
	REFERENCES	80
4	STRUCTURAL ANALYSIS OF LP-PLA ₂ COMPLEXES	83
4.1	Introduction	83
4.2	Materials and Methods	84
4.2.1	Materials	84
4.2.2	Crystallization screens	84
4.2.3	AutoDock4 modeling	86
4.2.3.1	Docking with darapladib	87
4.2.3.2	Docking with JMN21	88
4.2.3.3	Docking with PAF	89
4.3	Results and Discussion	91
4.3.1	Crystallization of Lp-PLA ₂	91
4.3.2	Lp-PLA ₂ complex models	96
4.3.2.1	Lp-PLA ₂ -darapladib complex	98
4.3.2.2	Lp-PLA ₂ -JMN21 complex	101
4.3.2.3	Lp-PLA ₂ -PAF complex	103
4.4	Conclusions	106
	REFERENCES	108
5	THE ROLE OF LP-PLA ₂ AND PAFAH-II IN PLATELETS	110
5.1	Introduction	110
5.2	Materials and Methods	112
5.2.1	Materials	112
5.2.2	Washing human platelets from whole blood	112
5.2.3	Activating and isolating platelet components	114
5.2.4	Western blotting of platelet samples	114
5.2.5	Thio-PAF Assay	116
5.2.6	Treatment of platelets with inhibitors	116

5.3	Results and Discussion	118
5.3.1	Localization of Lp-PLA ₂ and PAFAH-II	118
5.3.1.1	Western blotting analysis	120
5.3.1.2	Thio-PAF assay	121
5.3.1.2.1	Human platelet samples.....	123
5.3.1.2.2	Mouse platelet samples.....	123
5.3.2	Effects of inhibitors on Lp-PLA ₂ and PAFAH-II in platelets ...	125
5.3.2.1	Human releasate samples	127
5.3.2.2	Mouse releasate samples	127
5.4	Conclusions	129
	REFERENCES	134
6	CONCLUSIONS AND FUTURE DIRECTIONS	136
	REFERENCES	142
Appendix		
A	METHYLTRANSFERASE ENZYMES MtaABC	144
A.1	Introduction	144
A.2	Materials and Methods	145
A.2.1	Materials	145
A.2.2	Gene synthesis and subcloning of MtaA and MtaBC	146
A.2.3	Expression of recombinant MtaA in <i>E. coli</i>	148
A.2.4	Purification of recombinant MtaA.....	148
A.2.5	Methylcobalamin assay of MtaA.....	150
A.2.6	DTNB combined assays	150
A.2.6.1	Forward reaction.....	150
A.2.6.2	Reverse Reaction	151
A.3	Results and Discussion	151
A.3.1	Expression and purification of recombinant MtaA	151
A.3.2	Characterization of purified MtaA	152
A.3.3	Combined MtaABC assays.....	154

A.3.4	Conclusions	155
	REFERENCES	158
B	REPRINT PERMISSIONS	160

LIST OF TABLES

Table 2.1:	Lp-PLA ₂ detergent screening.....	47
Table 2.2:	Lp-PLA ₂ purification.....	49
Table 2.3:	Lp-PLA ₂ kinetics with PNPA as a substrate.....	51
Table 4.1:	Flexible residues for darapladib dockings.....	88
Table 4.2:	Flexible residues for JMN21 docking.....	89
Table 4.3:	Flexible residues of PAF docking.....	90

LIST OF FIGURES

Figure 1.1: Atherosclerotic plaque formation	2
Figure 1.2: PAF-AH's substrates.....	4
Figure 1.3: Structure of Lp-PLA ₂	8
Figure 1.4: Lp-PLA ₂ orientation in membrane	14
Figure 1.5: Lp-PLA ₂ -OP complexes.....	20
Figure 2.1: TEV cleavage site in pGEX-4T-3	35
Figure 2.2: PNPA Assay	39
Figure 2.3: Lp-PLA ₂ in pGEX-4T-3	42
Figure 2.4: Lipoprotein binding mutants.	45
Figure 2.5: Lp-PLA ₂ purification.....	49
Figure 2.6: Lp-PLA ₂ Michaelis–Menten saturation curve.....	51
Figure 3.1. FluoPol-ABPP assay	62
Figure 3.2. High throughput screening hits.	63
Figure 3.3: Fluorophosphonate-rhodamine probe.....	65
Figure 3.4: Inhibitor potency and selectivity determination	67
Figure 3.5: HT-01 Probe	68
Figure 3.6: <i>In vitro</i> evaluation of darapladib and JMN4.	70
Figure 3.7: Fluorophosphonate-biotin probe.	71
Figure 3.8: <i>In situ</i> evaluation of darapladib and JMN4	72
Figure 3.9: Structures of darapladib and its derivatives	73

Figure 3.10: Relative activity of Lp-PLA ₂ with inhibitors	75
Figure 3.11: Circular dichroism analysis of Lp-PLA ₂ with inhibitors.....	77
Figure 4.1: Lp-PLA ₂ crystal diffraction.....	92
Figure 4.2: Crystals of Lp-PLA ₂ inhibited with darapladib derivative SB-56.....	94
Figure 4.3: Crystals of Lp-PLA ₂ inhibited with carbamate inhibitor JMN21.....	95
Figure 4.4: Ligands for AutoDock modeling.....	97
Figure 4.5: Lp-PLA ₂ complexed with darapladib.....	99
Figure 4.6: Lp-PLA ₂ covalently complexed with JMN21	102
Figure 4.7: Predicted interactions of Lp-PLA ₂ and PAF	104
Figure 4.8: Lp-PLA ₂ covalently complexed with PAF	105
Figure 5.1: Thio-PAF Assay	117
Figure 5.2: Lp-PLA ₂ and PAFAH-II specific inhibitors.....	119
Figure 5.3: Activated human platelet Western blots.....	122
Figure 5.4: Human thio-PAF relative activity.	124
Figure 5.5: Mouse thio-PAF relative activity	126
Figure 5.6: Human releasate treated with Lp-PLA ₂ and PAFAH-II inhibitors	128
Figure 5.7: Mouse releasate treated with Lp-PLA ₂ and PAFAH-II inhibitors	130
Figure A.1: Methanol metabolism in <i>M. barkeri</i> with enzymes MtaABC	145
Figure A.2: MtaABC transcripts.....	147
Figure A.3: Expression and purification of MtaA	152
Figure A.4: Activity of MtaA.	153
Figure A.5: MtaABC Forward Reaction.....	154
Figure A.6: MtaABC Reverse Reaction.	156

LIST OF ABBREVIATIONS

ABPP	Activity based protein profiling
ATP	Adenosine-5'-triphosphate
BCA	Bicinchoninic acid
CHAPS	3-[(3-Cholamidopropyl)dimethylammonio]propanesulfonic acid
CHD	Coronary heart disease
DMSO	dimethyl sulfoxide
DTNB	5'5-dithiobis(2-nitrobenzoate)
DTT	Dithiothreitol
EDTA	Ethylenediamine- <i>N, N, N', N'</i> -tetraacetic acid
FluoPol-ABPP	Fluorescence polarization activity based protein profiling
FP-Rh	fluorophosphonate-rhodamine
GST	Glutathione S-transferase
HDL	High density lipoproteins
IPTG	Isopropyl- β -d-thiogalactopyranoside
LB	Luria-Bertani media
LDL	Low density lipoproteins
Lp-PLA ₂	Lipoprotein-associated phospholipase A ₂
Lyso-PAF	Lyso-platelet activating factor, 1-O-alkyl- <i>sn</i> -glycero-3-phosphocholine
OGP	octyl β -D-glucofuranoside
OP	Organophosphorus

OPM	Orientations of proteins in membranes
oxLDL	Oxidized low density lipoproteins
PAF	Platelet activating factor, 1-O-alkyl-2-acetyl- <i>sn</i> -glycero-3-phosphocholine
PAF-AH	Platelet activating factor-acetylhydrolase
PAFAH-II	Intracellular type II PAF-AH
PCR	Polymerase chain reaction
PMV	Python molecular viewer
PNPA	4-Nitro phenylacetate
POV-PC	1-(palmitoyl)-2-(5-oxovaleroyl)-phosphatidylcholine
PRP	Platelet rich pellet
RBC	Red blood cell
SDS	Sodium dodecyl sulfate
SDS-PAGE	Sodium dodecyl sulfate–polyacrylamide gel electrophoresis
TBS-T	Tris buffered saline with tween 20
TEV	Tobacco Etch Virus

ABSTRACT

Lipoprotein-associated phospholipase A₂ (Lp-PLA₂) is a membrane-associated enzyme that circulates in plasma primarily bound to low-density lipoprotein (LDL). The enzyme was discovered due to its ability to catalyze the hydrolysis of the acetyl group at the *sn*-2 position of the diverse signaling phospholipid platelet-activating factor (PAF) and is therefore also referred to as PAF acetylhydrolase. In addition to the substrate PAF, Lp-PLA₂ recognizes oxidatively fragmented phospholipids derived from polyunsaturated fatty acids at the *sn*-2 position as well as oxidatively fragmented phospholipids present on oxidized LDL. It is important to note that Lp-PLA₂ only recognizes oxidatively fragmented phospholipids and can therefore be constitutively active without compromising cellular integrity. Due to its associations with LDL, its cleavage products and the report that an increase in Lp-PLA₂ concentration or activity leads to an increase in the risk of atherosclerosis Lp-PLA₂ has been reported to play an important role in the progression of heart disease. Lp-PLA₂ has therefore become recognized as a viable drug target. The pharmaceutical company GlaxoSmithKline developed a specific inhibitor of Lp-PLA₂, darapladib, which was recently investigated for use as an add-on treatment for patients with heart disease.

The structure of Lp-PLA₂ was solved at a resolution of 1.5 Å and was determined to have the classic α/β hydrolase fold. This high resolution structure was then used to develop a model that mimics the association of Lp-PLA₂ in biological membranes. Using the knowledge of the structure of Lp-PLA₂, combined with its membrane associations as well as disease implications, the work of this thesis was

done to gain a better understanding of the structure-function relationship of the enzyme.

An *E. coli* over-expression construct of a truncated form of Lp-PLA₂ was created to resemble the sequence of protein samples of Lp-PLA₂ obtained from the company ICOS Corporation, as it was this truncated version whose crystal structure was solved. Expression and purification of the recombinant Lp-PLA₂, as well as point mutations created to minimize its membrane associations, were carried out using the *E. coli* expression construct. Activity assays using a general substrate were developed and demonstrated that there was no significant difference in specific activity, K_{cat} or V_{max} for any of the mutants; however, there was a decrease in the K_M for the Lp-PLA₂ lipoprotein binding mutants. The highly pure and concentrated samples of recombinant enzyme were used for protein crystallization trials.

Due to the fact that Lp-PLA₂ is a drug target, high throughput inhibitor screening was carried out at the Scripps Research Institute Molecular Screening Center for Lp-PLA₂ as well as with a homologous, intracellular enzyme, PAFAH-II. The highly potent preliminary hits were characterized in the lab of Dr. Benjamin Cravatt at the Scripps Research Institute and inhibitors were modified to specifically target Lp-PLA₂ *in vitro* and *in situ*. The inhibited recombinant Lp-PLA₂ was further studied in our lab for kinetic and biophysical properties.

In order to determine the structure of darapladib and the carbamate inhibitor complexed with Lp-PLA₂ crystallization trials were attempted. Though initial screening was promising, co-crystallization crystal structures were not determined. In turn, computational models of the enzyme-inhibitor complex were created to show the

binding interaction. In addition, a computational model of Lp-PLA₂'s interaction with its natural ligand, PAF, was modeled.

Previous reports indicated that Lp-PLA₂ was also carried in plasma associated with platelet derived microparticles. These microparticles are derived during platelet activation and are implicated in furthering the progression of atherosclerosis. This study confirms the presence of Lp-PLA₂ in both human and mouse platelets upon activation as well as PAFAH-II using Western blot analysis. It was also confirmed that the Lp-PLA₂ secreted from platelets is non-glycosylated, indicating that this enzyme was not taken up by the platelets from the plasma but was native to the platelet or its progenitor cells. The activity of the enzymes were assayed using a modified DTNB assay and activities contributed specifically to Lp-PLA₂ and PAFAH-II were determined by individually blocking each form's activity using the specific inhibitors developed through our collaboration with Scripps. It was shown that in human and mouse platelet releasate demonstrate Lp-PLA₂ and PAFAH-II activity, indicating a potential role in PAFAH-II advancing the progression of atherosclerosis.

In this study, we have broadened the knowledge base of Lp-PLA₂ and its structure-function relationship through the development and use of potent and specific inhibitors. We have also determined new potential roles for both Lp-PLA₂ and PAFAH-II in the progression of atherosclerosis due to their characterized release upon platelet activation. These roles can be explored in further studies and animal models to better understand the impact of these enzymes in disease.

Chapter 1

INTRODUCTION

1.1 Atherosclerosis

Coronary heart disease (CHD) is the leading cause of death for both males and females in the United States. An estimated 735,000 Americans suffer myocardial infarctions yearly and nearly 610,000 Americans die each year due to CHD related complications [1]. A leading cause of CHD is the inflammatory disease atherosclerosis, in which plaques form on the arterial inner lining and obstruct the blood flow [2]. These atherosclerotic plaques are composed of cell debris including the remnants of activated platelets, lipids, cholesterol, and inflammatory macrophage cells covered with the hallmark fibrous cap. The most dangerous plaques are those with unstable caps as they are prone to rupture. Plaque rupture can lead to thrombosis, strokes and myocardial infarction [2].

It is generally accepted that atherosclerotic plaque formation begins with activation of the blood vessel endothelial cells, shown in Figure 1.1. The activated endothelial cells begin to express cell adhesion molecules and pro-inflammatory chemokines that recruit inflammatory cells, such as T-cells and monocytes, to bind to the epithelium and enter the arterial intima [3,4]. After migrating into the inner most arterial lining, monocytes differentiate into macrophage cells. The macrophages express scavenger receptors, which engulf modified lipoprotein particles, such as oxidized low density lipoprotein (oxLDL). The cholesterol present in the oxLDL

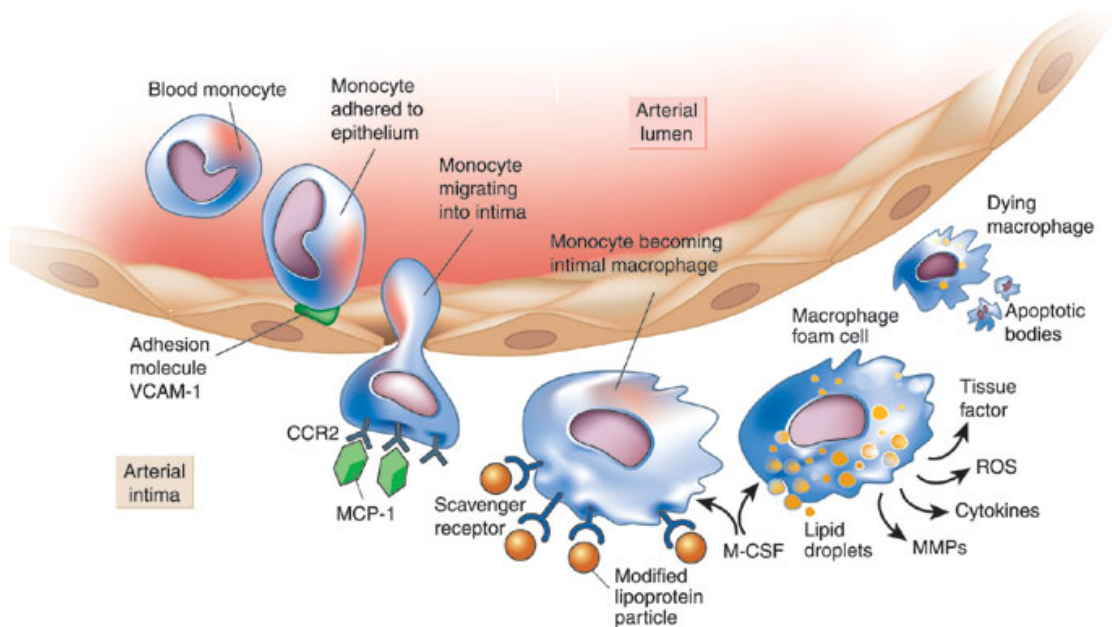


Figure 1.1: Atherosclerotic plaque formation. Monocytes are recruited to and migrate into the arterial intima. After migration, monocytes differentiate into macrophages and begin to engulf modified lipoprotein particles, such as oxidized LDL. This causes a buildup of cholesterol in cytosol and results in the cell transformation into foam cells. Foam cells secrete compounds that progress plaque formation. As foam cells die they form the necrotic core of the atherosclerotic lesion. Reprinted by permission from Macmillan Publishers Ltd: [NATURE] (Libby, P. Inflammation in atherosclerosis. 420, 868–74), copyright (2002)

begins to accumulate inside the cell, which causes the macrophage to differentiate into a foam cell. Foam cells secrete cytokines and reactive oxygen species in order to amplify the inflammatory response as well as matrix metalloproteinases that help form the hallmark fibrous cap. Eventually, the cells die and begin to form the central necrotic core of the atherosclerotic plaque [5].

The oxLDL engulfed by the macrophage cells is formed as a result of a build up of oxidatively fragmented phospholipids present on the lipoprotein particles. These fragments are caused by reactions with reactive oxygen species, like those secreted from the foam cells [6,7]. Oxidized LDL is responsible for several pro-inflammatory activities, including the activation of endothelial cells, monocyte chemotaxis, and smooth muscle cell proliferation [4,8,9]. Taken together, the pro-inflammatory activities of oxLDL lead to the progression of atherosclerosis [10].

1.2 Platelet-Activating Factor Acetylhydrolase (PAF-AH)

A group of Ca^{2+} -independent phospholipase A_2 (PLA_2) enzymes have been shown to hydrolyze oxidatively fragmented phospholipids [11]. The enzymes were discovered due to their ability to cleave the diverse phospholipid signaling molecule, platelet activating factor (PAF), 1-O-alkyl-2-acetyl-*sn*-glycerol-3-phosphocholine, and in turn were named platelet-activating factor acetylhydrolases (PAF-AH) [12]. The PAF-AH enzymes catalyze the hydrolysis of an acetyl group at the *sn*-2 position of PAF yielding lyso-PAF and acetate (Figure 1.2). Unlike other PLA_2 enzymes, PAF-AHs have a unique specificity for substrates with short acyl chains or polar chains at *sn*-2 position [12-14].

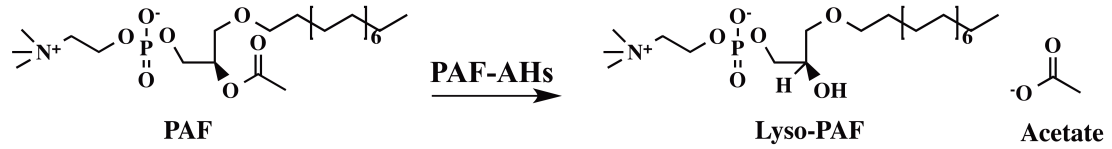
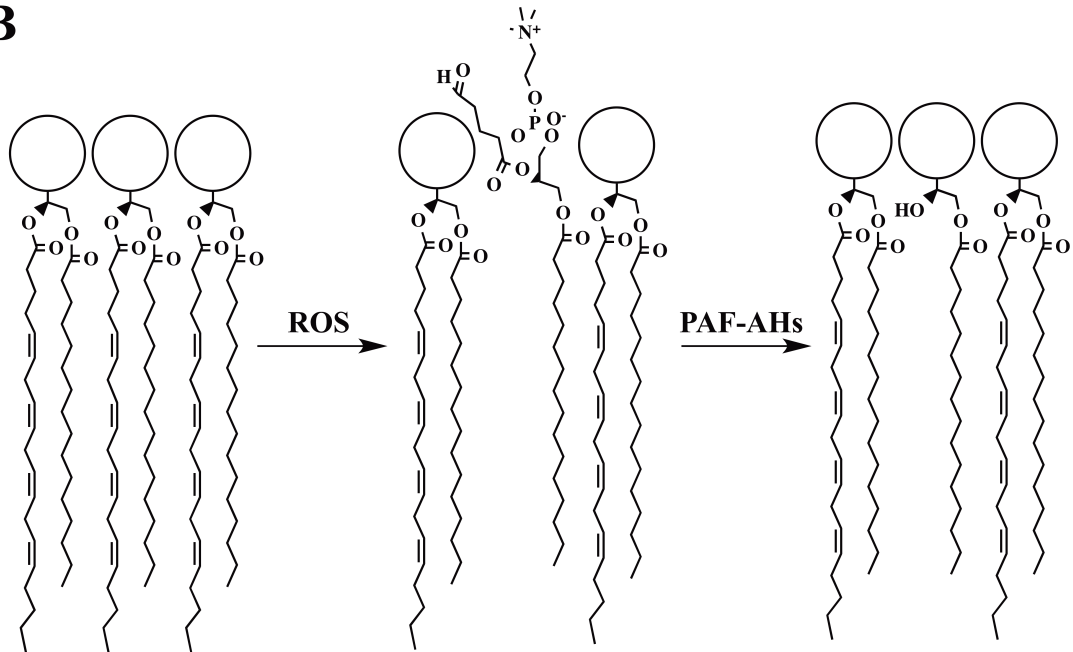
A**B**

Figure 1.2: PAF-AH's substrates. (A) PAF-AH cleaves at the *sn*-2 position of PAF yielding lyso-PAF and an acetate ion (B) Phospholipid monolayer can be oxidized by reactive oxygen species (ROS) yielding a fragmented phospholipid, 1-(palmitoyl)-2-(5-oxovaleroyl)-phosphatidylcholine (POV-PC). PAF-AH then recognizes that the oxidized *sn*-2 chain is flipped up or away from hydrophobic portion and accessible to the active site of the enzymes.

1.2.1 Types of PAF-AH

There are three types of PAF-AHs which comprise group VII and VIII of the PLA₂ superfamily [15]. These enzymes contain a *GXSXG* motif that is characteristic of neutral lipases and serine esterases, which includes the nucleophilic serine. There are two intracellular PAF-AHs and one secreted. The intracellular PAF-AH Ib (group VIIIA and group VIIIB) is a product of the Miller Dieker Lissencephaly gene and is primarily found in the brain. This enzyme exists as a heterotetramer containing regulatory β subunit (45 kDa) and two catalytic α subunits (26 kDa), where $\alpha 1$ and $\alpha 2$ are homologous and share 63% sequence identity [16,17]. The structure of PAF-AH Ib has been resolved by x-ray crystallography and this enzyme bears no sequence homology or identity to the other two PAF-AHs [18]. In addition, PAF-AH-Ib enzyme has been suggested to have a physiological function different than that of a true PAF-AH [19].

Plasma PAF-AH (group VIIA), also referred to as lipoprotein-associated phospholipase A₂ (Lp-PLA₂), is an extracellular 45 kDa monomer that circulates in the plasma and associates with lipoproteins [20]. The intracellular enzyme, PAF-AH-II (group VIIIB), is a 40 kDa myristoylated enzyme with 41% sequence identity to Lp-PLA₂ [21]. Research has shown that PAF-AH-II localizes in the cytoplasm of liver and kidney cells as a homodimer. In response to oxidative stress, PAF-AH-II becomes a monomer and binds the outer leaflet membranes of the Golgi and endoplasmic reticulum in order to prevent apoptosis [22,23].

The three PAF-AHs have varied substrate specificities. The intracellular brain enzyme, PAF-AH Ib has the most limited substrate specificity in which any *sn*-2 chains beyond 2 carbons greatly reduce the enzyme's catalytic efficiency [16]. Lp-PLA₂ and PAF-AH-II are more promiscuous and act on a wider range of substrates. In

addition to PAF, Lp-PLA₂ and PAFAH-II also hydrolyze oxidatively fragmented phospholipids that result from reactive oxygen species with polyunsaturated fatty acyl chains at *sn*-2 position. These enzymes are tolerable to *sn*-1 chains of up to 16 carbons before any effect occurs on catalysis at the *sn*-2 position. In addition, Lp-PLA₂ and PAFAH-II can affectively hydrolyze *sn*-2 chains with up to 5 carbons, though catalysis at this position is eliminated when the *sn*-2 chain exceeds 10 carbons [14,21,24]. It is important to note that non-oxidized, or normal longer *sn*-2 chain phospholipids are not recognized as substrates for PAF-AHs, allowing these enzymes to be active without compromising cellular integrity.

1.2.2 Lipoprotein-associated phospholipase A₂ (Lp-PLA₂)

The Lp-PLA₂ enzyme is secreted by macrophages into the plasma as they differentiate into monocytes. The enzyme naturally exists in a heterogeneous distribution as a 43-, 44-, or 45- kDa monomer with the N-terminus starting at residue Lys55, Ile42 or Ser35, respectively, and is glycosylated at residues Asn423 and Asn433, which are situated near the C-terminus. [25,26]. The ligand-free structure of Lp-PLA₂ (PDB ID: 3D59), spanning residues 47-429 was solved using x-ray diffraction data collected to a 1.5 Å resolution [27]. The protein sample used for structure determination was produced by the ICOS Corporation to be used as a potential protein therapeutic to treat patients with deficiencies in the enzyme who are afflicted with severe inflammatory diseases due to elevated levels of PAF in the body [27,28]. In addition to the ligand-free structure of Lp-PLA₂, structures of Lp-PLA₂ complexed with organophosphorus (OP) compounds were resolved and will be discussed further in section 1.5.

The structure confirmed that Lp-PLA₂ contained the classic α/β hydrolase fold, typical of lipases and neutral esterases. The active site serine is located in a conserved *GXSXG* motif. Although there is no evidence of Lp-PLA₂ forming oligomeric states in solution, the ligand-free crystal contained two subunits in the asymmetric unit. However, analysis with the PISA server of the interface between subunits A and B predicted this dimerization is strictly due to crystal packing and plays no role in enzyme function [29]. There is a rare, non-prolyl *cis*-peptide bond in Lp-PLA₂ between residues Phe72 and Asp73, with distinct electron density around the atoms supporting the presence of this unusual bond.

1.2.2.1 Active site

As originally predicted, the active site of Lp-PLA₂ was confirmed to be Ser273, Asp296 and His351 [26,30]. The nucleophilic serine is located at the N-terminal end of a core α -helix. The amide nitrogens of residues Leu153 and Phe274 are positioned around Ser273 in such a way that stabilizes the negative charge present on a tetrahedral intermediate during the reaction mechanism. This stabilization of the charged intermediate by Leu153 and Phe274 is better known as the oxyanion hole of this serine hydrolase enzyme.

The two other residues in the active site, Asp296 and His351, are positioned appropriately to Ser273 for catalysis, as shown in Figure 1.3. The residue Asp296 sits at the C-terminal end of a core β -sheet and residue His351 is positioned at the N-terminal end of a core α -helix. The catalytic triad is positioned inside the hydrophobic pocket of Lp-PLA₂, which is orientated toward its substrate, facing the aqueous phase, and sitting above the membrane interface. The positioning of the active site allows for

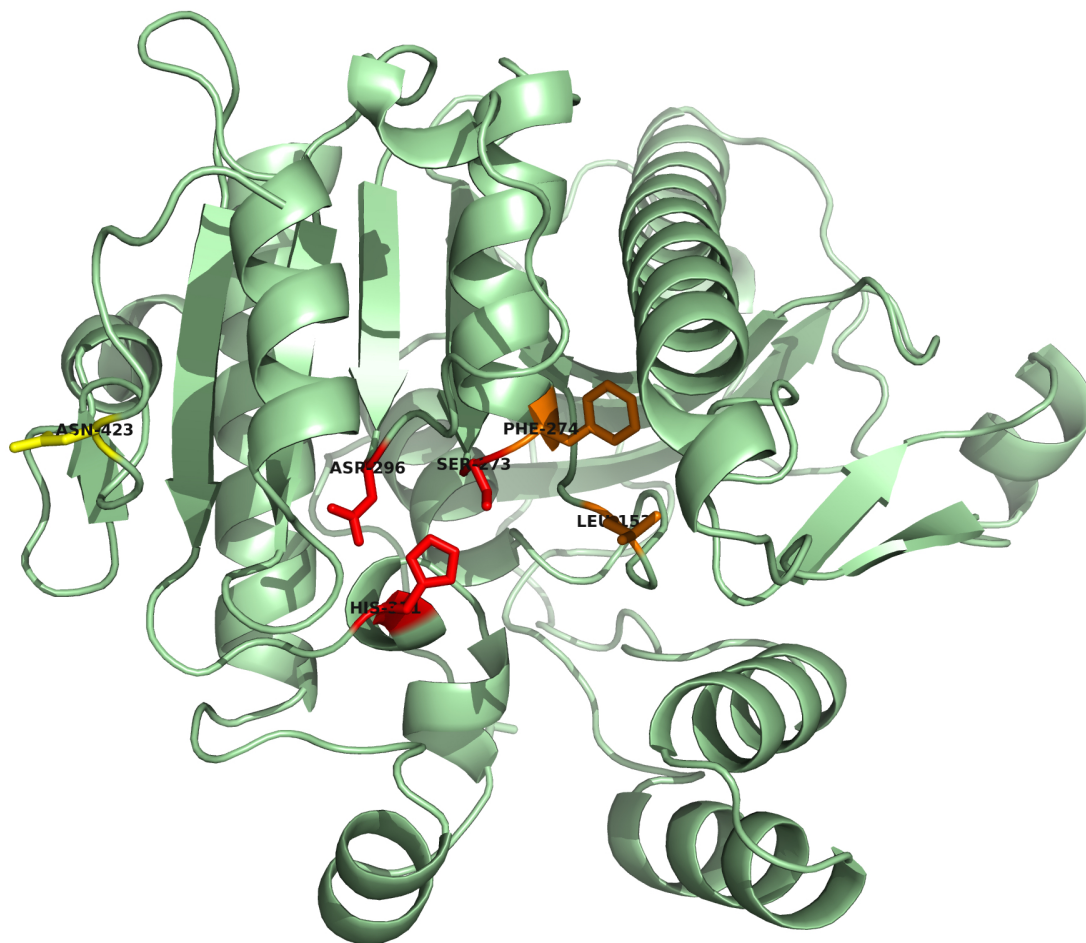


Figure 1.3: Structure of Lp-PLA₂. Cartoon view of Lp-PLA₂ structure with the catalytic triad active site residues Ser273, Asp296 and His351 shown in red ball and stick. The backbone amides of the two residues that compose the oxyanion hole, Leu153 and Phe274, are shown in orange. Glycosylation site Asn423 is shown in yellow.

substrate to enter the hydrophobic pocket of the enzyme from both lipoprotein carriers as well as from the aqueous phase, supporting other experimental findings [31-33]. The open channel active site of Lp-PLA₂ accounts for the substrate specificity of the enzyme whereby Lp-PLA₂ and lipophilic substrates are brought together by their common affinity for lipoproteins. Though the binding pocket of the enzyme can accommodate larger substrates, as previously mentioned, only phospholipids with short acyl chains at the *sn*-2 position can be hydrolyzed unless the substrate contains an oxidized functionality at the ω -position [13].

1.2.2.2 Lp-PLA₂ terminal flexibility and disordered regions

The recombinant enzyme construct, produced by the ICOS Corporation and used for crystallization, began at residue Ala47. However the crystal structure of Lp-PLA₂ was built and refined beginning at Thr54, one residue preceding an endogenous N-terminus for the enzyme found at Lys55 [26]. The residues between Ala47 and Thr54 were disordered and could not be modeled. The region at the C-terminus of the enzyme spanning residues 426-429 for subunit A, and 427-428 for subunit B, was disordered and was unable to be modeled [27].

Several other regions in the ligand-free structure were disordered and the residues were unable to be resolved. A portion of the membrane binding interface (i-face) region, containing residues His114, Trp116 and Leu116, in the ligand-free structure had weak electron density and was unable to be modeled. This is not surprising as this region of the enzyme is predicted to be flexible due to its superficial location and predicted membrane interactions, which will be discussed in section 1.3. These residues did have strong electron densities for the Lp-PLA₂ structure complexed with the OP compound paraoxon, and this region was able to be modeled [27].

1.2.2.3 Polymorphisms

There are several polymorphisms of Lp-PLA₂ reported in different populations, two of which result in a loss of enzyme function. These loss of function polymorphisms reported in 4% of the Japanese population are V279F and Q281R [34]. These two residues are located in the core of the enzyme and are critical for enzyme function. The residue Val279 is a conserved hydrophobic core residue that is critical for proper folding and therefore function of Lp-PLA₂. Residue Gln281 is located on the same α -helix as the nucleophilic active site Ser273; therefore, the Q281R variant disrupts the active site and results in a loss of the enzyme's function.

There are other polymorphic variants of Lp-PLA₂ reportedly linked to a variety of inflammatory diseases including asthma, atherosclerosis and coronary artery disease [35,36]. The three polymorphisms, R92H, I198T and A379V are all solvent exposed and each are far from the active site, and therefore are not believed to result in a loss of catalytic function of the enzyme [37]. The residue Ile198 is 71% solvent accessible and 35 Å away from the active site residue His351. Residue Ala379 is on a surface α -helix that is 39% solvent accessible and 15 Å from nucleophilic Ser273. The structure of Lp-PLA₂ and the locations of these polymorphisms, shown in Figure 1.4, suggest that the disease phenotype associated with these variants is likely a result of lipoprotein binding interaction and not due to a direct effect on the enzymes catalytic activity.

1.3 Lipoprotein Association of Lp-PLA₂

Lp-PLA₂ associates with both low density lipoprotein (LDL) and high density lipoprotein (HDL) in the plasma. The enzyme was initially isolated from human plasma using various detergents to aid in solubilization due to the enzyme's

interaction with these lipoprotein particles [38]. Using the structure of Lp-PLA₂ as a guide, a model of the enzyme bound to a hydrophobic/hydrophilic interface has been developed following the method of orientation of proteins in membranes (OPM) developed by A. Lomize (Figure 1.4) [39,40]. This model distinguishes membrane proteins and predicts their bilayer positioning based on transfer energy and membrane penetration depths. The plane of spheres represents the interface between the polar and non-polar components of membranes, with the polar head groups of the phospholipids extending about 10 Å above the plane. The OPM model predicts the interface (i-face) binding regions of Lp-PLA₂ with the phospholipid monolayer of LDL and HDL particles to occur at two α - helices. The residues in the i-face region helices are rich in hydrophobic residues that can insert into the interface region of the membranes.

It has been reported that certain alterations of the physiochemical properties of lipoprotein particles can play an important role in regulating the binding and activity of their associated enzymes, specifically varying levels of cholesterol which has a strong effect on membrane fluidity [41-43]. An increased level of cholesterol in membranes has a significant effect on the binding and penetration of Lp-PLA₂ in membranes, which varied based upon the membrane the enzyme is associated with [44]. Increasing levels of cholesterol induced changes in the order/disorder of the fatty acyl chains or polar interface region of membrane vesicles, which had a strong effect on the binding of Lp-PLA₂ to the membrane as well as its penetration depth; the more disordered, the better the enzyme binding. The presence of oxidized phospholipids, a substrate of Lp-PLA₂, intercalated into the membrane in a similar fashion as cholesterol, may also regulate the recruitment of Lp-PLA₂ to lipoprotein particles [45].

Lp-PLA₂ primarily associates with LDL while only a small percent of the enzyme circulating in plasma associates with HDL. The ratio of Lp-PLA₂ association with LDL and HDL varies due to the method of isolation. Using ultracentrifugation, Lp-PLA₂ was found to associate with LDL 70% of the time, but using size exclusion chromatography increased the amount of Lp-PLA₂ associated with LDL to 85% [20,46].

1.3.1 Lp-PLA₂ molecular interactions with LDL

Lp-PLA₂ is predicted to interact with the phospholipid monolayer of LDL and HDL particles at two α -helices. The helix containing residues 114-126 has been reported critical for interaction of the enzyme with LDL, shown in red in Figure 1.4 [47]. As previously stated, the weak electron density in the crystal structure surrounding the residues in this α -helix is likely due to the flexibility in this region. The residues Tyr205, Trp115, Leu116, and to a lesser extent Met117, have been reported critical for interaction with LDL and mutations of any of these residues greatly reduced the binding of Lp-PLA₂ to LDL [47]. In mice, the Lp-PLA₂ sequence is not conserved at residues corresponding to Trp115 and Leu116, and in turn the enzyme is not able to bind LDL. Site directed mutagenesis of the mouse homolog, which modified the enzyme to correspond to the human Trp115 and Leu116, allowed for the enzyme to bind LDL [47]. The residue Tyr205 is well above the plane of membrane interaction; however, this residue is involved in a cation-pi interaction with Lys109. This interaction at position 109 likely has an indirect effect on the α -helix interacting with LDL. Consistent with this prediction, a disruption of this cation-pi interaction between Try205 and Lys109 would result in a disruption to the lipoprotein binding helix reported critical for Lp-PLA₂ association with LDL.

The OPM model predicts that residue His114 is buried in the hydrophobic lipid phase. Previous studies have demonstrated a pH dependence on Lp-PLA₂ binding with LDL, and therefore the charged state of residue His114 supports its presence in the binding interface [38]. The importance of these residues was further confirmed by Dennis and coworkers using hydrogen-deuterium exchange experiments where it was shown that when Lp-PLA₂ is bound to LDL, the region spanning residues 113-120 had no exchange with deuterium, demonstrating that the residues are not solvent accessible, likely due to their penetration in the phospholipid monolayer of LDL [48].

The structure of Lp-PLA₂ also revealed an interesting feature: a region of conserved neighboring basic and acidic patches, which are potentially important for lipoprotein interactions. The region, shown in Figure 1.4 panel B, is comprised of 10 carboxylate residues (Asp374, Asp376, Asp382, Asp401, Asp403, Asp406, Glu410, Asp412, Asp413 and Glu414) adjacent to 3 basic residues (Lys55, Arg58, Lys363). This region of the enzyme has been implicated to mediate the binding of Lp-PLA₂ with apoB-100 present on LDL, as apoB-100 has been reported to mediate the electrostatic interactions of LDL with glycosaminoglycans (GAGs), exploiting clusters of charged residues on apoB-100 and GAGs [49,50].

It is interesting to note that Ala379, a residue with a naturally occurring non-synonymous polymorphism, falls at the base of the acidic patch and adjacent to the plane of lipoprotein binding as predicted by the OPM model. Due to its location, and the predicted electrostatic interactions, the A379V mutation plays a potential role in lipoprotein partition of Lp-PLA₂. It is probable that the Ala379 residue plays a role in maintaining the electrostatic interactions of Lp-PLA₂ with the polar head groups of phospholipids on the surface of lipoproteins [49].

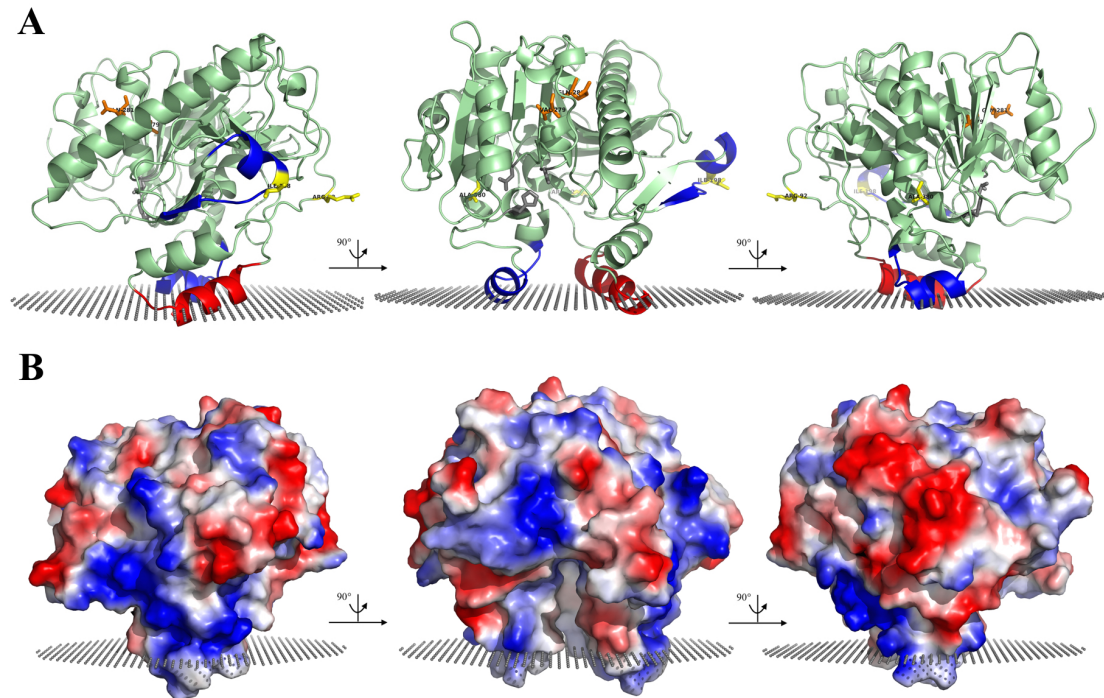


Figure 1.4: Lp-PLA₂ orientation in membrane. (A) The active site residues are shown in gray ball and stick and located at the core of the enzyme (unlabeled). The orange ball and stick residues Val279 and Gln281 are the polymorphisms that result in a loss of enzyme functions. The yellow ball and stick residues Ile198, Ala379 and Arg92 are polymorphisms that are solvent accessible and far from the active site, therefore do not result in a loss of function of the enzyme. The gray spheres at the base of the enzyme represents the predicted plane of hydrophobic/hydrophilic interaction as determined by the OPM method. The helix in red, spanning residues 113-126, represent the amino acids predicted critical for binding LDL while the helix in blue, spanning residues 360-369, represent the amino acids predicted critical for associates with HDL. The helix and turn shown in blue, near Ile198, spanning residues 192-204, represents the region predicted to interact with apoA-I. The figure shows two 90° rotation around the y-axis and corresponds to the panels in B. (B) Electrostatic view of Lp-PLA₂ OPM model. On the left shows the region predicted to interact with the apoA-I component of HDL, in the center is a 90° rotation around the y-axis and shows the hydrophobic binding pocket of Lp-PLA₂ and finally the right is another 90° rotation around the y-axis and shows the acidic/basic patch of Lp-PLA₂ predicted to interact with the apoB-100 portion of LDL.

1.3.2 Lp-PLA₂ interactions with HDL

The second α -helix at the membrane interface as predicted by the OPM model, containing residues 362-369, has been reported critical for interaction of Lp-PLA₂ with HDL, shown in blue in Figure 1.4 panel A [30]. The specific C-terminal residues on this α -helix reported critical for HDL include His367, Met368, Leu369 and Lys370, with residues Met368 and Leu369 reported to contain a more prominent role in the binding mechanism as determined by mutagenesis experiments. Hydrogen-deuterium exchange experiments, like those performed with LDL, confirmed that the region containing residues 360-368 were involved with the interface between Lp-PLA₂ and HDL [51].

An additional region, containing residues 192-204, was determined to bind the apoA-I component of HDL and is shown in blue in Figure 1.4 panel A [51]. This region contains a small cluster of acidic residues including Asp192, Glu197, and Asp200, adjacent to the basic residue Lys201 and polar residues Gln193, Ser194 and Ser202. This polar and charged region is similar to that of the acidic patch reported to associate with the apoB-100 portion of LDL, and is shown in Figure 1.4 panel B. Taking this together, it has been hypothesized that the interaction between Lp-PLA₂ and the apoA-I portion of HDL is predominantly electrostatic. Interestingly, the non-synonymous polymorphism I198T falls in the region predicted to associate with the apoA-I portion of HDL, and it can be hypothesized that mutations at this residue disrupt the association of Lp-PLA₂ with HDL. It is probable that the electrostatic interactions between residues of Lp-PLA₂ and apoB-100 on LDL and apoA-I on HDL play a role in the partitioning of the enzyme with its lipoprotein carriers.

Although the model of the Lp-PLA₂ membrane interaction predicted by OPM is in agreement with functional studies, there are no distinct structural features to

support the notion that specific regions interact with either LDL or HDL. It is important to note that hydrogen-deuterium exchange experiments demonstrated that the region containing residues 107-120 bound HDL. This same region had been previously reported critical for binding LDL with no previous implication on HDL binding. This data supports our previous proposal that the two i-face helices are involved in binding both LDL and HDL lipoproteins [49,52]. The studies, which identify the LDL and HDL binding regions, have been performed in isolation, using only one lipoprotein particle at a time. It is important to conduct experiments using both the lipoprotein particles in parallel before it can be concluded that specific regions of Lp-PLA₂ interact with only LDL or HDL.

1.4 Role of Lp-PLA₂ in Atherosclerosis

The carrier of Lp-PLA₂ may play a large effect on the enzyme's role in atherosclerosis [53]. As previously discussed, Lp-PLA₂ circulates in plasma associated with LDL and HDL. It has also been reported that the enzyme circulates in plasma associated with platelet derived microparticles [54]. Microparticles are shed from the platelets surface in response to platelet activation and have been reported to be carriers of proteins with known inflammatory roles [55]. To date, the role that Lp-PLA₂ associated with platelet derived microparticles plays on atherosclerosis has not been established.

The association of Lp-PLA₂ with HDL is decidedly anti-atherogenic, whereby associations with HDL contribute to preventing LDL oxidation [53]. As mentioned previously, mouse Lp-PLA₂ does not associate with LDL, and therefore the enzyme circulating in plasma is primarily associated with HDL [30,56]. Adenovirus-mediated Lp-PLA₂ gene transfer in atherosclerosis prone apoE^{-/-} mice showed anti-

atherosclerotic effects, providing further evidence that Lp-PLA₂ associated with HDL is protective against atherosclerosis [57]. In a follow-up study with the Lp-PLA₂ gene transfer in atherosclerotic mice, the enzyme bound all lipoprotein particles and was found to protect against oxidative stress [58].

While the role of Lp-PLA₂ associated with HDL is defined, the role of the enzyme associated with LDL remains controversial. Lp-PLA₂ has been known to associate with pro-inflammatory subclasses of lipoproteins. In patients with high levels of lipoprotein(a) [Lp(a)], Lp-PLA₂ preferentially associates with Lp(a) over LDL [59]. Lp(a) is a lipoprotein similar to LDL, but contains the additional glycoprotein, apo(a), which is associated with apoB-100 by a disulfide bond. This association of Lp-PLA₂ with Lp(a) is unsurprising, as it is known that Lp-PLA₂ associates with the apoB-100 portion of LDL. Lp(a) has been proposed to be a carrier of oxidatively fragmented phospholipids, and elevated levels of Lp(a) have been linked to increased risk of atherosclerosis [53,60]. In addition, it has been shown that Lp-PLA₂ associates with LDL(-), an increasingly electronegatively charged LDL [61]. LDL(-) is known to be atherogenic and proinflammatory, and it has cytotoxic effects on endothelial cells [62].

It was initially thought that the hydrolysis of oxidatively fragmented phospholipids on LDL by Lp-PLA₂ lead to a protective effect of the enzyme [63-65]. However, the hydrolysis reaction results in the formation of lysophosphatidylcholine and oxidized non-esterified fatty acids. These compounds are known to aid in atherosclerotic plaque development [66,67]. It has also been shown that the enzyme is present in the atherosclerotic plaques most prone to rupture and has been reported to promote the formation of the necrotic core [68,69]. An increase in Lp-PLA₂

concentration or activity present in human plasma is linked with an increased risk of developing atherosclerosis [70-72]. In addition, the enzyme has been used as a biomarker to assess the risk of CHD and has been shown to be a potential therapeutic target [73,74]. These pro-atherosclerotic properties of Lp-PLA₂ led GlaxoSmithKline to develop a potent and specific inhibitor of the enzyme, known as darapladib, which will be discussed further in Chapter 3 [75-77].

1.5 Lp-PLA₂ Complexes with Organophosphorus Compounds

Organophosphorus (OP) compounds have been primarily produced for use as insecticides; however, certain compounds such as sarin, soman and tabun have been developed as nerve agents in chemical warfare and pose a significant risk to human health. These compounds exhibit their toxicity by inhibition of acetylcholinesterase thus preventing the degradation of the neurotransmitter acetylcholine [78]. After binding acetylcholinesterase, the OP compounds typically undergo an aging process, which in turn prevents the enzyme from becoming reactivated and thus continues catalytic inhibition. However, if the compounds do not age upon binding, the complex can become reactivated by a water molecule or alternative nucleophile and the enzyme regains functionality [79].

It has been shown that serine hydrolase enzymes, including Lp-PLA₂, can bind these OP compounds and have potentially clinical consequences [78]. There have been efforts made to engineer various serine hydrolase enzymes to bind and hydrolyze these nerve agents and therefore function as catalytic bioscavengers [80]. Lp-PLA₂ is an excellent bioscavenger target due to its presence in human blood, the primary route nerve agents travel to reach acetylcholinesterase at nerve synapses. The structure of Lp-PLA₂ complexed with various nerve agents can be used as a starting point for

engineering hydrolase activity through strategic mutagenesis of residues around the active site.

Crystal structures of Lp-PLA₂ complexed with five OP compounds have been reported, including the insecticides paraoxon and DFP as well as the nerve agents sarin, soman and tabun solved to a resolution of 2.1, 2.3, 2.1, 1.7 and 1.7 Å respectively [27,81]. In all cases, the OP was found to be in the preferred non-aged form with the stability of these complexes demonstrated by a long incubation period (4-7 weeks) of protein co-crystallization.

While the Lp-PLA₂-OP structures themselves do not serve as definitive identification of another physiological substrate of the enzyme, they do provide insight into the hydrolase mechanism of Lp-PLA₂ and allow us to predict how the substrate would access and bind the active site. In each complexed structure, there is a reaction of the OP compound with Ser273 forming a covalent bond at the active site. First seen in paraoxon, and then demonstrated in each structure, the Lp-PLA₂-OP complexes serve as a mimic of the tetrahedral intermediate of the esterolysis reaction of the enzyme shown in Figure 1.5 [27,81]. The three catalytic residues, Ser273, Asp296 and His351, as well as neighboring active site residues, are positioned around the Lp-PLA₂-OP complexes in a manner consistent with the tetrahedral intermediate complex. The amide nitrogens of Leu154 and Phe274 make hydrogen bonds with an oxygen atom on the OP moiety, corresponding with the enolate oxygen of a tetrahedral intermediate. The interactions between the oxyanion hole of Lp-PLA₂-OP complexes revealed by the crystal structures allows for the engineering of catalytic hydrolase activity with low K_M values [82].

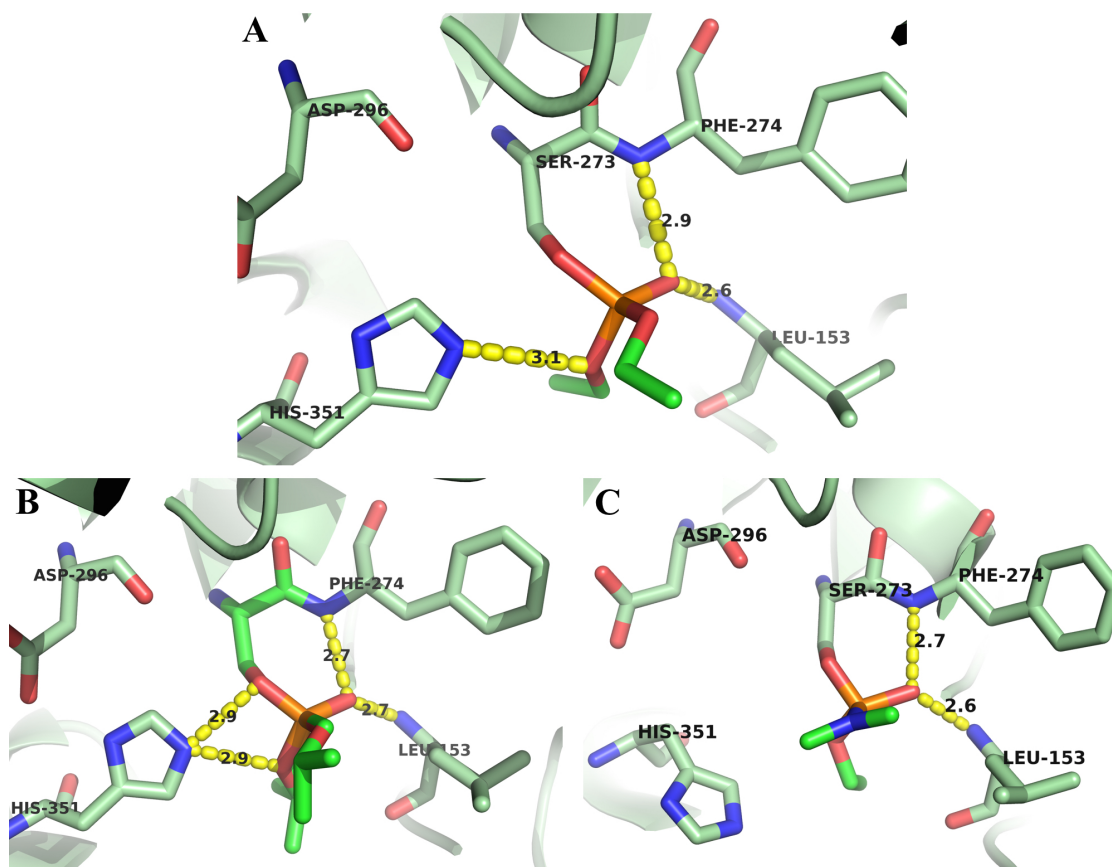


Figure 1.5: Lp-PLA₂-OP complexes representing tetrahedral intermediates of the reaction mechanism of the enzyme. (A) Paraoxon covalently bound at the nucleophilic Ser273 and contains hydrogen bond contacts with Leu153, Phe274 and active site residue His351. (B) The P_S stereoisomer of Sarin is covalently bound at Ser273 and also contains hydrogen bond contacts with Leu153, Phe274 and His351. Both the P_R and P_S stereoisomers are present in the enzyme at equal occupancy (C) Only the more toxic P_R stereoisomer of Tabun reacts with Lp-PLA₂ forming a covalent bond at Ser273 and contains hydrogen bond interactions with Leu153 and Phe274. The active site His351 is positioned away from the complex and is not in close proximity to interact with the OP.

The Lp-PLA₂-OP complexes of sarin and soman react non-selectivity with both the P_R and the more toxic P_S stereoisomers. In contrast, the Lp-PLA₂ complex with tabun is specific for the more toxic P_R stereoisomer. It has been shown, with limited success, that nascent reactivity with these nerve agents can serve as a starting point for engineering the enzyme to display OP hydrolase catalytic activity [82,83]. Currently, the versatility of Lp-PLA₂, due to its ability to bind the various stereoisomers of sarin, soman and tabun, is being exploited to generate catalytic bioscavengers that will work at the low, physiologically relevant concentrations of these lethal nerve agents *in vivo*.

In summary, Lp-PLA₂ is a secreted enzyme circulating in plasma associated with LDL, HDL and platelet derived microparticles. The enzyme catalyzes the hydrolysis of platelet activating factor (PAF) and oxidatively fragmented phospholipids at the *sn*-2 position. The crystal structure of human Lp-PLA₂ was solved to a 1.5 Å resolution revealing that the enzyme contained the classic α/β hydrolase fold, typical of lipases and neutral esterases. The catalytic triad of Lp-PLA₂ consists of Ser273, Asp296 and His351, containing the nucleophilic serine and the conserved *GXSXG* motif. A mimic of the tetrahedral intermediate of the esterolysis reaction of Lp-PLA₂ was modeled using OP compounds covalently bound at Ser273. These complexed structures can be used to provide insight into the hydrolase mechanism of Lp-PLA₂.

The role of Lp-PLA₂ in atherosclerosis remains controversial and we seek to further the understanding of the enzyme's role in disease using potent and specific inhibitors. In addition to the inhibitor developed by GlaxoSmithKline, a potent and specific carbamate inhibitor was developed through a high throughput inhibitor

screening that was carried out in collaboration with the Molecular Libraries Screening Center Network at The Scripps Research Institute Florida and the lab of Prof. Ben Cravatt from The Scripps Research Institute La Jolla. Chapter 3 describes the *in vitro* and *in situ* characterization of the carbamate inhibitors that was performed at The Scripps Research Institute, in addition to kinetic and biophysical studies performed in the lab using the recombinant source of Lp-PLA₂ described in Chapter 2.

Two site-directed mutant constructs of Lp-PLA₂ that interrupt the membrane binding regions were constructed with the aim of producing higher yields of pure protein. Kinetic analyses of the wild type and mutant Lp-PLA₂ constructs were carried out and are described in Chapter 2. In an effort to determine the binding interaction between darapladib and the carbamate inhibitor developed through high throughput screening, the recombinant enzyme sources were used for crystallization trials and are described in Chapter 4. In addition, using the crystal structure of Lp-PLA₂ as a guide, computational modeling was performed to predict the interactions of the enzyme with inhibitor as well as the physiological substrate PAF. The endogenous Lp-PLA₂ and its homologous enzyme PAFAH-II were studied in human and mouse platelets and their activities were probed using specific inhibitors as described in Chapter 5. This work aimed to further the understanding of Lp-PLA₂ and its structure-function relationship utilizing potent and specific inhibitors.

REFERENCES

1. Murphy, S. L., Xu, J. & Kochanek, K. D. Deaths: final data for 2010. *Natl. Vital Stat. Rep.* **61**, 1–117 (2013).
2. Hallenbeck, J. M., Hansson, G. K. & Becker, K. J. Immunology of ischemic vascular disease: plaque to attack. *Trends Immunol.* **26**, 550–6 (2005).
3. Stocker, R. & Keaney, J. F. Role of oxidative modifications in atherosclerosis. *Physiol. Rev.* **84**, 1381–478 (2004).
4. Witztum, J. L. & Steinberg, D. The oxidative modification hypothesis of atherosclerosis: does it hold for humans? *Trends Cardiovasc. Med.* **11**, 93–102
5. Libby, P. Inflammation in atherosclerosis. *Nature* **420**, 868–74 (2002).
6. Watson, A. D. *et al.* Structural identification of a novel pro-inflammatory epoxyisoprostane phospholipid in mildly oxidized low density lipoprotein. *J. Biol. Chem.* **274**, 24787–98 (1999).
7. Navab, M. *et al.* The oxidation hypothesis of atherogenesis: the role of oxidized phospholipids and HDL. *J. Lipid Res.* **45**, 993–1007 (2004).
8. Subbanagounder, G., Watson, A. D. & Berliner, J. A. Bioactive products of phospholipid oxidation: isolation, identification, measurement and activities. *Free Radic. Biol. Med.* **28**, 1751–61 (2000).
9. Blank, M. L., Lee, T., Fitzgerald, V. & Snyder, F. A specific acetylhydrolase for 1-alkyl-2-acetyl-sn-glycero-3-phosphocholine (a hypotensive and platelet-activating lipid). *J. Biol. Chem.* **256**, 175–8 (1981).
10. Marathe, G. K. *et al.* Bioactive phospholipid oxidation products. *Free Radic. Biol. Med.* **28**, 1762–70 (2000).
11. Farr, R. S., Cox, C. P., Wardlow, M. L. & Jorgensen, R. Preliminary studies of an acid-labile factor (ALF) in human sera that inactivates platelet-activating factor (PAF). *Clin. Immunol. Immunopathol.* **15**, 318–330 (1980).
12. Honda, Z., Ishii, S. & Shimizu, T. Platelet-activating factor receptor. *J. Biochem.* **131**, 773–9 (2002).

13. Stremler, K., Stafforini, D., Prescott, S. & McIntyre, T. Human plasma platelet-activating factor acetylhydrolase - oxidatively fragmented phospholipids as substrate. *J. Biol. Chem.* **266**, 11095–11103 (1991).
14. Min, J.-H. H. *et al.* Platelet-activating factor acetylhydrolases: Broad substrate specificity and lipoprotein binding does not modulate the catalytic properties of the plasma enzyme. *Biochemistry* **40**, 4539–4549 (2001).
15. Six, D. A. & Dennis, E. A. The expanding superfamily of phospholipase A(2) enzymes: classification and characterization. *Biochim. Biophys. Acta* **1488**, 1–19 (2000).
16. Hattori, M., Arai, H. & Inoue, K. Purification and characterization of bovine brain platelet-activating factor acetylhydrolase. *J. Biol. Chem.* **268**, 18748–53 (1993).
17. Hattori, M., Adachi, H., Tsujimoto, M., Arai, H. & Inoue, K. Miller-Dieker lissencephaly gene encodes a subunit of brain platelet-activating factor acetylhydrolase [corrected]. *Nature* **370**, 216–8 (1994).
18. Tarricone, C. *et al.* Coupling PAF signaling to dynein regulation: structure of LIS1 in complex with PAF-acetylhydrolase. *Neuron* **44**, 809–21 (2004).
19. Epstein, T. M. Structural and kinetic studies of two enzymes catalyzing phospholipase A2 activity. *Ph.D. thesis, Univ. Delaware, Newark*, (2005).
20. Stafforini, D. M., McIntyre, T. M., Carter, M. E. & Prescott, S. M. Human plasma platelet-activating factor acetylhydrolase. Association with lipoprotein particles and role in the degradation of platelet-activating factor. *J. Biol. Chem.* **262**, 4215–22 (1987).
21. Hattori, K. *et al.* Purification and characterization of platelet-activating factor acetylhydrolase II from bovine liver cytosol. *J. Biol. Chem.* **270**, 22308–13 (1995).
22. Thevenin, a F., Monillas, E. S., Winget, J. M., Czymbek, K. & Bahnson, B. J. Trafficking of platelet-activating factor acetylhydrolase type II in response to oxidative stress. *Biochemistry* **50**, 8417–8426 (2011).
23. Monillas, E. S., Caplan, J. L., Thévenin, A. F. & Bahnson, B. J. Oligomeric state regulated trafficking of human platelet-activating factor acetylhydrolase type-II. *Biochim. Biophys. Acta* **1854**, 469–75 (2015).
24. Stafforini, D. M., McIntyre, T. M., Zimmerman, G. A. & Prescott, S. M. Platelet-activating factor acetylhydrolases. *J. Biol. Chem.* **272**, 17895–8 (1997).

25. Elstad, M. R., Stafforini, D. M., McIntyre, T. M., Prescott, S. M. & Zimmerman, G. A. Platelet-activating factor acetylhydrolase increases during macrophage differentiation. A novel mechanism that regulates accumulation of platelet-activating factor. *J. Biol. Chem.* **264**, 8467–70 (1989).
26. Tjoelker, L. W. *et al.* Plasma platelet-activating factor acetylhydrolase is a secreted phospholipase A2 with a catalytic triad. *J. Biol. Chem.* **270**, 25481–7 (1995).
27. Samanta, U. & Bahnson, B. J. Crystal structure of human plasma platelet-activating factor acetylhydrolase: structural implication to lipoprotein binding and catalysis. *J. Biol. Chem.* **283**, 31617–24 (2008).
28. Tjoelker, L. W. *et al.* Anti-inflammatory properties of a platelet-activating factor acetylhydrolase. *Nature* **374**, 549–53 (1995).
29. Krissinel, E. & Henrick, K. Inference of macromolecular assemblies from crystalline state. *J. Mol. Biol.* **372**, 774–97 (2007).
30. Gardner, A. a., Reichert, E. C., Topham, M. K. & Stafforini, D. M. Identification of a domain that mediates association of platelet-activating factor acetylhydrolase with high density lipoprotein. *J. Biol. Chem.* **283**, 17099–17106 (2008).
31. Min, J. H. *et al.* Platelet-activating factor acetylhydrolases: broad substrate specificity and lipoprotein binding does not modulate the catalytic properties of the plasma enzyme. *Biochemistry* **40**, 4539–49 (2001).
32. Min, J.-H. *et al.* Membrane-Bound Plasma Platelet Activating Factor Acetylhydrolase Acts on Substrate in the Aqueous Phase. *Biochemistry* **38**, 12935–12942 (1999).
33. Gelb, M. H., Min, J.-H. & Jain, M. K. Do membrane-bound enzymes access their substrates from the membrane or aqueous phase: interfacial versus non-interfacial enzymes. *Biochim. Biophys. Acta - Mol. Cell Biol. Lipids* **1488**, 20–27 (2000).
34. Abuzeid, A. M., Hawe, E., Humphries, S. E. & Talmud, P. J. Association between the Ala379Val variant of the lipoprotein associated phospholipase A2 and risk of myocardial infarction in the north and south of Europe. *Atherosclerosis* **168**, 283–288 (2003).
35. Ninio, E. *et al.* Platelet-activating factor-acetylhydrolase and PAF-receptor gene haplotypes in relation to future cardiovascular event in patients with coronary artery disease. *Hum. Mol. Genet.* **13**, 1341–51 (2004).

36. Kruse, S. *et al.* The Ile198Thr and Ala379Val variants of plasmatic PAF-acetylhydrolase impair catalytical activities and are associated with atopy and asthma. *Am. J. Hum. Genet.* **66**, 1522–30 (2000).
37. Samanta, U., Bahadur, R. P. & Chakrabarti, P. Quantifying the accessible surface area of protein residues in their local environment. *Protein Eng. Des. Sel.* **15**, 659–667 (2002).
38. Stafforini, D. M., Prescott, S. M. & McIntyre, T. M. Human plasma platelet-activating factor acetylhydrolase. Purification and properties. *J. Biol. Chem.* **262**, 4223–30 (1987).
39. Lomize, M. A., Lomize, A. L., Pogozheva, I. D. & Mosberg, H. I. OPM: orientations of proteins in membranes database. *Bioinformatics* **22**, 623–5 (2006).
40. Lomize, A. L., Pogozheva, I. D., Lomize, M. A. & Mosberg, H. I. The role of hydrophobic interactions in positioning of peripheral proteins in membranes. *BMC Struct. Biol.* **7**, 44 (2007).
41. Pande, A. H., Qin, S. & Tatulian, S. A. Membrane fluidity is a key modulator of membrane binding, insertion, and activity of 5-lipoxygenase. *Biophys. J.* **88**, 4084–94 (2005).
42. Lobo, L. I. & Wilton, D. C. Effect of lipid composition on lipoprotein lipase activity measured by a continuous fluorescence assay: effect of cholesterol supports an interfacial surface penetration model. *Biochem. J.* **321** (Pt 3, 829–35 (1997).
43. Pandit, S. A., Chiu, S.-W., Jakobsson, E., Grama, A. & Scott, H. L. Cholesterol packing around lipids with saturated and unsaturated chains: a simulation study. *Langmuir* **24**, 6858–65 (2008).
44. Pande, A. H. & Tillu, V. A. Membrane lipid composition differentially modulates the function of human plasma platelet activating factor-acetylhydrolase. *Biochim. Biophys. Acta* **1811**, 46–56 (2011).
45. Kar, S., Bajaj, P., Tripathy, R. K. & Pande, A. H. The chemical nature of the polar functional group of oxidized acyl chain uniquely modifies the physicochemical properties of oxidized phospholipid-containing lipid particles. *J. Membr. Biol.* **246**, 443–52 (2013).
46. Karabina, S. A., Liapikos, T. A., Grekas, G., Goudevenos, J. & Tselepis, A. D. Distribution of PAF-acetylhydrolase activity in human plasma low-density lipoprotein subfractions. *Biochim. Biophys. Acta* **1213**, 34–8 (1994).

47. Stafforini, D. M. *et al.* Molecular Basis of the Interaction between Plasma Platelet-activating Factor Acetylhydrolase and Low Density Lipoprotein. *J. Biol. Chem.* **274**, 7018–7024 (1999).
48. Cao, J., Hsu, Y.-H., Li, S., Woods, V. L. & Dennis, E. A. Lipoprotein-associated phospholipase A(2) interacts with phospholipid vesicles via a surface-disposed hydrophobic α -helix. *Biochemistry* **50**, 5314–21 (2011).
49. Srinivasan, P. & Bahnson, B. J. Molecular Model of Plasma PAF Acetylhydrolase-Lipoprotein Association: Insights from the Structure. *Pharmaceuticals* **3**, 541–557 (2010).
50. Camejo, G., Olofsson, S. O., Lopez, F., Carlsson, P. & Bondjers, G. Identification of Apo B-100 segments mediating the interaction of low density lipoproteins with arterial proteoglycans. *Arteriosclerosis* **8**, 368–77
51. Cao, J., Hsu, Y.-H., Li, S., Woods, V. L. & Dennis, E. A. Structural basis of specific interactions of Lp-PLA₂ with HDL revealed by hydrogen deuterium exchange mass spectrometry. *J. Lipid Res.* **54**, 127–33 (2013).
52. Srinivasan, P. Characterization of the association of human plasma platelet-activating factor acetyl hydrolase with lipoproteins. *University of Delaware ProQuest Dissertations & Theses A&I* (2010).
53. Tellis, C. C. & Tselepis, A. D. The role of lipoprotein-associated phospholipase A2 in atherosclerosis may depend on its lipoprotein carrier in plasma. *Biochim. Biophys. Acta* **1791**, 327–38 (2009).
54. Mitsios, J. V, Vini, M. P., Stengel, D., Ninio, E. & Tselepis, A. D. Human platelets secrete the plasma type of platelet-activating factor acetylhydrolase primarily associated with microparticles. *Arterioscler. Thromb. Vasc. Biol.* **26**, 1907–13 (2006).
55. Coppinger, J. A. & Maguire, P. B. Insights into the platelet releasate. *Curr. Pharm. Des.* **13**, 2640–6 (2007).
56. Tsaoussis, V. & Vakirtzi-Lemonias, C. The mouse plasma PAF acetylhydrolase: II. It consists of two enzymes both associated with the HDL. *J. Lipid Mediat. Cell Signal.* **9**, 317–31 (1994).
57. Theilmeier, G. *et al.* HDL-associated PAF-AH reduces endothelial adhesiveness in apoE^{-/-} mice. *FASEB J.* **14**, 2032–9 (2000).

58. Quarck, R. *et al.* Adenovirus-mediated gene transfer of human platelet-activating factor-acetylhydrolase prevents injury-induced neointima formation and reduces spontaneous atherosclerosis in apolipoprotein E-deficient mice. *Circulation* **103**, 2495–500 (2001).
59. Erqou, S. *et al.* Lipoprotein(a) concentration and the risk of coronary heart disease, stroke, and nonvascular mortality. *JAMA* **302**, 412–23 (2009).
60. Tsimikas, S. & Witztum, J. L. The role of oxidized phospholipids in mediating lipoprotein(a) atherogenicity. *Curr. Opin. Lipidol.* **19**, 369–77 (2008).
61. Sánchez-Quesada, J. L., Benítez, S. & Ordóñez-Llanos, J. Electronegative low-density lipoprotein. *Curr. Opin. Lipidol.* **15**, 329–35 (2004).
62. Blencowe, C., Hermetter, A., Kostner, G. M. & Deigner, H. P. Enhanced association of platelet-activating factor acetylhydrolase with lipoprotein (a) in comparison with low density lipoprotein. *J. Biol. Chem.* **270**, 31151–7 (1995).
63. Watson, A. D. *et al.* Effect of platelet activating factor-acetylhydrolase on the formation and action of minimally oxidized low density lipoprotein. *J. Clin. Invest.* **95**, 774–82 (1995).
64. Tjoelker, L. W. & Stafforini, D. M. Platelet-activating factor acetylhydrolases in health and disease. *Biochim. Biophys. Acta* **1488**, 102–23 (2000).
65. McIntyre, T. M., Prescott, S. M. & Stafforini, D. M. The emerging roles of PAF acetylhydrolase. *J. Lipid Res.* **50 Suppl**, S255–9 (2009).
66. Wilensky, R. L. & Macphee, C. H. Lipoprotein-associated phospholipase A(2) and atherosclerosis. *Curr. Opin. Lipidol.* **20**, 415–20 (2009).
67. Zalewski, A. & Macphee, C. Role of lipoprotein-associated phospholipase A2 in atherosclerosis: biology, epidemiology, and possible therapeutic target. *Arterioscler. Thromb. Vasc. Biol.* **25**, 923–31 (2005).
68. Kolodgie, F. D. *et al.* Lipoprotein-associated phospholipase A2 protein expression in the natural progression of human coronary atherosclerosis. *Arterioscler. Thromb. Vasc. Biol.* **26**, 2523–9 (2006).
69. Tselepis, A. F., Rizzo, M. & Goudevenos, I. A. Therapeutic modulation of lipoprotein-associated phospholipase A2 (Lp-PLA₂). *Curr. Pharm. Des.* **17**, 3656–61 (2011).

70. Sudhir, K. Clinical review: Lipoprotein-associated phospholipase A2, a novel inflammatory biomarker and independent risk predictor for cardiovascular disease. *J. Clin. Endocrinol. Metab.* **90**, 3100–5 (2005).
71. Anderson, J. L. Lipoprotein-associated phospholipase A2: an independent predictor of coronary artery disease events in primary and secondary prevention. *Am. J. Cardiol.* **101**, 23F–33F (2008).
72. Koenig, W. & Khuseyinova, N. Lipoprotein-Associated and Secretory Phospholipase A2 in Cardiovascular Disease: The Epidemiological Evidence. *Cardiovasc. Drugs Ther.* **23**, 85–92 (2008).
73. Carlquist, J. F., Muhlestein, J. B. & Anderson, J. L. Lipoprotein-associated phospholipase A2: a new biomarker for cardiovascular risk assessment and potential therapeutic target. *Expert Rev. Mol. Diagn.* **7**, 511–7 (2007).
74. Corson, M. A., Jones, P. H. & Davidson, M. H. Review of the evidence for the clinical utility of lipoprotein-associated phospholipase A2 as a cardiovascular risk marker. *Am. J. Cardiol.* **101**, 41F–50F (2008).
75. Boyd, H. F. *et al.* Potent, orally active inhibitors of lipoprotein-associated phospholipase A(2): 1-(biphenylmethylamidoalkyl)-pyrimidones. *Bioorg. Med. Chem. Lett.* **12**, 51–5 (2002).
76. O'Donoghue, M. L. *et al.* Effect of darapladib on major coronary events after an acute coronary syndrome: the SOLID-TIMI 52 randomized clinical trial. *JAMA* **312**, 1006–15 (2014).
77. White, H. D. *et al.* Darapladib for preventing ischemic events in stable coronary heart disease. *N. Engl. J. Med.* **370**, 1702–11 (2014).
78. Casida, J. E. & Quistad, G. B. Organophosphate toxicology: safety aspects of nonacetylcholinesterase secondary targets. *Chem. Res. Toxicol.* **17**, 983–98 (2004).
79. Harris, L. W., Fleisher, J. H., Clark, J. & Cliff, W. J. Dealkylation and loss of capacity for reactivation of cholinesterase inhibited by sarin. *Science* **154**, 404–7 (1966).
80. Broomfield, C. A., Lockridge, O. & Millard, C. B. Protein engineering of a human enzyme that hydrolyzes V and G nerve agents: design, construction and characterization. *Chem. Biol. Interact.* **119-120**, 413–418 (1999).

81. Samanta, U., Kirby, S. D., Srinivasan, P., Cerasoli, D. M. & Bahnson, B. J. Crystal structures of human group-VIIA phospholipase A2 inhibited by organophosphorus nerve agents exhibit non-aged complexes. *Biochem. Pharmacol.* **78**, 420–9 (2009).
82. Amitai, G. *et al.* Enhanced stereoselective hydrolysis of toxic organophosphates by directly evolved variants of mammalian serum paraoxonase. *FEBS J.* **273**, 1906–19 (2006).
83. Millard, C. B., Lockridge, O. & Broomfield, C. A. Organophosphorus acid anhydride hydrolase activity in human butyrylcholinesterase: synergy results in a somanase. *Biochemistry* **37**, 237–47 (1998).

Chapter 2

EXPRESSION AND PURIFICATION OF LP-PLA₂

2.1 Introduction

The enzyme Lp-PLA₂ was first discovered due to its ability to catalyze the hydrolysis of platelet-activating factor (PAF) and is therefore also referred to as PAF acetylhydrolase. Lp-PLA₂ is a glycosylated enzyme which is secreted by macrophages in the plasma as they differentiate into monocytes [1]. The enzyme was initially isolated from human plasma using various detergents to aid in solubilization and further purified using affinity chromatography and ion exchange chromatography. The endogenous enzyme isolated from lipoprotein molecules was reported to have an activity of 170 $\mu\text{mol min}^{-1} \text{mg}^{-1}$ and a K_M of 12 μM for the radiolabeled substrate [³H]PAF [2,3].

Lp-PLA₂ is encoded by the *PLA2G7* gene and is comprised of 12 exons found on chromosome 6p12-21.1 [4]. In 1995, the Lp-PLA₂ cDNA was cloned by Tjoelker et. al from the mRNA of monocyte derived macrophages, thus making recombinant expression and purification possible for the first time. The enzyme is 441 amino acids in length where the first 18 residues represent a signal sequence and residues 18-42 are cleaved as a post translational modification, thus making the active Lp-PLA₂ residues 42-441 with a predicted molecular weight of 45 kDa [5]. The enzyme is very hydrophobic and therefore requires the use of detergent to maintain solubility.

The purification and expression of recombinant Lp-PLA₂ residues 42-441 from an *E. coli* source was developed in our laboratory. The enzyme was further truncated

to residues 49-423 in order resemble the amino acid sequence of the structure of Lp-PLA₂ which was solved previously in our laboratory [6,7]. This construct is expressed as a GST fusion protein, and modified to contain either a thrombin, TEV or PreScission Protease recognition site in order to optimize the cleavage of the fusion tag. Mutants of Lp-PLA₂ were generated by site-directed mutagenesis with the aim of reducing the enzyme's hydrophobicity to disrupt the association of Lp-PLA₂ with membranes. Finally, kinetic analyses of recombinant Lp-PLA₂ and its mutants were performed using a general substrate for serine hydrolase enzymes.

2.2 Materials and Methods

2.2.1 Materials

The pGEX-4T-3 vector was from GE Healthcare, the pMHTΔ238 plasmid expressing TEV protease was purchased from the Protein Structure Initiative-Material Repository, and the pGEX-6P-1 vector was a gift from the lab of Dr. Catherine Grimes. The cDNA of human Lp-PLA₂ (also known as plasma PAF-AH) was from Invitrogen. *Sall*, *BamHI*, *NotI*, *rSAP* and T4 DNA ligase were purchased from New England Biolabs and dithiothreitol (DTT) was from Acros Organics. The PCR primers, ampicillin, ATP, MgCl₂, 3-[3-(Cholamidopropyl) dimethylammonio] propanesulfonic acid (CHAPS), Octyl β-D-glucopyranoside (OGP), reduced glutathione, 4-nitro phenylacetate (PNPA), Triton DF-16, Triton X-100 and lysozyme were from Sigma-Aldrich. Isopropyl β-D-1-thiogalactopyranoside (IPTG) was from Goldbio.com. Luria-Bertani media (LB), LB Agar, agarose, TrisBase, NaCl, pepstatin, and ethylenediaminetetraacetic acid (EDTA) were purchased from Fisher Scientific.

2.2.2 Subcloning

The construct of human Lp-PLA₂ cDNA spanning amino acids 49-423 in a pGEX-4T-3 vector was obtained from a previous lab member, Dr. Prabha Srinivasan [7,8]. The desired construct, containing Lp-PLA₂ residues 49-423, was PCR amplified using the forward primer 5' – AAAAAAGGATCCTCCTTTGGCCAAACT – 3' (*Bam*HI site underlined) and the reverse primer 5' – AAAAAACAGCTGGTTAATGTTGGTCCCT – 3' (*Sal*I site underlined).

Approximately 1 µg of vector pGEX-6P-1 as well as 1 µg of amplified insert were digested with 20 units of *Bam*HI and 20 units of *Sal*I in the presence of bovine serum albumen (BSA) for 2 h at 37 °C. One hour into the pGEX-6P-1 vector digestion, 1 unit of *rSAP* was added in order to prevent vector recircularization. The Lp-PLA₂ insert was then ligated into the pGEX-6P-1 vector at a molar ratio of 8:1 insert to vector. The successful ligation of Lp-PLA₂ into pGEX-6P-1 was confirmed via DNA sequencing performed by GENEWIZ and a glycerol stock of the construct in DH5α cells was made and stored at -80 °C.

2.2.3 Mutations of Lp-PLA₂

2.2.3.1 Insertion of TEV recognition site

Prior to the cloning Lp-PLA₂ (49-423) into pGEX-6P-1, an insertion was made to the Lp-PLA₂-pGEX-4T-3 construct in order to introduce a TEV cleavage site. This was done due to the possibility of thrombin contamination and non-specific proteolysis sensitivity using the present Lp-PLA₂-pGEX-4T-3 construct and will be discussed further in the results section. In order to insert the TEV protease recognition site (ENLYFQG) a series of primers were designed to disrupt the current thrombin cleavage site and exploit the glycine residue that remains fused to the Lp-PLA₂ after

TEV cleavage (Figure 2.1). The overall strategy to insert the TEV site utilized a stepwise PCR addition of nucleotides to the N-terminal end of Lp-PLA₂ with primers containing restriction enzymes for PCR amplification, digestion and ligation into empty pGEX-4T-3. The first step of TEV recognition site addition used the forward primer 5' – TTTTTTGTCGACGTATTTTCAGGGCTCCTTTGGC – 3' (*Sall* site underlined, TEV insert bold) and reverse primer aligning with the C-terminus of Lp-PLA₂ (49-423) 5' – TTTTTTGCGGCCCGCCTAGTTAATGTTGG – 3' (*NotI* underlined, stop codon bold). Both insert and pGEX-4T-3 were digested with the restriction enzymes *Sall* and *NotI* and then ligated at a molar ratio of 8:1 insert to vector. The addition of the four amino acids included in the TEV recognition site were confirmed by DNA sequencing. The second step of the TEV recognition site addition used the forward primer 5' – AAAAAAAGGATCCGAAAACCTCTATTTTCAGGGC – 3' (*BamHI* site underlined, remaining TEV insert bold) and the same reverse primer that was used in the first step. Again, the insert and vector were digested with restriction enzymes (*BamHI* and *NotI*) and then ligated at a molar ration of 8:1 insert to vector. After successful transformation into DH5 α cells, the DNA was sequenced and the addition of the complete TEV recognition site was confirmed.

2.2.3.2 Lipoprotein binding mutations

Two different constructs were made using the Lp-PLA₂ (49-423) in pGEX-6P-1 as a template with the aim of disrupting the lipoprotein binding site. The first was a point mutation at residue 205 from the native tyrosine to alanine. This was done with the forward primer 5' – GTCTTGGCTCGCGCTTAGAACCC – 3' and the reverse

Vector	Disrupted Thrombin Cleavage	TEV Cleavage Recognition Site	Lp-PLA ₂
Pro Lys Ser Asp	Leu Val Pro Arg	Ser Gly Glu Asn Leu Tyr Phe Gln	Gly Ser Phe Gly Gln
CCC AAA TCG GAT	CTG GTT CCG CGT GGA TCC	GAA AAC CTC TAT TTT CAG	GGC TCC TTT GGC CAA

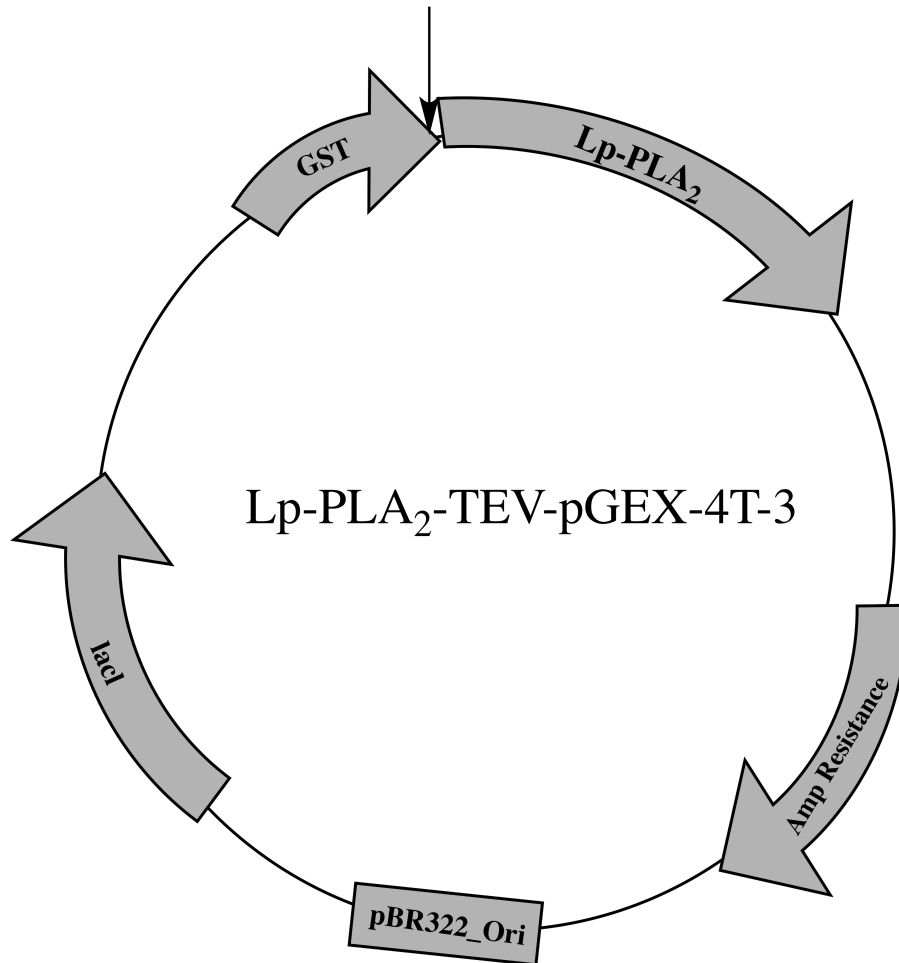


Figure 2.1: TEV cleavage site in pGEX-4T-3. Vector map of pGEX-4T-3 depicting the insert of the TEV cleavage site. The insertion was incorporated through a series of PCR amplifications, restriction enzyme digestions and ligations into pGEX-4T-3. In the process the thrombin cleavage site was disrupted and the GST-Lp-PLA₂ fusion protein can only be cleaved using TEV protease.

primer 5' – GGGTTCTAAGCGCGAGCCAAGAC – 3'. The other construct made was the triple mutant, I120A/L123A/L124A in the hydrophobic patch of Lp-PLA₂. This was created with the forward primer 5' – CTTATGGGCAACGCGTTGAGGGCGGCGTTTGGTTCAATG – 3' and the reverse primer 5' – CATTGAACCAAACGCCGCCCTCAACGCGTTGCCATAAG – 3'. All constructs were transformed into DH5 α cells and were sequenced to confirm the presence of the desired mutations and ensure that no undesired DNA mutations were made in the process. Glycerol stocks were made of both lipoprotein binding mutants and stored at -80 °C.

2.2.4 Expression of recombinant Lp-PLA₂ in *E. coli*

The expression of Lp-PLA₂ was carried out using pGEX vectors containing either a thrombin or TEV cleavage site and with all mutants described above. The Lp-PLA₂ expression construct was transformed into *E. coli* BL21 cells and plated on LB agar plates with 100 μ g/mL ampicillin and grown overnight at 37 °C. A single colony was grown in 5 mL of LB with 100 μ g/mL ampicillin at 37 °C overnight and the following morning was made into a glycerol stock to be stored at -80 °C for starter cultures. For expression, a starter culture was made using a scrape of the glycerol stock, was grown overnight in 200 mL of LB with 100 μ g/mL ampicillin at 30 °C. In the morning 20 mL of the overnight growth was inoculated into 1 L of fresh LB containing 100 μ g/mL ampicillin and grown shaking at 30 °C until it reached an OD₆₀₀ ~ 0.8. The culture was then induced with 0.5 mM IPTG and expressed shaking overnight at 18 °C. The cells were harvested by centrifugation at 8,000 rpm (Sorvall SLA-3000) for 10 min at 4 °C and pellets were stored at -80 °C until purification.

2.2.5 Purification of recombinant Lp-PLA₂

The purification of Lp-PLA₂ was developed based upon the work of previous lab member, Dr. Prabha Srinivasan. The cell pellet was thawed at room temperature for 30 min (average 0.10 g wet weight of cells per 1 mL buffer) and suspended in 50 mM Tris base buffer, pH 7.8, containing 100 mM NaCl, 5 mM DTT, 1 μM pepstatin, and 0.1 mg/mL lysozyme. The suspended cells were then lysed by sonication twice for 2 min each with 5 min rest in between. The lysed cells were incubated with detergent, 0.2% Triton X-100, and rocked at 4 °C for 30 min to solubilize the Lp-PLA₂ fusion and dislodge it from the cell membrane. The suspension was then clarified by centrifugation at 13,000 rpm (Sorvall SS-34) for 20 min at 4 °C. Afterwards, the supernatant was incubated with 10 mM ATP and 20 mM MgCl₂ for 20 min at RT to prevent chaperone proteins from co-purifying and then clarified by centrifugation at 13,000 rpm a second time for 20 min at 4 °C. The supernatant was applied to Glutathione Sepharose resin (GE Life Sciences) on a column equilibrated with 50 mM Tris base buffer, pH 7.8, containing 100 mM NaCl, 1 mM DTT, 5 mM ATP, 20 mM MgCl₂ and 0.2% Triton X-100 and incubated rocking at 4 °C for 1 h to ensure fusion protein binding to the resin. After the incubation, the column was washed with 10 column volumes of the equilibration buffer to remove nonspecifically bound proteins.

Using the construct in the pGEX-4T-3 vector, which has either a thrombin or TEV protease recognition site, the GST-Lp-PLA₂ fusion protein was eluted off the resin with 30 mL of 50 mM Tris base, pH 8.0, containing 100 mM NaCl, 25 mM reduced glutathione, 1 mM EDTA, 1 mM DTT and 0.2% Triton X-100. The eluted protein was pooled and concentrated using Amicon Ultra centrifugal filter units (30 kDa molecular weight cut-off, Millipore) at 2,000 rpm to a final volume of 3 mL. For the pGEX-4T-3 constructs, either thrombin or TEV protease was added to cleave the

fusion protein and the sample was dialyzed overnight against 50 mM Tris base, pH 7.8, containing 1 mM EDTA.

Using the Lp-PLA₂ in pGEX-6P-1 vector, which has a PreScission Protease recognition site, the GST-Lp-PLA₂ fusion protein bound to the glutathione resin was washed with 6 column volumes of 50 mM Tris HCl, pH 7.5, containing 150 mM NaCl, 1 mM EDTA, 1 mM DTT and 0.2% Triton X-100. PreScission Protease (HRV 3C with a GST Fusion tag, GE Life Sciences) was added to the column and rocked at 4 °C overnight for on column cleavage. The next day the cleaved Lp-PLA₂ was drained from the column and then dialyzed against 50 mM Tris base, pH 7.8, containing 1 mM EDTA. The PreScission Protease and remaining free GST was eluted from the column and discarded.

Further purification of all constructs was done using an FPLC (BioRad) with an anion exchange column. After overnight dialysis the cleaved enzyme, Lp-PLA₂ was loaded onto the FPLC and bound to a Q-Sepharose resin (GE Life Sciences) equilibrated with the no salt buffer of 50 mM Tris base, pH 7.8, containing 1 mM EDTA, 1 mM DTT and 0.2% Triton X-100. The resin was washed with 20 mL at a 1.5 mL/min flow rate of no salt buffer to remove any nonspecific binding. A gradient was then introduced with high salt buffer of 50 mM Tris base, pH 7.8, containing 750 mM NaCl, 1 mM EDTA, 1 mM DTT and 0.2% Triton X-100, ranging from 0% - 100% high salt buffer over 75 mL at a 1 mL/min flow rate. Finally the Q-Sepharose column is washed with the high salt buffer over 20 mL at a flow rate of 1.5 mL/min to remove all remaining bound proteins. Fractions from the gradient were collected and the pure Lp-PLA₂ began to elute between 300 and 350 mM NaCl. These fractions were pooled and dialyzed against 10 mM Tris base, pH 7.8, containing, 0.01%

CHAPS, at 4 °C overnight. The following day the dialyzed protein was concentrated using Amicon Ultra centrifugal filter units, characterized and stored at -80 °C.

2.2.6 PNPA Assay

Lp-PLA₂ was assayed using p-nitrophenol acetate (PNPA) as a general substrate to assess serine hydrolase activity (Figure 2.2). The assay was performed in a 1 mL reaction volume of 50 mM Tris base, pH 7.5, containing 5 mM of PNPA. The reaction was initiated with the addition of 1 μL of Lp-PLA₂ in concentrations ranging from 1-4 μg of the enzyme. The rate of formation of p-nitrophenoxide ion (PNP) was measured over 1 min at 405 nm and the activity of Lp-PLA₂ was determined.

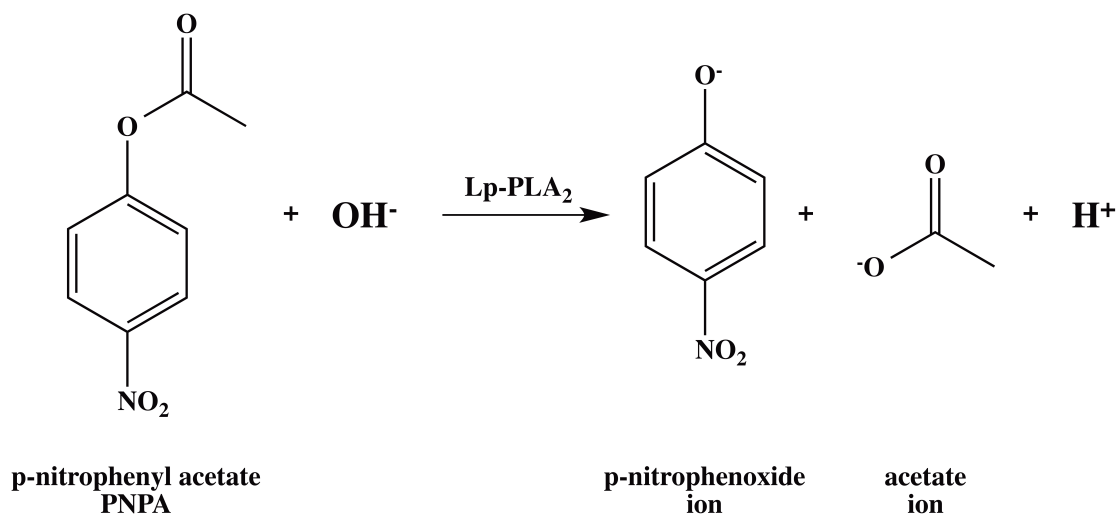


Figure 2.2: PNPA Assay. Lp-PLA₂ cleaves the acetyl group from PNPA and the rate of formation of p-nitrophenoxide ion is measured at 405 nm to determine enzyme activity.

2.3 Results and Discussion

2.3.1 Lp-PLA₂ constructs

The Lp-PLA₂ (49-423) construct was developed to resemble the sequence of protein samples of Lp-PLA₂ obtained from the ICOS Corporation, as it was this truncated version whose crystal structure was solved in our lab. This construct has a molecular weight of 43 kDa and lacks the Western blotting antibody recognition site as those C-terminal residues were truncated from this expression construct. Due to Lp-PLA₂ association with membranes, a vector expressing a large fusion tag like GST aids in the solubilization of the enzyme. The initial construct of Lp-PLA₂ in pGEX-4T-3 was not ideal and the change to a TEV protease site showed improvements to the quality of the protein preparations. Also, several hydrophobic patch mutants were made in order to increase the solubility and optimize the expression and purification of Lp-PLA₂. There were also two constructs made to disrupt the lipoprotein binding and aid in overall quantity of purified enzyme.

2.3.1.1 Lp-PLA₂ in pGEX-4T-3

The Lp-PLA₂ construct in p-GEX-4T-3 created by Dr. Srinivasan was expressed, purified and characterized using the methods previously described. The enzyme was expressed with a GST fusion tag and contained a thrombin cleavage site. The protein concentration was estimated using a BCA (bicinchoninic acid) assay and the construct was found to yield 1.25 mg of Lp-PLA₂ per 1 L bacterial culture. Lp-PLA₂ was able to be concentrated down to 4.5 mg/mL and had an average purity of 94% as determined by the ImageJ software. As seen on the SDS PAGE gel (Figure 2.3), there is a strong band at 43 kDa, representing Lp-PLA₂ as well as a band at 25 kDa for GST. There was a consistent impurity around 35 kDa which was not

identified, but thought to be thrombin which has a molecular weight of 37 kDa. Thrombin contamination is very detrimental to the enzyme sample as it will continue to proteolyze Lp-PLA₂. This will affect the stability of the enzyme, alter its activity, and preclude protein crystallization due to the heterogeneity introduced to the sample. For this reason, it was decided to use a different enzyme to cleave the GST-Lp-PLA₂ fusion protein, and the first alternate protease site substituted was TEV protease.

TEV protease is a 27 kDa catalytic domain of the enzyme Nuclear Inclusion A from Tobacco Etch Virus, which is commonly used for the cleavage of fusion proteins. A TEV protease recognition site was cloned into pGEX-4T-3 as described previously, disrupting the native thrombin cleavage site. This construct was able to express GST-Lp-PLA₂ fusion protein and purification of this construct was carried out successfully. The commercially available TEV protease (AcTEV, Life Technologies) successfully cleaved the GST fusion tag from Lp-PLA₂ and the enzyme was further characterized with PNPA assay and determined to be active (Figure 2.3).

A pMHTΔ238 plasmid expressing TEV protease fused to the cytoplasmic maltose binding protein (MBP) was purchased from the Protein Structure Initiative-Material Repository in order to produce our own source of TEV, due to the high costs of the commercially available enzyme [9]. Expression and purification of this construct were carried out according to the previously published protocol; however, the attempts were unsuccessful at producing high quantities of purified active TEV protease (Figure 2.3). For this reason, it was decided to once again find an alternative protease to cleave the fusion protein, and PreScission Protease was chosen.

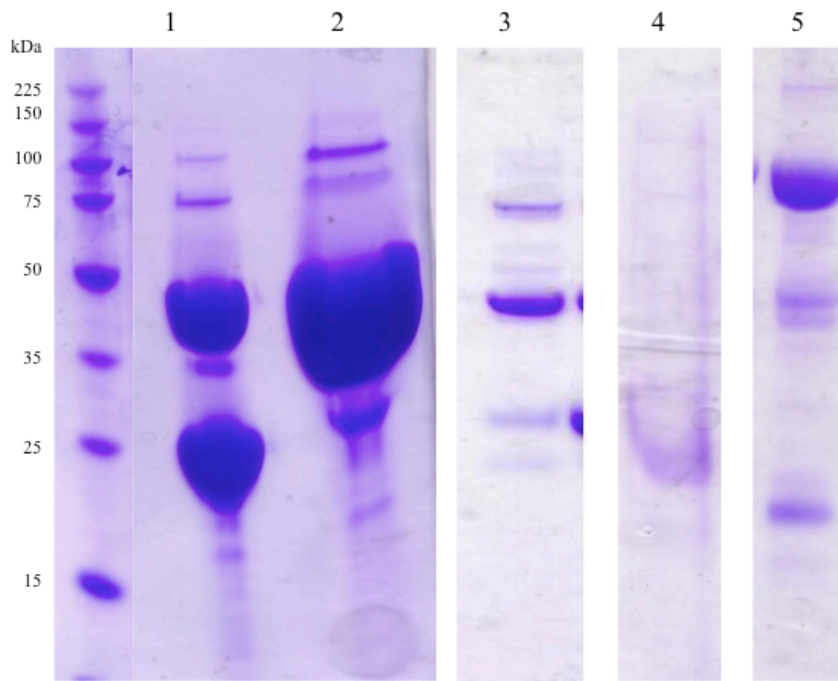


Figure 2.3: Lp-PLA₂ in pGEX-4T-3. SDS PAGE gels representing purifications of Lp-PLA₂ in the various pGEX-4T-3 constructs. Molecular Weights: GST-Lp-PLA₂ fusion: 70 kDa, Lp-PLA₂: 43 kDa, GST: 25 kDa, thrombin: 37 kDa, TEV protease: 25 kDa. Lanes: 1. Post thrombin cleavage of GST-Lp-PLA₂*; 2. Purified Lp-PLA₂ using thrombin*; 3. Purified Lp-PLA₂ using AcTEV commercial TEV protease; 4. Purified TEV protease from pMHTDelta238 plasmid; 5. Post pMHTDelta238 plasmid TEV protease cleavage of GST-Lp-PLA₂. * denotes very overloaded sample thus skewing molecular weight marker approximations

2.3.1.2 Lp-PLA₂ in pGEX-6P-1

The cloning of Lp-PLA₂ into pGEX-6P-1 expression vector containing the PreScission Protease cleavage site required the use of recombinant Shrimp Alkaline Phosphatase (*rSAP*, NEB) to prevent vector recircularization. *rSAP* dephosphorylates at the 5' and 3' ends of DNA, RNA and dNTPs and is commonly used in blunt end ligations. Although the restriction enzymes used (*BamHI* and *Sall*) do not give blunt ends, the absence of *rSAP* always resulted in the ligation of pGEX-6P-1 without the Lp-PLA₂ gene inserted. All results regarding recombinant Lp-PLA₂ and its mutants discussed from this point on will refer to Lp-PLA₂ in the pGEX-6P-1 expression vector unless otherwise stated.

2.3.1.3 Lipoprotein binding mutants

The two Lp-PLA₂ mutations, Y205A and I120A/L123A/L124A were created with the aim at disrupting the lipoprotein associations of Lp-PLA₂. Although there was no interaction of recombinant Lp-PLA₂ from *E. coli* with lipoproteins it was hypothesized that the mutations would disrupt membrane binding in general, thus resulting in higher yields of Lp-PLA₂ per 1 L of expression media.

As shown in the OPM model of Lp-PLA₂, there is an interaction with the enzyme and membrane at two helices, referred to as the interface binding region (i-face). The residues 363-369 have been reported critical for association with HDL and residues on helix 114-125 have been reported critical for LDL association [10,11]. The mutation of I120A/L123A/L124A will disrupt the hydrophobic patch of the i-face and will reduce Lp-PLA₂ membrane binding capabilities (Figure 2.4).

The mutation at Y205A exploits an indirect association with lipoprotein binding. As seen in the OPM model, Y205 is at the C-terminal end of a beta hairpin

and the residue sits well above the membrane plane, demonstrating that it does not directly interact with membrane binding. However, Y205 has a cation- π interaction with residue K109 on the helix containing residues 101-111 and also has an interaction with the i-face helix 114-125 (Figure 2.4). The conformational change to the enzyme induced by a mutation at Y205 has a downstream effect on the helix critical for lipoprotein association and thus disrupts Lp-PLA₂ membrane association.

2.3.2 Expression of recombinant Lp-PLA₂

The expression of Lp-PLA₂ was carried out in *E. coli* BL21 cells as the gene was optimized to remove any rare codons unable to be recognized in an *E. coli* system. The enzyme is hydrophobic due to its membrane interactions, thus a GST tag was used to aid in solubility. Although the tag does help pull the enzyme from the membranous portion, it alone cannot fully solubilize Lp-PLA₂. Several conditions were varied during the expression trials including growing temperature, IPTG concentration, expression temperature as well as expression time. It was determined that Lp-PLA₂-pGEX-6P-1 has optimal expression when grown at 30 °C, differing from the growth at 37 °C which had been used for the pGEX-4T-3 constructs. Growth of Lp-PLA₂-pGEX-6P-1 at the higher temperature resulted in the formation of inclusion bodies and almost all protein was lost during purification attempts. It was also found that Lp-PLA₂-pGEX-6P-1 has an optimal expression temperature of 18 °C, unlike the pGEX-4T-3 constructs which were expressed at room temperature. This lower temperature slowed the protein expression and resulted in higher amounts of functional and soluble enzyme.

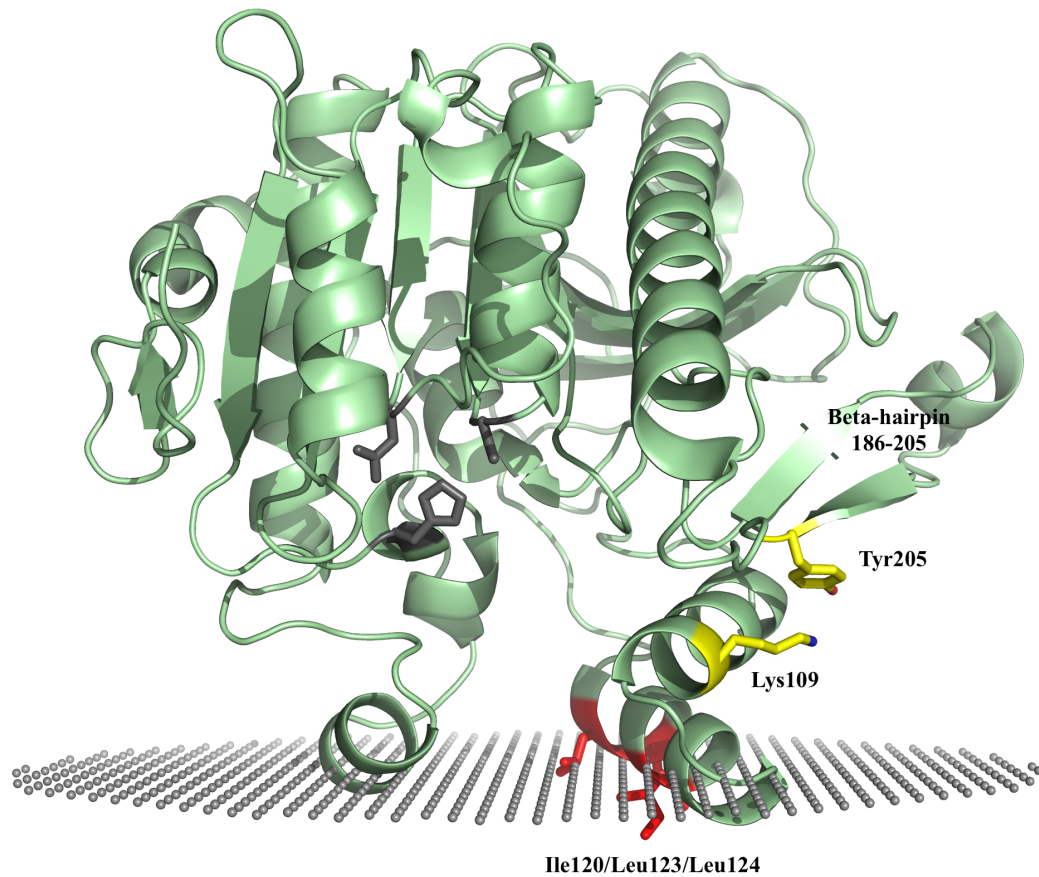


Figure 2.4. Lipoprotein binding mutants. OPM model of Lp-PLA₂ and its association with membranes. Highlighted in red on helix 114-125 are residues I120, L123, and L124, all prominently interfacing with predicted membrane. Highlighting in yellow are the residues Y205 and K109 who have a cation- π interaction and a downstream effect on membrane binding. Highlighting in gray are the active site residues of Lp-PLA₂.

2.3.3 Purification of recombinant Lp-PLA₂

Due to the hydrophobicity of Lp-PLA₂, it is essential to have detergent present throughout the entire purification to maintain enzyme solubility. Initial purification attempts used 0.2% v/v of the non-ionic detergent Triton DF-16 (Sigma); however this product was discontinued and it became necessary to use a different detergent. Several commercially available detergents were screened and it was determined that a similar non-ionic detergent, Triton X-100 (Sigma), was a suitable substitute for Triton DF-16.

One concern regarding Triton X-100 is that detergent micelles are approximately 80 kDa and are therefore non-dialyzable. The detergent also cannot pass through the Amicon Ultra centrifugal filter units (30 kDa molecular weight cutoff) and causes clogging at the bottom of the filter unit, leading to precipitation of the Lp-PLA₂. The initial purification modifications aimed at reducing the concentration of Triton X-100 present in solution at the end of the purification scheme. The initial attempts included reducing the detergent for the washes on the Glutathione Sepharose column (0.1– 0.2% v/v), and/or reducing the concentration of detergent from the anion exchange column on the FPCL (0.1 – 0.2% v/v); however, all attempts resulted in almost a complete loss of Lp-PLA₂. The next modifications aimed at using different detergents, including the zwitterionic detergent CHAPS and the non-ionic detergent octyl β-D-glucopyranoside (OGP), due to their small micelle molecular weights, 6 kDa and 8 kDa, respectively. This resulted in improved dialysis of the sample as well as a significant improvement in the ability of the detergent solution to pass through the centrifugal filter units when concentrating the enzyme. These two detergents were not as effective at solubilizing Lp-PLA₂ to remove it from the membrane and there was a loss of protein when either CHAPS or OGP were used throughout the purification (Table 2.1).

Table 2.1: Lp-PLA₂ detergent screening. All data representative of one purification attempt of Lp-PLA₂ in pGEX-6P-1 with specific detergent treatment.

Treatment	Concentration (mg/L expression media)	Specific Activity ($\mu\text{M min}^{-1} \text{mg}^{-1}$)
0.2% v/v Triton X-100 entire purification	1.05	21.9
0.2% v/v Triton X-100 extraction, 0.1% v/v Triton X-100 washes and FPLC	0.75	22.0
0.2% v/v Triton X-100 extraction and washes, 0.1% v/v Triton X-100 FPLC	0.36	21.0
0.2% v/v Triton X-100 extraction, 0.1% v/v Triton X-100 washes and FPLC	0.21	21.7
0.2% v/v OGP entire purification	No data	No data
0.2% w/v CHAPS entire purification	No data	No data

0.2 % v/v Triton X-100 entire purification, dialyze against CHAPS after FPLC

Treatment	Concentration (mg/mL sample volume)	Specific Activity ($\mu\text{M min}^{-1} \text{mg}^{-1}$)
Pre dialysis (0.2% v/v Triton X-100)	0.29	22.3
Post dialysis (0.01 w/v CHAPS)	0.22	21.6
Post dialysis (0.001 w/v CHAPS)	0.23	29.5

It had been reported that CHAPS can form mixed micelles with Triton X-100, thus drastically reducing the micelle size and allowing for the detergent to be removed during dialysis [12]. Using this approach, purification of Lp-PLA₂ was carried out using 0.2% Triton X-100 in each step, and then dialysis of the purified enzyme collected off of the anion exchange was done against buffer containing CHAPS of various concentrations (0.001 – 1% w/v). After dialysis, the protein sample was concentrated using the Amicon Ultra centrifugal filter units and did not have the build up of detergent that had been observed with Triton X-100, and most importantly, Lp-PLA₂ remained soluble. The enzyme was assayed before dialysis (containing only Triton X-100), after dialysis (for varying CHAPS concentrations) and after concentration, with no observed changes in specific activity (Table 2.1).

2.3.4 Characterization of purified Lp-PLA₂ constructs

After detergent optimization for Lp-PLA₂ purification, the enzyme was characterized for purity, concentration and activity. The quality of Lp-PLA₂ was determined by SDS PAGE gels and purity estimated from the program ImageJ (Research Services Branch of the NIH). The concentration of enzyme was determined using a BCA protein assay and the activity was assessed using the PNPA assay described previously.

The two lipoprotein binding mutants of Lp-PLA₂ gave higher yields of protein compared to wild type (Table 2.2). This was as expected because the mutations disrupted membrane binding and more enzyme was diverted to the soluble fraction from the insoluble portion. There were, however, differences in the enzymes purity between wild type and site-directed mutants. As seen in the SDS PAGE gel (Figure 2.5), the wild type Lp-PLA₂ contains significantly fewer impurities than either the

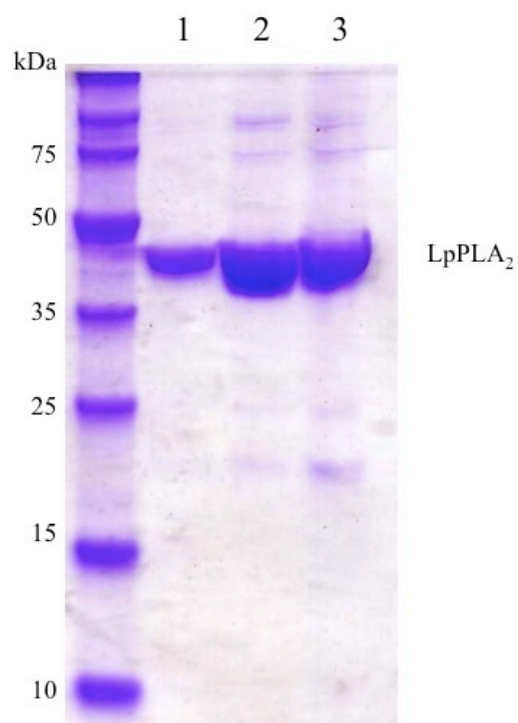


Figure 2.5: Lp-PLA₂ purification. SDS PAGE showing the relative purity of Lp-PLA₂ WT and lipoprotein mutants. Enzyme concentration was normalized to volume after enzyme was pooled from FPLC. Lanes: 1. WT Lp-PLA₂, 2. I120A/L123A/L124A hydrophobic patch mutant, 3. Y205A mutant

Table 2.2: Lp-PLA₂ purification. Protein yield and average purity of the Lp-PLA₂ constructs.

	Lp-PLA₂	I120A/L123A/L124A	Y205A
Concentration (mg L ⁻¹ expression)	1.8 ± 0.3	3.6 ± 0.5	2.2 ± 0.3
Average Purity	95%	93%	88%

I120A/L123A/L124A or Y205A mutants. Analysis with ImageJ confirms that WT Lp-PLA₂ has a higher level of purity (95%) than either of the mutants. Although attempts were made to increase the purity of the mutants, only I120A/L123A/L124A showed any improvement, while Y205A did not (Table 2.2). Due to the fact that the mutants were made to help with crystallography, the Y205A mutant was not pursued further. All constructs, however, were further characterized to determine their activity.

The PNPA assay previously described was used to determine the specific activity, K_{cat} , K_M and catalytic efficiency for Lp-PLA₂ as well as the lipoprotein binding mutants I120A/L123A/L124A and Y205A (Table 2.3). An attempt at this study was made, following a procedure described later in Chapter 5. However, even with maintaining the reaction conditions at very low concentrations of Lp-PLA₂, the amount of the substrate, 2-ThioPAF (Caymen Chemicals), required to carry out the Michaelis-Menten calculations was greater than that of the stock solution. For these purposes, the PNPA assay was deemed sufficient.

In addition to similar specific activities between all constructs, the Michaelis-Menten saturation curve shows that the V_{max} for Lp-PLA₂ and the lipoprotein binding mutants is comparable (Figure 2.6). It was also determined that the K_{cat} did not show any significant differences between the three constructs.

There was, however, a decrease in the K_M for the I120A/L123A/L124A and Y205A mutants compared to the wild type. As evident in the Michaelis-Menten saturation curve (Figure 2.6), the majority of the differences between Lp-PLA₂ and the lipoprotein binding mutants take place at very low substrate concentrations. The decreased K_M for the lipoprotein binding mutants indicates that these mutants have a

Table 2.3: Lp-PLA₂ kinetics with PNPA as a substrate. * denotes student's *t* test p value < 0.05 in comparison to WT. Specific activity n = 6; K_M, K_{cat} n = 3

	Lp-PLA ₂	I120A/L123A/L124A	Y205A
Specific activity μM min ⁻¹ mg ⁻¹	27.6 ± 2.9	27.1 ± 1.4	27.9 ± 3.7
K_M μM	464 ± 71	349 ± 36 *	415 ± 34 *
K_{cat} min ⁻¹	708 ± 40	676 ± 24	692 ± 20

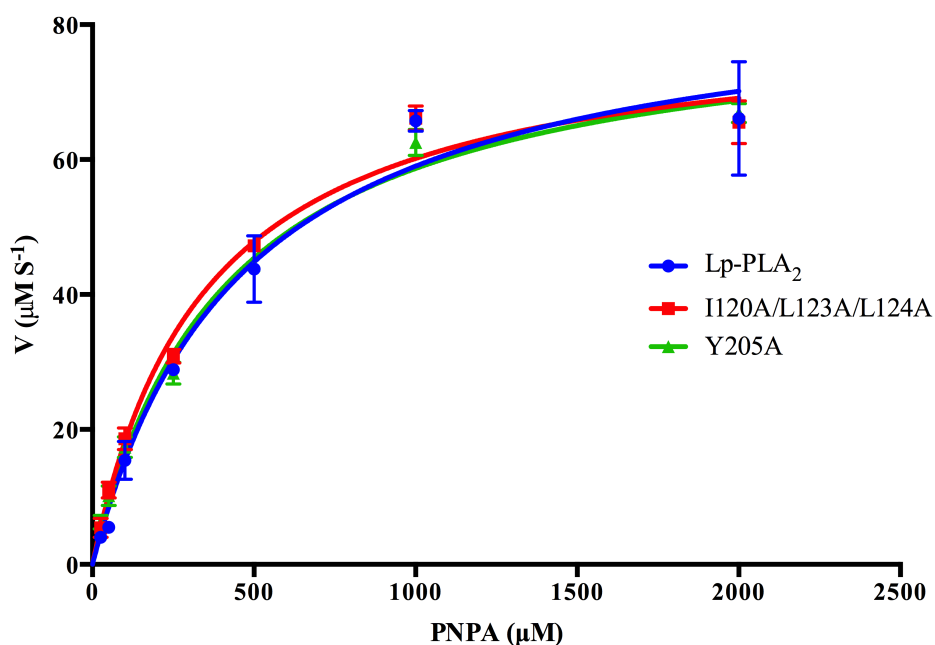


Figure 2.6: Lp-PLA₂ Michaelis–Menten saturation curve with PNPA as the substrate. WT Lp-PLA₂ represented by blue circles, Lipoprotein binding mutant I120A/L123A/L124A curve shown with red squares and Y205A mutant represented with green triangles. Michaelis–Menten kinetics data was fit using the GraphPad Prism version 6.00 for Mac, GraphPad Software, La Jolla California USA, www.graphpad.com

higher binding affinity for the substrate PNPA. The K_M for the endogenous enzyme using the radiolabeled substrate [^3H]PAF (hexadecyl-2- ^3H]acetyl-sn-glycerol-3-phosphorylcholine) was reported to be 12 μM [3]. It is likely that the recombinant enzyme would also have a lower K_M using a natural substrate for Lp-PLA₂ instead of the general substrate PNPA. It would also be interesting to see if a decreased K_M would still be as evident between the wild type Lp-PLA₂ and the lipoprotein binding mutants using the native substrate PAF.

2.4 Conclusions

Presented in this chapter was the cloning, expression, purification and characterization of the membrane-associated enzyme Lp-PLA₂. Due to potential thrombin contamination from the pGEX-4T-3 vector, two new protease cleavage sites were introduced into the GSP-Lp-PLA₂ fusion construct. The first, TEV protease, yielded limited success following a procedure for a recombinant production of the protease. It was determined that a pGEX-6P-1 vector containing the cleavage site for PreScission Protease was the most optimal for our purposes.

An expression procedure was determined for the Lp-PLA₂ construct in pGEX-6P-1. After detergent screening to best isolate Lp-PLA₂ from the insoluble portion, a purification scheme was optimized and activity was assayed using a PNPA assay.

In addition to the WT Lp-PLA₂ expression, purification, and characterization, two site-directed mutants were made. The I120A/L123A/L124A and Y205A mutant constructs were created to disrupt the membrane-associated portion of Lp-PLA₂ with the goal of higher protein yields per liter of expression media. These mutants were expressed and purified in the same manner as the wild type, Lp-PLA₂. Assessment of the activity of these mutants demonstrated no significant differences in the specific

activity, V_{\max} or K_{cat} between the lipoprotein binding mutants and wild type; however there was a decrease in the K_M for the mutants using PNPA as a substrate.

REFERENCES

1. Elstad, M. R., Stafforini, D. M., McIntyre, T. M., Prescott, S. M. & Zimmerman, G. A. Platelet-activating factor acetylhydrolase increases during macrophage differentiation. A novel mechanism that regulates accumulation of platelet-activating factor. *J. Biol. Chem.* **264**, 8467–70 (1989).
2. Stafforini, D. M., Prescott, S. M. & McIntyre, T. M. Human plasma platelet-activating factor acetylhydrolase. Purification and properties. *J. Biol. Chem.* **262**, 4223–30 (1987).
3. Tew, D. G. *et al.* Purification, properties, sequencing, and cloning of a lipoprotein-associated, serine-dependent phospholipase involved in the oxidative modification of low-density lipoproteins. *Arterioscler. Thromb. Vasc. Biol.* **16**, 591–9 (1996)
4. Stafforini, D. M. *et al.* Platelet-activating factor acetylhydrolase deficiency. A missense mutation near the active site of an anti-inflammatory phospholipase. *J. Clin. Invest.* **97**, 2784–91 (1996).
5. Tjoelker, L. W. *et al.* Anti-inflammatory properties of a platelet-activating factor acetylhydrolase. *Nature* **374**, 549–53 (1995).
6. Samanta, U., Kirby, S. D., Srinivasan, P., Cerasoli, D. M. & Bahnson, B. J. Crystal structures of human group-VIIA phospholipase A2 inhibited by organophosphorus nerve agents exhibit non-aged complexes. *Biochem. Pharmacol.* **78**, 420–9 (2009).
7. Srinivasan, P. Characterization of the association of human plasma platelet-activating factor acetyl hydrolase with lipoproteins. *University of Delaware ProQuest Dissertations & Theses A&I* (2010).
8. Srinivasan, P. & Bahnson, B. J. Molecular Model of Plasma PAF Acetylhydrolase-Lipoprotein Association: Insights from the Structure. *Pharmaceuticals* **3**, 541–557 (2010).
9. Blommel, P. G. & Fox, B. G. A combined approach to improving large-scale production of tobacco etch virus protease. *Protein Expr. Purif.* **55**, 53–68 (2007)
10. Gardner, A. a., Reichert, E. C., Topham, M. K. & Stafforini, D. M. Identification of a domain that mediates association of platelet-activating factor acetylhydrolase with high density lipoprotein. *J. Biol. Chem.* **283**, 17099–17106 (2008).

11. Stafforini, D. M. *et al.* Deficiency of platelet-activating factor acetylhydrolase is a severity factor for asthma. *J. Clin. Invest.* **103**, 989–97 (1999).
12. O'Malley, M. A., Helgeson, M. E., Wagner, N. J. & Robinson, A. S. Toward rational design of protein detergent complexes: determinants of mixed micelles that are critical for the in vitro stabilization of a G-protein coupled receptor. *Biophys. J.* **101**, 1938–48 (2011).

Chapter 3

SELECTIVE INHIBITOR DISCOVERY OF LP-PLA₂

3.1 Introduction

Lipoprotein-associated phospholipase A₂ contains both pro and anti-inflammatory properties, making its role in the progression of coronary heart disease (CHD) controversial. On the pro-inflammatory side, there have been reports that an association between an increase in Lp-PLA₂ activity and/or concentration increases the risk of CHD. It has also been shown that the enzyme is present in the atherosclerotic plaques most prone to rupture and has been reported to promote the formation of the necrotic core [1,2]. For these reasons, Lp-PLA₂ has risen as a promising target for the development of therapeutics used in the treatment of CHD.

The pharmaceutical company GlaxoSmithKline developed a series of substituted pyrimidone compounds that selectively inhibit Lp-PLA₂ *in vitro* at nanomolar concentrations, the most promising of which was darapladib. A phase I trial established the safety of darapladib in healthy patients and determined that the drug effectively lowers Lp-PLA₂ levels in plasma without affecting the lipid profile or platelet function [3-5]. There were two phase II trials in which stable CHD patients were administered darapladib daily. The outcome of these studies was that darapladib effectively lowered Lp-PLA₂ activity and prevented the increase in necrotic core volume [6,7]. Taken together, the studies showed positive effects on those treated with darapladib and the drug moved into phase III clinical trials.

There were two phase III, randomized, placebo-controlled clinical trials carried out to determine if darapladib is an effective add-on treatment for those with CHD. The first study being the Stabilization of Atherosclerotic Plaque by Initiation of Darapladib Therapy (STABILITY) which aimed to determine if treatment with darapladib prevents coronary events in those with stable CHD [8,9]. The second study was the Stabilization of Plaques using Darapladib-Thrombolysis in Myocardium Infarction (SOLID-TIMI 52), in which patients were treated with darapladib within 30 days of a cardiac event and the ability of the drug to prevent another cardiac event was assessed [10,11]. Recently, to GlaxoSmithKline's disappointment, both studies showed no significant differences in primary endpoints between darapladib and placebo and the STABILITY study only showed a minor improvement in the total coronary events upon treatment with darapladib.

With the results of the STABILITY and SOLID-TIMI 52 studies, the exact determination of the physiological and pathophysiological role for Lp-PLA₂ remains unknown. A recent study using a diabetic/high cholesterol pig model demonstrated that the development of atherosclerosis in the coronary arteries is markedly different than in the distal abdominal arteries. Treatment with darapladib in this model inhibited the progression of coronary atherosclerotic plaques with no reduction of inflammation or plaque development in the distal abdominal aortae, thus demonstrating that the effect of darapladib on plaque progression was highly site specific [12].

In collaboration with our lab, a high throughput screen was carried out to determine new compounds that will inhibit Lp-PLA₂ at the Molecular Libraries Screening Center Network at The Scripps Research Institute Florida. The compounds were characterized and optimized in the lab of our collaborator Dr. Ben Cravatt of The

Skaggs Institute for Chemical Biology at The Scripps Research Institute and the potency and selectivity of the new compounds were determined. A comparison between the optimized inhibitors and darapladib were carried out *in vitro* as well as *in situ* and the results have been published [13]. Here I present studies that were carried out with recombinant Lp-PLA₂ to compare inhibition by the optimized inhibitors and darapladib derivatives by PNPA activity assay as well as determination of any potential changes to the secondary structure upon inhibitor binding.

3.2 Materials and Methods

3.2.1 Materials

The materials used for the kinetic and biochemical analysis include sodium chloride, potassium chloride, sodium phosphate dibasic anhydrous, sodium phosphate monobasic monohydrate, calcium chloride and dimethyl sulfoxide (DMSO) which were purchased from Fisher Scientific. All other materials for the production of recombinant Lp-PLA₂ as well as the PNPA assay are listed in Chapter 2.

3.2.2 Scripps BioAssay

In order to determine the compounds that can inhibit Lp-PLA₂, a fluorescence polarization activity based protein profiling (FluoPol-ABPP) assay was performed at The Scripps Research Institute. This assay utilizes a plate reader in which recombinant enzyme sent to Scripps from our lab is placed into each well, and then a potential inhibitor compound is added to the individual wells. Following the incubation of enzyme and potential inhibitor, an ABPP probe is added to the well. The probe contains a reactive group to bind the enzyme active site serine (S273 for Lp-PLA₂) and a fluorophore reporter tag. If the compound is an effective inhibitor, the ABPP

probe will not bind the enzyme and the resulting fluorescence polarization remains low and does not increase compared to the uninhibited enzyme. Conversely, if the compound is not an effective inhibitor, the probe will bind the enzyme and the fluorescence polarization is increased accordingly [14].

A preliminary ABPP screening was performed in the lab of our collaborator, Dr. Ben Cravatt, to determine if Lp-PLA₂ was a candidate for a high throughput screening. The high throughput inhibitor screening of recombinant Lp-PLA₂ was then carried out at the Molecular Libraries Screening Center Network at The Scripps Research Institute Florida where 326,141 compounds were screened at a concentration of 3.39 μ M and the full results can be found on PubChem AID 463092. It is important to note that in addition to the FluoPol-ABPP high throughput inhibitor screen performed for Lp-PLA₂, the homologous enzyme PAFAH-II (PubChem AID 492969) was screened as well as the PAF-AH Ib isoforms (PubChem AID 492971, 492979, and 493032). This high throughput screening was funded by a supplement award to NIH 5R01HL084366 (P.I. Bahnson).

3.2.3 Circular dichroism

Recombinant Lp-PLA₂ was expressed and purified as previously described in Chapter 2. The samples were diluted to around 10 μ M and treated with each inhibitor compound of interest. After inhibition, all samples were dialyzed into 0.5x PBS buffer (5 mM Na₂HPO₄ and 0.9 mM NaH₂PO₄, pH 7.4, containing 68.5 mM NaCl, 1.35 mM KCl, and 0.5 mM CaCl₂) overnight to ensure complete buffer transfer in all samples. Circular dichroism was performed in Colburn Laboratory using a JASCO Spectropolarimeter. Samples were maintained at 25 °C with a Julabo F25 water bath and controlled with a JASCO Peltier Controller. Measurements were performed in

triplicate with a data pitch of 1 nM, scanning speed of 20 nm/min, and a response of 4 s. A blank was run of 0.5x PBS buffer and baseline was automatically corrected.

3.3 Results and Discussion

All inhibitor screening discussed in this chapter was conducted at the Molecular Libraries Screening Center Network at The Scripps Research Institute Florida. In addition, the lead targets from the screening were optimized and characterized *in vitro* and *in situ* in the lab of our collaborator, Dr. Ben Cravatt, of The Skaggs Institute for Chemical Biology at The Scripps Research Institute. These results have been published as J. M. Nagano, K. L. Hsu, L. R. Whitby, M. J. Niphakis, A. E. Speers, S. J. Brown, T. Spicer, V. Fernandez-Vega, J. Ferguson, P. Hodder, P. Srinivasan, T. D. Gonzalez, H. Rosen, B. J. Bahnson, and B. F. Cravatt.

Selective inhibitors and tailored activity probes for lipoprotein-associated phospholipase A(2), (2013) *Bioorg. Med. Chem. Lett.*, 23, 839-943. The kinetic and biophysical analysis of the inhibitor complexed with recombinant Lp-PLA₂ were performed in our lab.

3.3.1 Scripps BioAssay results and inhibitor optimization

In an initial experiment, Lp-PLA₂ as well as an Lp-PLA₂ S273 activity knockout mutant were assayed using the FluoPol-ABPP technique in the Cravatt lab. This assay demonstrated that only Lp-PLA₂ with an intact active site would bind the probe. In addition, a preliminary screen of Lp-PLA₂ against a library of 3,200 compounds was tested and the relative fluorescence polarization was read. Of the compounds screened, a few displayed inhibition of the enzyme (Figure 3.1). Taken together, this data suggested Lp-PLA₂ and the designed assay was a prospect for a

high throughput inhibitor screen in collaboration with the Molecular Libraries Screening Center Network at The Scripps Research Institute Florida.

The library for at the Molecular Libraries Screening Center Network screened 326,141 compounds, of which 4,934 showed a reduction in fluorescence polarization, thus providing some inhibition of Lp-PLA₂. Upon replication, it was revealed that of the 1,675 compounds that inhibited Lp-PLA₂, only 153 showed greater than 60% inhibition when retested. The 153 compounds were screened for their selectivity using gel-based competitive ABPP against recombinant mouse enzyme as well as lysate from HEK-293T cells expressing mouse Lp-PLA₂ [15]. From the gel-based competitive ABPP screen, only 12 of the compounds were confirmed to inhibit the enzyme at greater than 75% at 5 μ M concentration [13].

Eight of the 12 hits happen to be carbamates, a class of inhibitor compounds previously demonstrated to have excellent selectivity for serine hydrolases both *in vivo* and *in situ*. This selectivity of carbamate inhibitors can be achieved with slight modifications around the central carbonyl [16]. The general mechanism for the carbamate inhibition of serine hydrolases involves nucleophilic attack of the active site serine to the carbonyl of the carbamate, resulting in a covalent bond at the active site (Figure 3.2). Portions of two of the lead hits, WWL153 and P9, were combined to form the optimized inhibitor JMN4 with the hopes of increasing selectivity and potency [13]. On the biphenyl moiety of JMN4, an amine was substituted at carbon 5 creating the inhibitor to JMN21 (Figure 3.2).

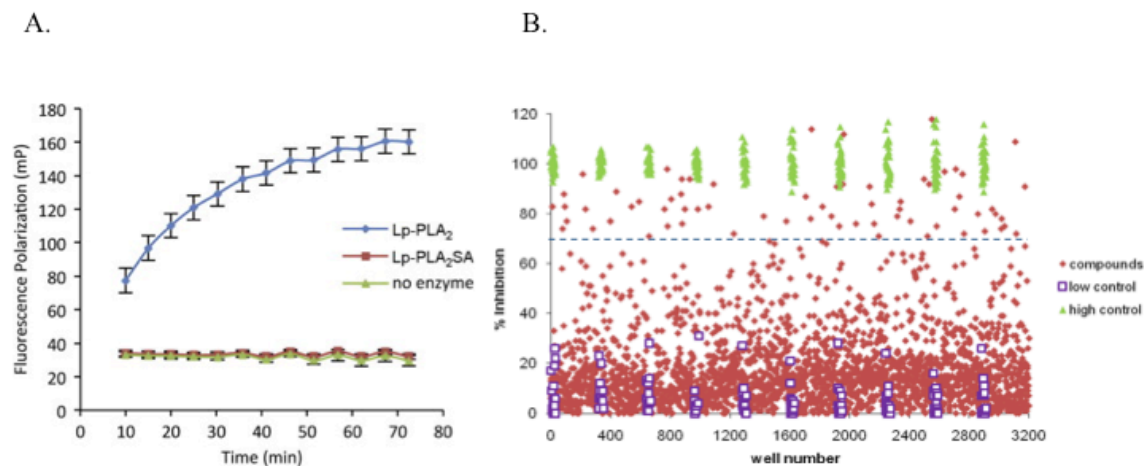


Figure 3.1. FluoPol-ABPP assay. (A) 10 nM sample of purified human Lp-PLA₂, (Lp-PLA₂ SA), or no enzyme was incubated with 75 nM probe at room temperature and fluorescence polarization was measured. B. Preliminary screening of Lp-PLA₂ against a library of 3,200 compounds. Reprinted from *Bioorg. Med. Chem. Lett.* 23, Nagano, J. M. G. *et al.* Selective inhibitors and tailored activity probes for lipoprotein-associated phospholipase A(2), 839–43, Copyright (2012), with permission from Elsevier. (B) Initial inhibitor compound screening of Lp-PLA₂ displaying only a handful of compounds inhibit the enzyme. The low control contained no compound and high control contained no enzyme. The Z' average was 0.63 with an inhibition cutoff at 70% yielding a hit rate of 2% (69 compounds).

3.3.2 Inhibitor characterization

The specific inhibitors of Lp-PLA₂ developed through our collaboration's high throughput screening were analyzed for their potency using recombinant sources of the enzyme as well as the specificity of the inhibitors using mouse brain proteome with experimentation carried out at The Scripps Research Institute. The potency and selectivity of the optimized inhibitor JMN4 was determined in mouse brain proteome

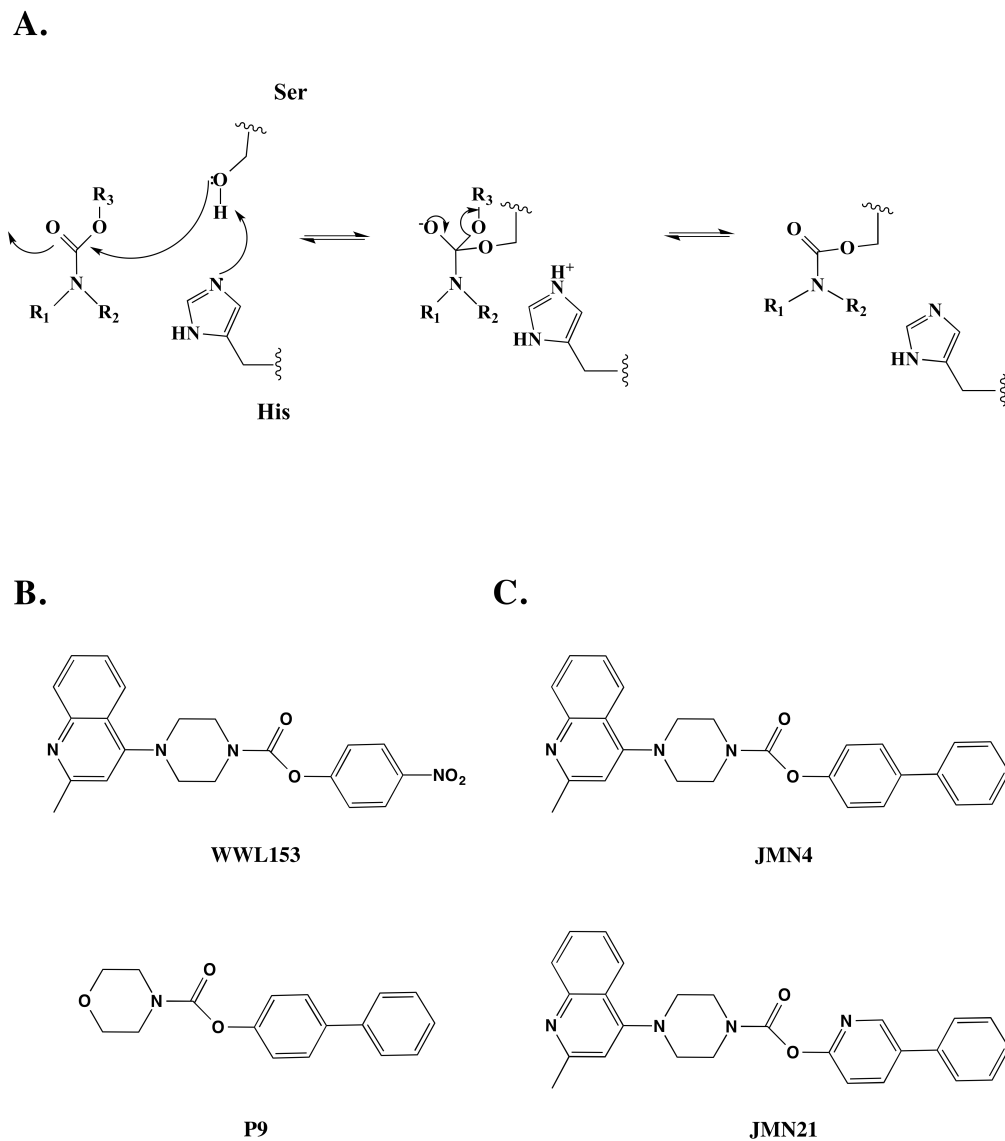


Figure 3.2. High throughput screening hits. (A) General mechanism of carbamate inhibitors with serine hydrolase enzymes. Histidine (or other general base) in active site deprotonates active site serine, which then has a nucleophilic attack of the carbonyl on the carbamate, resulting in covalent bond to active site. (B) Structures of lead inhibitors from the high throughput screen. (C) Structures of optimized inhibitors developed from the lead inhibitors from the high throughput screen.

as well as human prostate cancer (PC3) cells and ultimately compared darapladib, the specific inhibitor developed by GlaxoSmithKline.

3.3.2.1 Potency

The potency of the lead inhibitors WWL153, P9 and optimized compounds JMN4 and JMN21 were determined using a gel based activity based protein profiling approach. In this experiment, recombinant mouse or human Lp-PLA₂ was incubated with various concentrations of each inhibitor compound (10 μ M to 1 nM) as well as DMSO (negative control). A fluorophosphonate-rhodamine (FP-Rh) probe (Figure 3.3) designed to target the active site of serine hydrolase enzymes was then added to the recombinant Lp-PLA₂ mixtures and inhibition was determined by the difference in optical density of the bands on an SDS-PAGE gel (Figure 3.4, panels A and B).

This data was used to determine the IC₅₀ for each of the inhibitors in both human and mouse Lp-PLA₂. The two leading hits from the high throughput screen had higher IC₅₀ than JMN4 and JMN21 in both mouse and human Lp-PLA₂. The compound WWL153 had an IC₅₀ of 250 nM in human and 290 nM in mouse Lp-PLA₂ and the P9 inhibitor had an IC₅₀ of 100 nM and 470 nM respectively. The optimized inhibitors had significantly lower IC₅₀ values than either of the lead compounds from the high throughput screen; JMN4 has an IC₅₀ of 5.9 nM in human and 90 nM in mouse Lp-PLA₂ and JMN21 has an IC₅₀ of 2.8 nM for human Lp-PLA₂. This effectively demonstrates that slight modifications to the moieties around the carbonyl on a carbamate can significantly increase the potency of the inhibitor for Lp-PLA₂ [13].

3.3.2.2 Selectivity

Once it was established that the optimized inhibitor JMN4 (as well as JMN21) displayed more potency than either of the lead inhibitors from the high throughput screening, it was necessary to determine if the optimized compound also displayed greater selectivity *in vitro*.

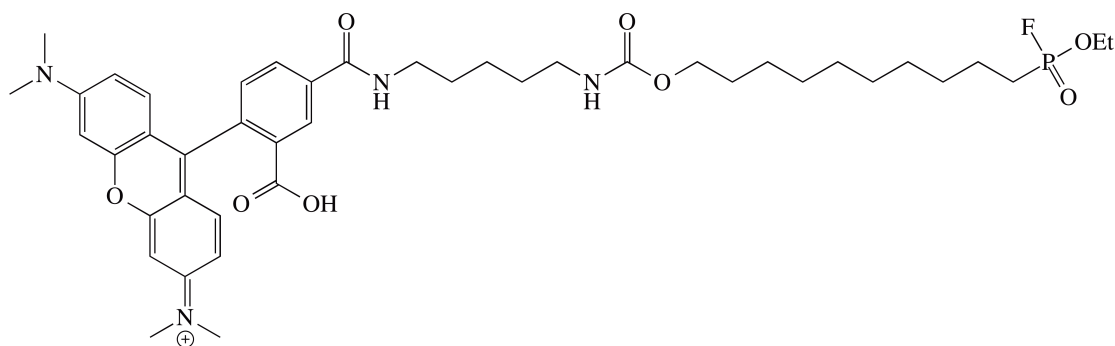


Figure 3.3: Fluorophosphonate-rhodamine probe. Used as a general ABPP probe to detect serine hydrolase enzymes.

3.3.2.2.1 Comparison of lead inhibitors and JMN4

To determine the selectivity of the lead compounds WWL153 and P9, as well as our optimized inhibitor JMN4, studies were performed using mouse brain proteome. The mouse brain lysate was treated with the inhibitor compounds at various concentrations (10 μ M – 1 nM) and subsequently labeled with the FP-Rh probe to determine cross reactivity of the compounds with other serine hydrolases present in mouse brain (Figure 3.4, panel C).

It was found that both WWL153 and P9 displayed cross reactivity with Fatty Acid Amide Hydrolase (FAAH) at concentrations of 10 nM and 10 μ M, respectively. However, this off target reaction is not desirable, and importantly, FAAH did not show any sensitivity to the optimized inhibitor JMN4 [13]. There were two other

enzymes that displayed sensitivity only to compound WWL153; Monoacylglycerol lipase (MAGL) and α/β Hydrolase Domain 6 (ABHD6). Neither MAGL nor ABHD6 showed any sensitivity to P9 or our optimized inhibitor JMN21. Taken together, JMN21 displays greater potency than WWL153 or P9 as well as more selectivity *in vitro* than the lead compounds, thus making JMN4 a potent and selective inhibitor of Lp-PLA₂ [13].

3.3.2.2.2 Comparison of JMN4 and darapladib

Once it was determined that JMN4 was a more potent and selective inhibitor of Lp-PLA₂, studies were performed to compare its efficacy with the GlaxoSmithKline drug darapladib. It became necessary to use a different probe for the gel-based competitive ABPP studies due to the fact that the FP-Rh probe can only detect those serine hydrolases present in high abundance.

A 1,2,3-triazole urea (HT-01) probe had been developed previously in order to detect the low abundant DAGL β in cell and tissue proteomes (Figure 3.5) [17]. This probe was synthesized based on the general structure of the 1,2,3-triazole urea with a BODIPY fluorophore modification for use in ABPP. It had also been previously shown that 1,2,3-triazole urea compounds, including HT-01, inhibit mouse Lp-PLA₂ (IC₅₀ of 39 nM, Figure 3.6 panel A); therefore, it was necessary to be mindful of the concentration of HT-01 used for mouse studies [18]. For these reasons, the HT-01 probe (Sigma Aldrich) was utilized in order to positively identify Lp-PLA₂ in both mouse brain proteome and human prostate cancer cell lysate samples.

Similar to the previously described experiments, mouse brain proteome was used to study the selectivity of the inhibitory compounds darapladib and JMN4

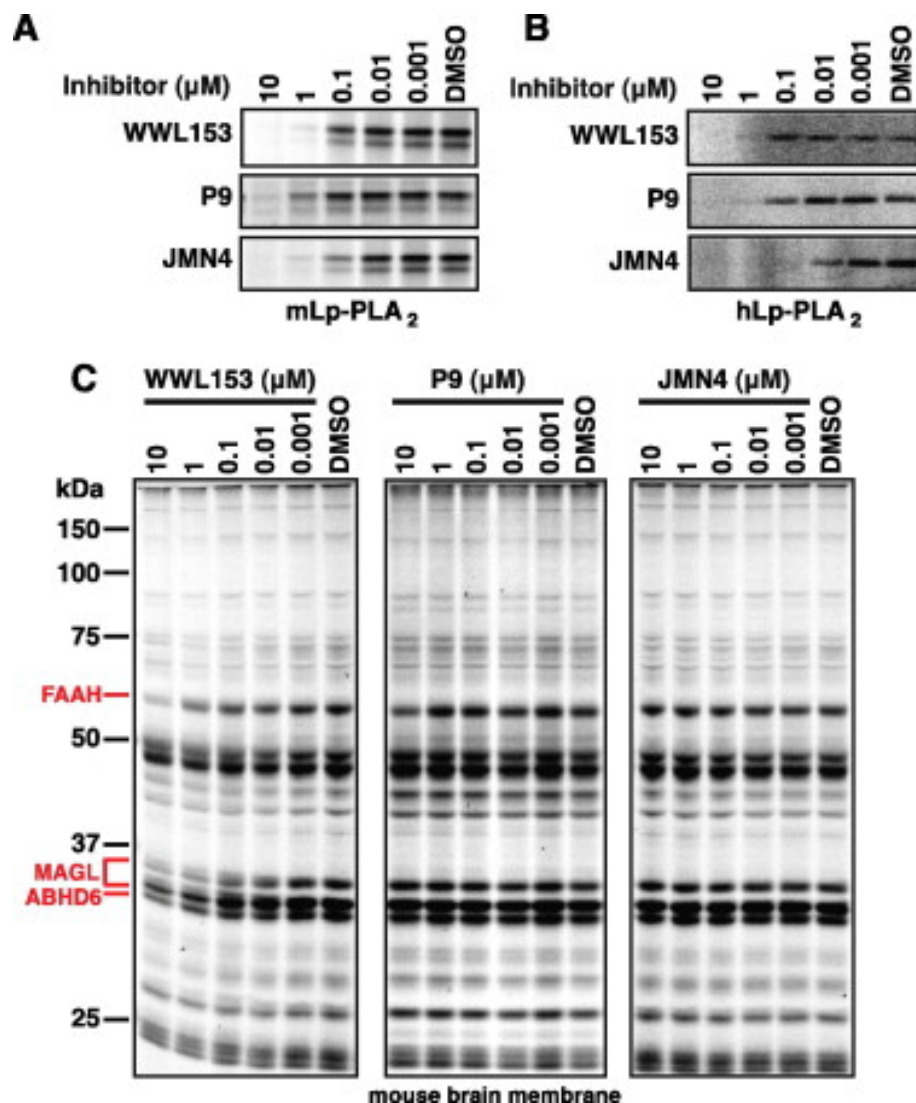


Figure 3.4: Inhibitor potency and selectivity determination. (A) and (B) IC_{50} determination of Lp-PLA₂ inhibitors using competitive ABPP with the FP-Rh probe (A) Mouse Lp-PLA₂. (B) Human Lp-PLA₂. (C) Selectivity determination for WWL153, P9, and JMN21 using competitive ABPP with the FP-Rh probe in mouse brain. Fluorescent gels are shown in gray scale. Reprinted from *Bioorg. Med. Chem. Lett.* 23, Nagano, J. M. G. *et al.* Selective inhibitors and tailored activity probes for lipoprotein-associated phospholipase A(2), 839–43, Copyright (2012), with permission from Elsevier.

not show sensitivity to any other enzymes using HT-01 labeling as shown in Figure 3.6 panels A and B. As expected, the FP-Rh probe was unable to detect Lp-PLA₂ in the mouse brain lysate. This labeling showed that darapladib and JMN4 did not cross-react with any highly abundant hydrolase at any concentration of compound tested, as shown in Figure 3.6 panel C [13].

Human prostate cancer (PC3) cell lines were used to determine the specificity of darapladib and JMN4 *in vitro* and *in situ* as they have been previously reported to express endogenous enzyme [21]. The ABPP experiments previously described for the mouse brain lysate were repeated with the PC3 cells. Using both the sensitive HT-01 probe and the FP-Rh probe for high abundant serine hydrolases, no other enzymes showed inhibitory effects with either compound at any concentration (Figure 3.6 panels D and E). Similar to the mouse lysate, FP-Rh probe was not able to detect Lp-PLA₂ for the membrane fraction or soluble fraction of the PC3 cells. [13].

In order to evaluate the *in situ* inhibitory effects of darapladib and our optimized inhibitor JMN4, PC3 cells were once again used. However, treatment with the inhibitors was done to the whole cell prior to lysis. After the PC3 cells were treated with either darapladib or JMN4 (heavy cells) or the negative control DMSO (light cells), they were harvested, lysed, and incubated with an FP-Biotin probe (Figure 3.7) [15]. This probe exploits the biotin/avidin relationship and allows for labeled enzymes to bind avidin resin while all unlabeled enzymes (either non serine hydrolases or those with inhibited active sites) will not bind. The heavy and light labeled lysates are mixed at equal ratios and applied to avidin resin. While bound to the resin, the peptides were digested with trypsin and then analyzed with liquid chromatography-tandem MS in order to quantify the light (DMSO) and heavy (darapladib or JMN4) signals from the

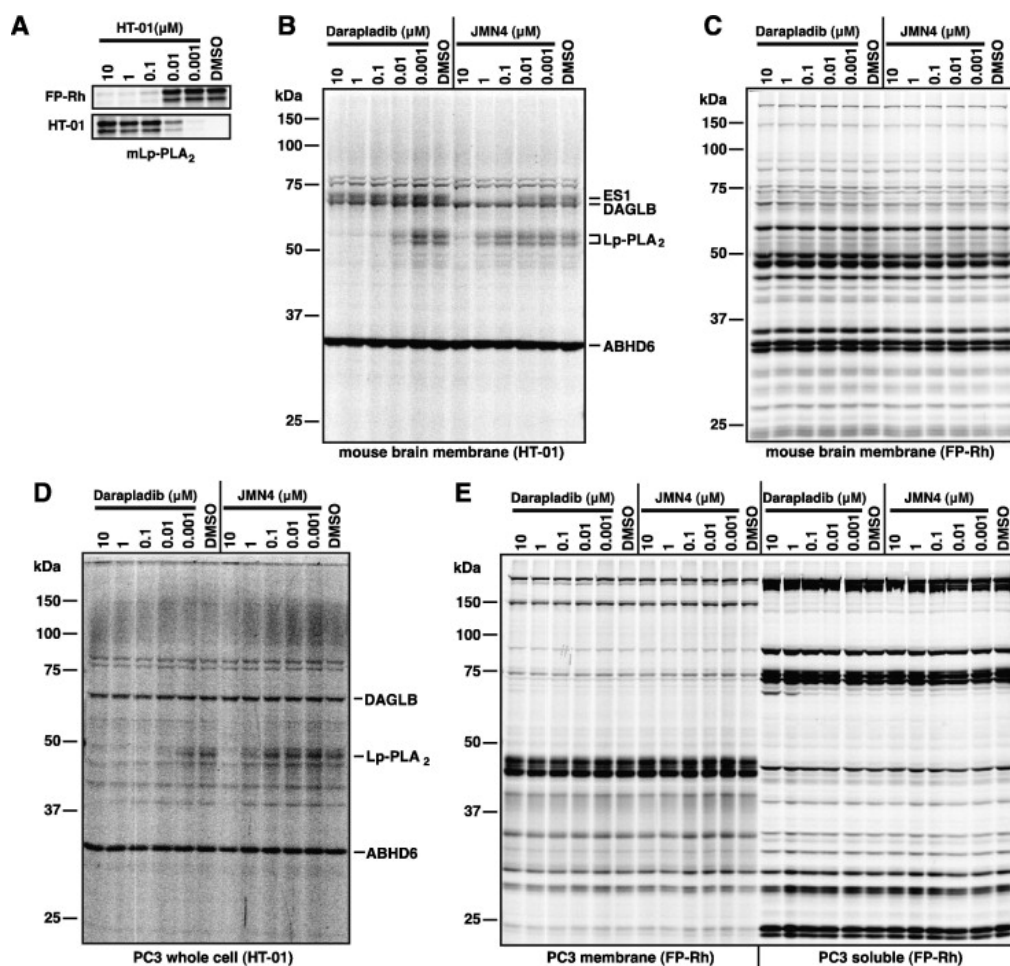


Figure 3.6: *In vitro* evaluation of darapladib and JMN4. (A) Inhibition of mouse Lp-PLA₂ with HT-01 probe. Competitive ABPP with FP-RH probe determined IC₅₀ of HT-01 to be 39 nM. (B) Mouse brain proteome analysis of darapladib and JMN4 selectivity using HT-01 probe and (C) FP-Rh probe. (D) Prostate cancer cells (PC3) analysis of darapladib and JMN4 selectivity using HT-01 probe. (E) PC3 cells partitioned to membrane and soluble fraction with analysis of darapladib and JMN4 selectivity using FP-Rh probe. Reprinted from *Bioorg. Med. Chem. Lett.* 23, Nagano, J. M. G. *et al.* Selective inhibitors and tailored activity probes for lipoprotein-associated phospholipase A(2), 839–43, Copyright (2012), with permission from Elsevier.

parent ion (MS1) peaks [22]. Finally, the serine hydrolase enzyme identities were determined from the product ion (MS2). The ratio of the heavy (darapladib or JMN4) over light (DMSO) was determined for each protein and plotted in Figure 3.8 [13].

It was apparent that both darapladib and JMN4 exclusively inhibit only Lp-PLA₂ *in situ* for PC3 cells shown in Figure 3.8. None of the 40 other serine hydrolases in PC3 cells showed any sensitivity to either inhibitor. The enzyme ABDH6, which showed sensitivity to the lead inhibitor WWL153, did not display inhibition *in vitro* (mouse or human with HT-01 probe) or *in situ* with either darapladib or JMN4. Importantly, the homologous PAFAH-II (Figure 3.8, 10 from the left, both panels) and PAFAH-Ib isoform (Figure 3.8, panel A. 8 from the left, panel B. 9 from the left) did not display any sensitivity to either treatment *in situ*.

The findings presented here and published in J. M. G. Nagano *et al* in 2013 represent the evaluation of inhibitors for only Lp-PLA₂. As mentioned previously, similar studies were performed for the PAFAH-II homolog [23] and the PAF-AH Ib isoform [24], and whose findings were published independently.

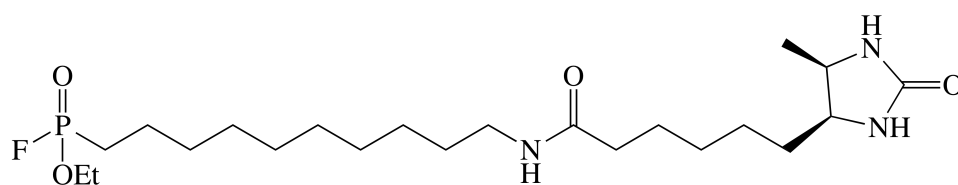


Figure 3.7: Fluorophosphonate-biotin probe. FP-biotin. Used as a general to detect serine hydrolases and can be used in pull down experiments through exploitation of the biotin/avidin relationship.

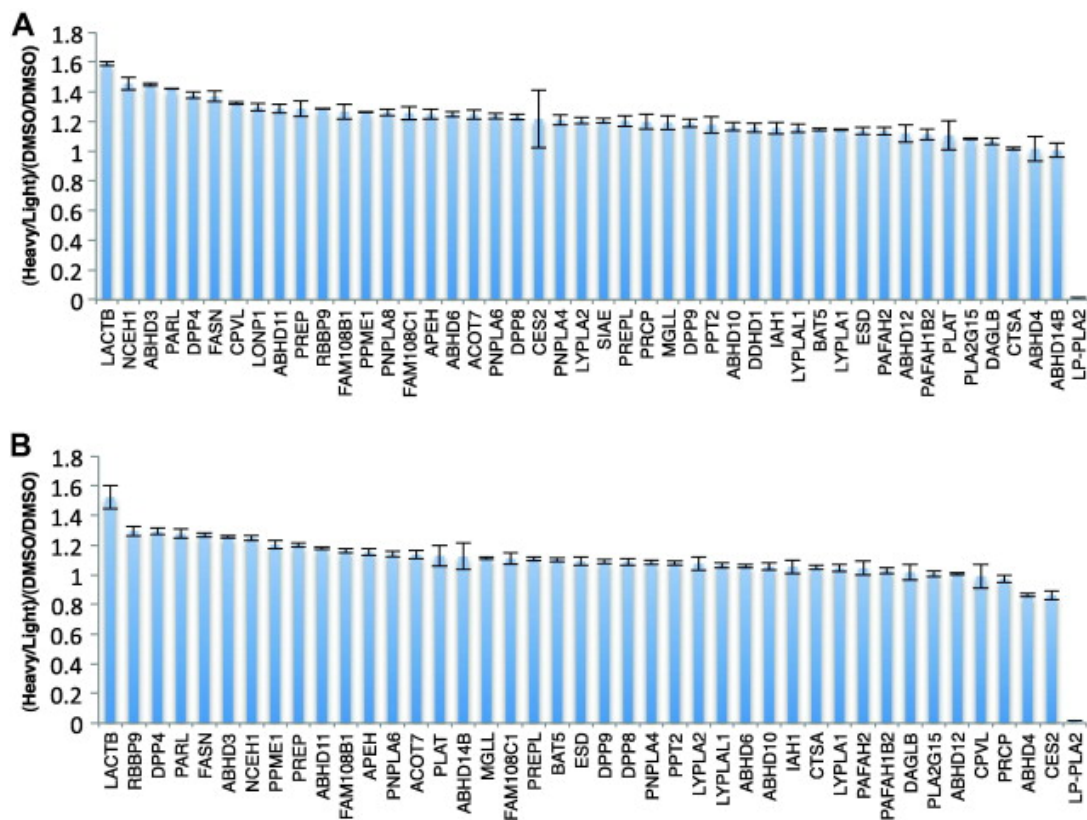


Figure 3.8: *In situ* evaluation of darapladib and JMN4. ABPP-SILAC analysis of PC3 cells with inhibitor treatment (heavy) or DMSO (light). (A) Darapladib treatment and (B) JMN4 treatment. Reprinted from *Bioorg. Med. Chem. Lett.* 23, Nagano, J. M. G. *et al.* Selective inhibitors and tailored activity probes for lipoprotein-associated phospholipase A(2), 839–43, Copyright (2012), with permission from Elsevier.

3.3.3 Kinetic and biophysical characterization of Lp-PLA₂ inhibitor complexes

Both kinetic and biophysical studies were performed using the recombinant human Lp-PLA₂ (49-423) construct described in Chapter 2 complexed with derivatives of darapladib, SB-567952 and SB-595058 (HLW Compound Management, Figure 3.9) and our optimized inhibitor JMN21 (Figure 3.2).

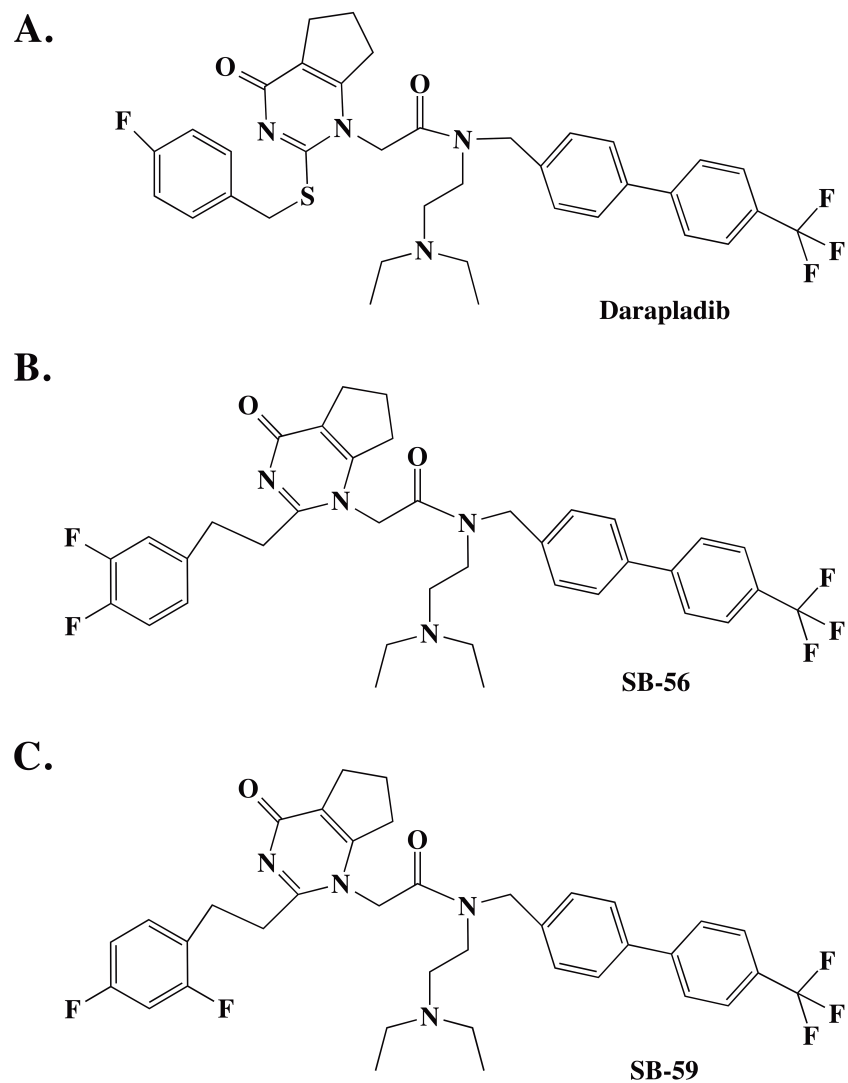


Figure 3.9: Structures of darapladib and its derivatives. (A) Darapladib (B) SB-567952 (referred to as SB-56) (C) SB-595058 (referred to as SB-59)

3.3.3.1 Kinetic analysis of inhibited complexes

The PNPA assay described in the previous chapter was used to characterize the inhibitor's effects on the recombinant enzyme over time. Samples were prepared of Lp-PLA₂ with saturating concentrations of inhibitor SB-56, SB-59 and JMN21 and assayed immediately. The samples were then stored at 4 °C for 60 days and the assay was repeated. The data was normalized to wild type Lp-PLA₂ incubated with DMSO (JMN21 solvent) that was assayed and stored under the same conditions (Figure 3.10). It is clear that initial PNPA assay demonstrate complete inhibition of Lp-PLA₂ activity by all of the compounds, as expected. In the activity assessment of the 60-day-old samples, as expected, the control wild type Lp-PLA₂ lost some activity during storage due to protein degradation. The Lp-PLA₂ treated with SB-56 and SB-59 displayed some activity, likely due to the reversible nature of the darapladib compounds, while Lp-PLA₂ treated with JMN21 remained completely inhibited. The retained inhibition of Lp-PLA₂ treated with JMN21 further validates the covalent bond of the active site serine to the carbamate inhibitor. Due to the similar results obtained between SB-56 and SB-59, all other experiments using the darapladib derivatives only used SB-56 due to limited quantities of SB-59 available in our lab.

3.3.3.2 Circular dichroism analysis

The circular dichroism spectrum was obtained for wild type ligand free Lp-PLA₂ and inhibited Lp-PLA₂ with either SB-56 and JMN21 as described previously in order to determine if there were any major changes to the secondary structure upon inhibition. It was necessary to dialyze the enzyme samples after inhibition as the DMSO, which JMN21 was dissolved in, caused the voltage of the CD to rise above 600 around 225 nm and a large portion of the spectral data was not reliable. Dialyzing

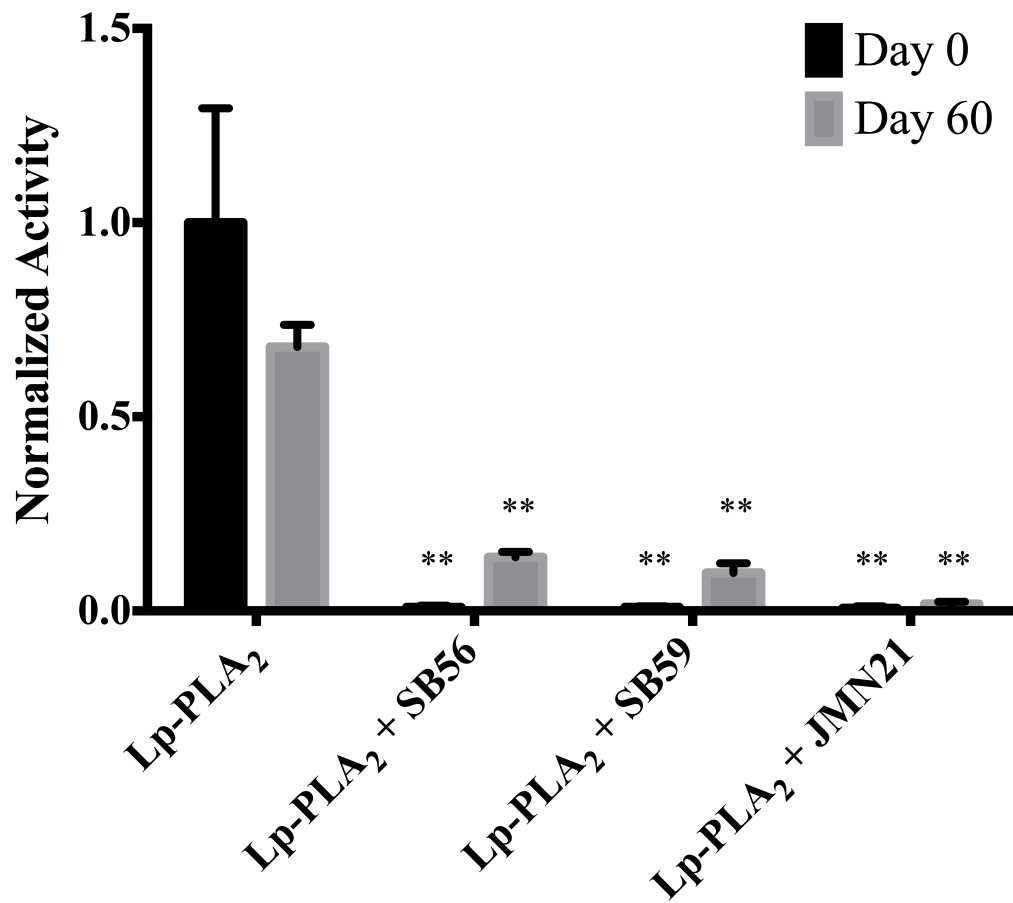


Figure 3.10: Relative activity of Lp-PLA₂ with inhibitors. PNPA assay was performed on Lp-PLA₂ samples treated with inhibitors immediately (black bars) or after 60 day incubation at 4 °C (gray bars). Data was normalized to WT Lp-PLA₂ activity on Day 0. T-test performed analyzing inhibited samples to WT taken at its respective time point. There was no significant difference between the WT activities on Day 0 and Day 60 ($p = 0.06$). ** denotes $p < 0.001$

against 0.5X PBS buffer prevented this early voltage jump and reliable data was obtained from 200 – 250 nm for all samples (Figure 3.11). Dialysis in a PBS buffer also had the benefit of removing the organic cosolvent DMSO that may influence CD spectral changes.

Though the baseline was automatically deducted from the runs of the CD, the data set formulated by the instrument's software required additional analysis. The ellipticity measured from the CD was reported as mdeg, and it was necessary to convert that to deg. The concentration of enzyme was calculated in $\mu\text{mol/mL}$ and the number of residues was accounted for in order to determine the mean molar ellipticity per residue as $\text{deg cm}^2 \text{dmol}^{-1}$. Once this conversion was calculated, the mean molar ellipticity per residue was determined at each wavelength on the CD spectrum.

The CD spectra of WT Lp-PLA₂, Lp-PLA₂ inhibited with SB-56 and Lp-PLA₂ inhibited with JMN21 did not show any apparent differences. All inhibited samples studied remained fully folded, thereby confirming that the loss of activity was only due to inhibition at the active site. Analysis with the K2D3 software predicted no significant differences in the α -helices or β -sheets for any of the inhibited Lp-PLA₂ samples, also indicating no significant changes to the secondary structure upon inhibitor binding [25].

Taken together, this data confirms that the carbamate inhibitors JMN4 and JMN21, which were developed from a high throughput screening at The Scripps Research Institute Molecular Screening Center and optimized in the Cravatt lab at The Scripps Research Institute, are potent and selective inhibitors of Lp-PLA₂. The selectivity of the inhibitor was confirmed in representative mouse and human models.

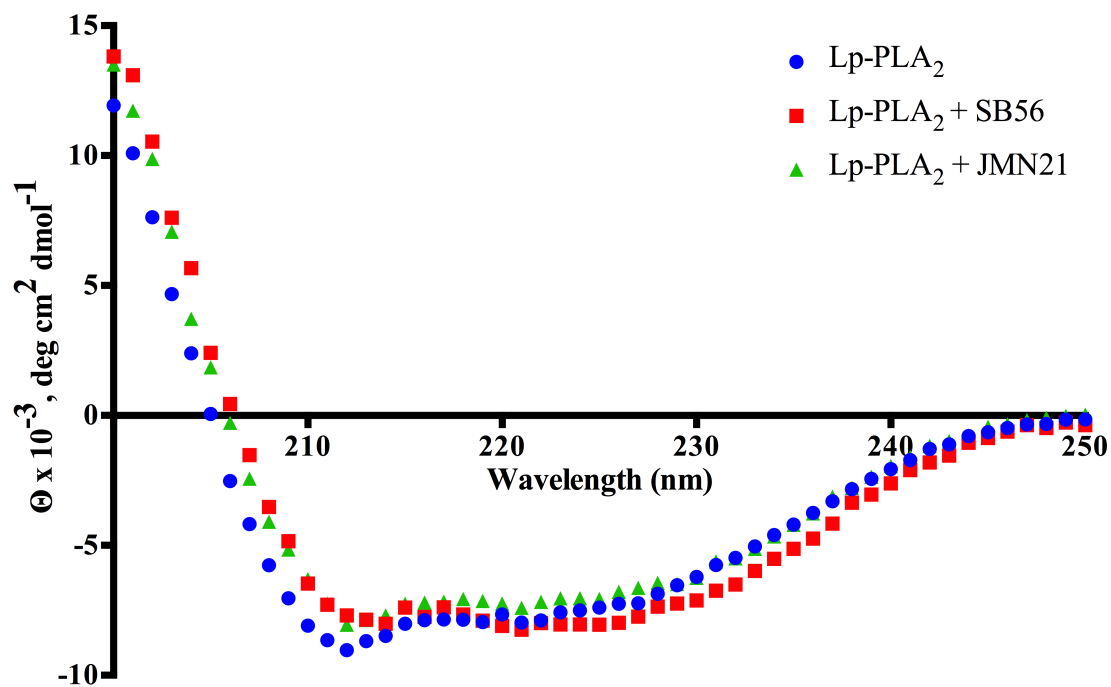


Figure 3.11: Circular dichroism analysis of Lp-PLA₂ with inhibitors. Active Lp-PLA₂ represented with blue circles, Lp-PLA₂ inhibited with the darapladib derivative SB-56 shown in red squares and Lp-PLA₂ inhibited with carbamate JMN21 represented with green triangles. There are no significant changes in the spectrum for any of the constructs.

this inhibitor is mechanistically different than darapladib, as the carbamate forms a covalent bond with the active site serine while darapladib is presumed to be a reversible active site inhibitor. The CD secondary structure analysis revealed that no significant changes occurred to Lp-PLA₂ in the presence of either inhibitor compound.

3.4 Conclusions

In summary, a high throughput inhibitor screen was carried out at the Molecular Libraries Screening Center Network at The Scripps Research Institute, and a variety of new compounds, which display inhibition of Lp-PLA₂, were determined. The most prominent inhibitor leads were determined to be from a class of compounds known as carbamates. These compounds have been shown to demonstrate excellent selectivity with serine hydrolases *in vivo* and inhibit through a reaction with nucleophilic serine, resulting in a covalent bond at the active site. The top hits from the screen were optimized by the lab of Dr. Ben Cravatt of The Skaggs Institute for Chemical Biology at The Scripps Research Institute and the potency and selectivity of the new compounds were determined. It was determined that the optimized inhibitor, JMN4, demonstrated both increased potency and selectivity for Lp-PLA₂.

The optimized inhibitor, JMN4, was then studied in comparison to the GlaxoSmithKline inhibitor darapladib. Through a variety of activity-based protein profiling experiments, it was determined that JMN4 was as selective of an inhibitor *in vitro* and *in situ* as darapladib. It was, however, determined that the IC₅₀ of darapladib is significantly lower than that of JMN4, 0.25 nM and 5.9 nM, respectively.

A similar optimized carbamate inhibitor, JMN21, was sent to our lab for further analysis. This compound has an IC₅₀ of 2.8 nM and was used in recombinant studies to compare its inhibitory effects to that of two darapladib derivatives, SB-

567952 and SB-595058. Using the PNPA assay previously described in Chapter 2, it was shown that initial inhibition with either the carbamate inhibitor JMN21 or darapladib derivatives SB-56 or SB-59 was identical. However, after 60 days, the catalytic activity of the darapladib inhibited compounds returned, while the activity of the JMN21 inhibited Lp-PLA₂ did not. This plays to the nature of darapladib binding Lp-PLA₂ in a reversible manner and JMN21 binding covalently at the nucleophilic Ser273. In addition, the CD spectra of WT Lp-PLA₂, Lp-PLA₂ inhibited with SB-56 and Lp-PLA₂ inhibited with JMN21 did not show any apparent differences, confirming loss of activity was only due to inhibition at the active site. Using this data, models of inhibitor binding will be presented in the next chapter.

REFERENCES

1. Kolodgie, F. D. *et al.* Lipoprotein-associated phospholipase A2 protein expression in the natural progression of human coronary atherosclerosis. *Arterioscler. Thromb. Vasc. Biol.* **26**, 2523–9 (2006).
2. Tselepis, A. F., Rizzo, M. & Goudevenos, I. A. Therapeutic modulation of lipoprotein-associated phospholipase A2 (Lp-PLA₂). *Curr. Pharm. Des.* **17**, 3656–61 (2011).
3. Boyd, H. F. *et al.* Potent, orally active inhibitors of lipoprotein-associated phospholipase A(2): 1-(biphenylmethylamidoalkyl)-pyrimidones. *Bioorg. Med. Chem. Lett.* **12**, 51–5 (2002).
4. Blackie, J. A. *et al.* The discovery of SB-435495. A potent, orally active inhibitor of lipoprotein-associated phospholipase A(2) for evaluation in man. *Bioorg. Med. Chem. Lett.* **12**, 2603–6 (2002).
5. Blackie, J. A. *et al.* The identification of clinical candidate SB-480848: a potent inhibitor of lipoprotein-associated phospholipase A2. *Bioorg. Med. Chem. Lett.* **13**, 1067–70 (2003).
6. Mohler, E. R. *et al.* The effect of darapladib on plasma lipoprotein-associated phospholipase A2 activity and cardiovascular biomarkers in patients with stable coronary heart disease or coronary heart disease risk equivalent: the results of a multicenter, randomized, double-bl. *J. Am. Coll. Cardiol.* **51**, 1632–41 (2008).
7. Serruys, P. W. *et al.* Effects of the direct lipoprotein-associated phospholipase A(2) inhibitor darapladib on human coronary atherosclerotic plaque. *Circulation* **118**, 1172–82 (2008).
8. White, H. *et al.* Study design and rationale for the clinical outcomes of the STABILITY Trial (STabilization of Atherosclerotic plaque By Initiation of darapLadIb TherapY) comparing darapladib versus placebo in patients with coronary heart disease. *Am. Heart J.* **160**, 655–61 (2010).
9. White, H. D. *et al.* Darapladib for preventing ischemic events in stable coronary heart disease. *N. Engl. J. Med.* **370**, 1702–11 (2014).

10. O'Donoghue, M. L. *et al.* Study design and rationale for the Stabilization of pLaques using Darapladib-Thrombolysis in Myocardial Infarction (SOLID-TIMI 52) trial in patients after an acute coronary syndrome. *Am. Heart J.* **162**, 613–619.e1 (2011).
11. O'Donoghue, M. L. *et al.* Effect of darapladib on major coronary events after an acute coronary syndrome: the SOLID-TIMI 52 randomized clinical trial. *JAMA* **312**, 1006–15 (2014).
12. Fenning, R. S. *et al.* Atherosclerotic plaque inflammation varies between vascular sites and correlates with response to inhibition of lipoprotein-associated phospholipase A2. *J. Am. Heart Assoc.* **4**, (2015).
13. Nagano, J. M. G., Hsu, K. L., Whitby, L. R., Niphakis, M. J., Speers, A. E., Brown, S. J., Spicer, T., Fernandez-Vega, V., Ferguson, J., Hodder, P., Srinivasan, P., Gonzalez, T. D., Rosen, H., Bahnson, B. J., and Cravatt, B. F. Selective inhibitors and tailored activity probes for lipoprotein-associated phospholipase A(2). *Bioorg. Med. Chem. Lett.* **23**, 839–43 (2013).
14. Bachovchin, D. A., Brown, S. J., Rosen, H. & Cravatt, B. F. Identification of selective inhibitors of uncharacterized enzymes by high-throughput screening with fluorescent activity-based probes. *Nat. Biotechnol.* **27**, 387–94 (2009).
15. Liu, Y., Patricelli, M. P. & Cravatt, B. F. Activity-based protein profiling: the serine hydrolases. *Proc. Natl. Acad. Sci. U. S. A.* **96**, 14694–9 (1999).
16. Alexander, J. P. & Cravatt, B. F. Mechanism of carbamate inactivation of FAAH: implications for the design of covalent inhibitors and in vivo functional probes for enzymes. *Chem. Biol.* **12**, 1179–87 (2005).
17. Hsu, K.-L. *et al.* DAGL β inhibition perturbs a lipid network involved in macrophage inflammatory responses. *Nat. Chem. Biol.* **8**, 999–1007 (2012).
18. Hoover, H. S., Blankman, J. L., Niessen, S. & Cravatt, B. F. Selectivity of inhibitors of endocannabinoid biosynthesis evaluated by activity-based protein profiling. *Bioorg. Med. Chem. Lett.* **18**, 5838–41 (2008).
19. Bachovchin, D. A. *et al.* Superfamily-wide portrait of serine hydrolase inhibition achieved by library-versus-library screening. *Proc. Natl. Acad. Sci. U. S. A.* **107**, 20941–6 (2010).
20. Satoh, T. & Hosokawa, M. Structure, function and regulation of carboxylesterases. *Chem. Biol. Interact.* **162**, 195–211 (2006).

21. Vainio, P. *et al.* Phospholipase PLA2G7, associated with aggressive prostate cancer, promotes prostate cancer cell migration and invasion and is inhibited by statins. *Oncotarget* **2**, 1176–90 (2011).
22. Weerapana, E. *et al.* Quantitative reactivity profiling predicts functional cysteines in proteomes. *Nature* **468**, 790–5 (2010).
23. Adibekian, A. *et al.* Optimization and characterization of a triazole urea inhibitor for platelet-activating factor acetylhydrolase type 2 (PAFAH2). (2013). at <<http://www.ncbi.nlm.nih.gov/books/NBK133429/>>
24. Chang, J. W. *et al.* Selective inhibitor of platelet-activating factor acetylhydrolases 1b2 and 1b3 that impairs cancer cell survival. *ACS Chem. Biol.* **10**, 925–32 (2015).
25. Louis-Jeune, C., Andrade-Navarro, M. A. & Perez-Iratxeta, C. Prediction of protein secondary structure from circular dichroism using theoretically derived spectra. *Proteins* **80**, 374–81 (2012).

Chapter 4

STRUCTURAL ANALYSIS OF LP-PLA₂ COMPLEXES

4.1 Introduction

The high resolution structure of ligand-free Lp-PLA₂ was solved using x-ray diffraction data collected to a resolution of 1.5 Å [1]. In addition, five structures of Lp-PLA₂ complexed with the organophosphorus (OP) compounds paraoxon, DFP, sarin, soman or tabun were solved to a resolution of 2.1, 2.3, 2.1, 1.7 and 1.7 Å respectively [2]. The ligand-free structure as well as the OP-complexed structures have allowed for the development of a model of Lp-PLA₂ bound to a hydrophobic/hydrophilic interface using the orientation of proteins in membranes (OPM) method developed by A. Lomize [3,4]. Using the OPM model, the predicted interface (i-face) binding regions of Lp-PLA₂ were determined and a working model of how substrates enter the active site of the enzyme was developed. The catalytic triad is positioned inside the hydrophobic pocket, facing the aqueous phase and sitting above the membrane interface. This allows for substrates to enter the active site from the aqueous phase or lipoprotein carriers, supporting other experimental findings [5-7].

In addition to the information about the active site provided by the OPM model, the Lp-PLA₂-OP complexes provided insight into the enzyme's hydrolase activity. The three catalytic residues, Ser273, Asp296 and His351, as well as neighboring active site residues, are positioned around the Lp-PLA₂-OP complex in a manner consistent with the tetrahedral intermediate of the esterolysis reaction. In each complexed structure, the amide nitrogens of Leu153 and Phe274 form hydrogen bonds

with an oxygen atom on the OP moiety, corresponding with the enolate oxygen of a tetrahedral intermediate [2]. Though the structures of the Lp-PLA₂-OP complexes provide insight into the hydrolase mechanism of the enzyme and allow for the prediction of active site access, these OP complex structures do not serve as definitive models of the physiological substrates of the enzyme.

Crystallization screens were performed with the aim of determining the structures of Lp-PLA₂ complexed with two specific and potent inhibitors, darapladib and JMN21, the carbamate inhibitor developed through high throughput screening as discussed in Chapter 3 [8]. Using the structures of the ligand-free Lp-PLA₂ as well as the OP complexed structures, models have been developed to represent the interaction of Lp-PLA₂ with the inhibitors, darapladib and JMN21, as well as with its native substrate, PAF.

4.2 Materials and Methods

4.2.1 Materials

The crystallography screening kits, including Screen 1, Screen 2, PEG/Ion, A/S grid, and additive screens were purchased from Hampton Research. Ammonium sulfate and xylitol were purchased from Sigma-Aldrich. The isopropanol and MES (2-(4-Morpholino)ethane Sulfonic Acid, 2-(N-Morpholino)ethanesulfonic acid hydrate) are from Fisher Scientific.

4.2.2 Crystallization screens

Recombinant Lp-PLA₂ samples, both wild type and I120A/L123A/L124A lipoprotein binding mutant, were screened for crystallization of Lp-PLA₂ inhibitor complexes. Each protein sample was expressed and purified as described in Chapter 2

and concentrated in a buffer of 10 mM Tris Base, pH 7.8 containing 0.01% w/v CHAPS. The Lp-PLA₂ samples used for crystallization ranged in purity from 95 – 97%, as determined by Image_J, and the concentrations screened ranged from 3.7 – 6.5 mg/mL, estimated from the BCA assay.

Hampton Research screening kits were used as starting points for determining appropriate crystallization conditions for Lp-PLA₂. The protein sample was mixed with an equal volume of well solution (1 µL each) and the hanging drop vapor diffusion method was used. In this method the protein solution drop is placed on a cover slip, and then affixed to 48- or 24- well pre-greased plates from Hampton Research. After initial crystal hits were identified, the crystallization well conditions were optimized by refining the crystallization conditions through trials in which one variable was altered.

With the ultimate goal of co-crystallization of Lp-PLA₂ with either the darapladib derivative, SB-56, or the carbamate inhibitor, JMN21, two crystallization methods were approached in parallel. The first aimed to determine conditions in which non-inhibited, or apo, Lp-PLA₂ formed diffraction quality crystals. Once the ligand free enzyme crystals are grown, they are then soaked with the inhibitor in order to form the Lp-PLA₂-inhibitor complex. Alternatively, the enzyme is incubated with saturating concentrations of inhibitor prior to laying the crystal screen. Using this co-crystallization method, any protein crystals that form will be of the Lp-PLA₂-inhibitor complex.

The crystals were visualized using a Nikon SMZ 1500 stereomicroscope whose software provided a method for measuring the crystal dimensions. Suitable crystals were picked from their drops using cryo-loops and transferred into a cryo-

protectant solution of 25% xylitol. The cryo-protectant solution was composed of a 100% xylitol solution mixed with an appropriate volume of well solution to achieve the desired concentration. Immediately upon removal from the cryo-protectant, the crystals were flash frozen by submersion in liquid nitrogen. The crystal screening was carried out using our home source x-ray diffraction equipment comprised of a Rigaku RU-H3R with R-axis IV detector.

4.2.3 AutoDock4 modeling

Molecular docking calculations were carried out using the program AutoDock4.2 and AutoDockTools1.5.4 (Scripps) due to its capabilities of predicting side chain motions as well as covalently attached ligands [9]. The crystal structure of human Lp-PLA₂ (PDB 3D59) was used to model the two inhibitor complexes as well as the natural substrate, platelet activating factor (PAF) covalently bound to Ser273 as a tetrahedral intermediate [1]. The structure files for the inhibitor and substrate ligands were created using ChemDraw 14.0 and converted to .pdb files using iBabel 4.

For the Lp-PLA₂ structure, all water molecules were removed, non-polar hydrogen molecules were merged and Gasteiger charges were applied using AutoDockTools1.5.4. The ligands, which will be discussed in more detail later in the chapter, were also assigned Gasteiger charges. Flexible residues predicted to make contact with the ligands were selected from the Lp-PLA₂ molecule and torsions were assigned to these residues, which was then subsequently saved as a flexible .pdbqt file. The residues without torsions were also saved as a rigid .pdbqt file and used to compute the grid boxes using AutoGrid4. Docking calculations were performed using AutoDock4.2 and the Lamarckian genetic algorithm using the default parameters with the exception of energy evaluations set to 5.0 million [10]. For each docking

experiment, 100 – 200 conformations were computed, and the results were clustered within a 2.0 Å tolerance. The most populated clusters with the most ideal predicted free energy of binding were selected for further analysis. All ligand and inhibitor conformations, as well as docking experiments were visualized using the Python Molecular Viewer (PMV) [11,12].

4.2.3.1 Docking with darapladib

The structure of darapladib contains 14 rotatable bonds, discussed in detail in the results section 4.3.2 and shown in Figure 4.4. AutoDock4.2 contains a limit of 32 total torsions for computation; therefore it was necessary to keep the torsions in the flexible residue files to 18 or fewer. There were three different flexible residues sets created to generate the maximum amount of possible dockings for darapladib on Lp-PLA₂, referred to as 1GSK, 2GSK and 3GSK which are listed in Table 4.1. Grid boxes were centered on Ser273 and contained 70 points in the X and Z directions and 60 points in the Y direction of 0.375 Å spacing to ensure complete coverage of the binding pocket. Grid maps were created using AutoGrid4 for each type of atom present in darapladib and Lp-PLA₂, which included maps for carbon (C), aromatic carbon (A), fluorine (F), oxygen (aromatic OA), nitrogen (N, aromatic NA), sulfur (aromatic SA), hydrogen (HD) as well as an electrostatic potential map (e) and a desolvation potential map (d).

The docking calculations were performed using AutoDock4.2 and the Lamarckian genetic algorithm was used as previously described. Clustering was performed to 2.0 Å and those clusters with the highest number of conformations and the most ideal energy conformations were selected for further analysis. Any interactions (hydrogen bonding, stacking, hydrophobic interactions, etc.) between

darapladib and the residues of Lp-PLA₂ were taken into account to determine the most appropriate binding mode.

Table 4.1: Flexible residues for darapladib dockings. Catalytic residues underlined.

	1GSK	2GSK	3GSK
Flexible Residues	<u>Ser273</u> , <u>Asp296</u> , <u>His351</u> ,	<u>Ser273</u> , <u>Phe274</u> , <u>His351</u> ,	<u>Ser273</u> , <u>Phe274</u> , <u>His351</u> , <u>Gln352</u>
Torsions	7	7	10

4.2.3.2 Docking with JMN21

As described in chapter 3 (and shown in Fig. 3.2) the carbamate inhibitor JMN21 forms a covalent complex with Ser273 of Lp-PLA₂. In order to create a covalent docking of a ligand such as JMN21, two approaches have been reported. The first uses a grid based approach and the second models the inhibitor onto the flexible side chain [9]. Using the grid-based approach, covalent maps were created centered on the OG atom of Ser273 and contained 2 points in each direction of 0.375 Å spacing to only cover the location of binding. The grid maps created for the grid-based covalent docking included carbon (C, covalent CZ), aromatic carbon (A), oxygen (aromatic OA, covalent OZ), nitrogen (N, aromatic NA), hydrogen (HD) as well as an electrostatic potential map (e) and a desolvation potential map (d) and carried out using AutoGrid4. The docking calculations were performed using AutoDock4.2 and the Lamarckian genetic algorithm was used as previously described.

The second approach to covalent docking involved modeling the inhibitor (JMN21) onto the flexible residue file (.pdbqt) by superimposing the coordinates onto

the OG atom of Ser273 and docking a water molecule as the ligand. Using this approach four different flexible files were created, referred to as 1JMN, 2JMN, 3JMN and 4JMN whose flexible residues are listed in Table 4.2. Grid boxes were centered on Ser273 and contained 55 points in the X and Y directions and 65 points in the Z direction of 0.375 Å spacing to demonstrate adequate coverage of the binding pocket. Grid maps were created for each type of atom present in JMN21 and Lp-PLA₂, which included maps for carbon (C), aromatic carbon (A), oxygen (aromatic OA), nitrogen (N, aromatic NA), hydrogen (HD) as well as an electrostatic potential map (e) and a desolvation potential map (d). The docking calculations were performed using AutoDock4.2 and the Lamarckian genetic algorithm creating 100 conformations and performing 2,500,000 evaluations. Clustering was performed with a 2.0 Å tolerance and analysis of docked conformations was performed as previously described.

Table 4.2: Flexible residues for JMN21 docking. Inhibitor built on to active site Ser273, all catalytic residues underlined.

	1JMN	2JMN	3JMN	4JMN
Flexible residues	<u>Ser273</u>	<u>Ser273</u> , <u>Asp296</u> , <u>His351</u>	<u>Ser273</u> , Phe274, <u>His351</u>	<u>Ser273</u> , Phe274, <u>His351</u> , Gln352
Torsions	3	7	7	10

4.2.3.3 Docking with PAF

Using the superimposed coordinate covalent docking technique previously described for JMN21 modeling, a model of the enzyme's substrate PAF was created to mimic the tetrahedral intermediate of the catalytic reaction. The substrate PAF was

assigned flexibility to 12 torsions, and the long C₁₈ chain's torsions were fixed at a 180 degree torsion angle to be non-rotatable. There were three different flexible residue files created, 1PAF, 2PAF and 3PAF, whose residues are shown in Table 4.3. The grid maps were centered on Ser273 and contained 70 points in the X and Z directions with 55 points in the Y direction with spacing of 0.375 Å to fully cover the binding pocket. The docking maps, which were created using AutoGrid4, included maps for each atom type present in PAF as well as the enzyme and contained carbon (C), aromatic carbon (A), phosphorus (P), oxygen (aromatic OA), nitrogen (N), hydrogen (HD) in addition to the electrostatic potential map (e) and a desolvation potential map (d). The program AutoDock4.2 was used for the docking calculation with the Lamarckian genetic algorithm. For each set of flexible residues, 200 conformations were created with 5 million energy evaluations. Clustering was performed with a 2.0 Å tolerance and analysis of docked conformations was performed as previously described.

Table 4.3: Flexible residues of PAF docking. Inhibitor built on to active site Ser273, all catalytic residues underlined.

	1PAF	2PAF	3PAF
Flexible Residues	<u>Ser273, Asp296,</u> <u>His351</u>	<u>Ser273, Phe274,</u> Gln352	<u>Ser273, Phe274,</u> <u>His351, Gln352</u>
Torsions	7	8	10

4.3 Results and Discussion

4.3.1 Crystallization of Lp-PLA₂

Crystal screens were performed in parallel using the WT Lp-PLA₂ and the I120A/L123A/L124A lipoprotein binding mutant for both apo-enzyme as well as enzyme pre-mixed with saturating concentrations of either the darapladib derivative SB-56 or the carbamate inhibitor JMN21. Crystals began to form 4-6 weeks after the trays were laid, similar to the time frame previously reported for the crystal formed by the protein from the ICOS Corporation [1,2].

Using the WT apo LP-PLA₂, 97% pure and concentrated to 6.5 mg/mL, an initial hit was found using Hampton Research Screen 1, condition 32, containing 2.0 M ammonium sulfate. The protein crystals, like the one shown in Figure 4.1, were monoclinic in shape and were between 100 and 150 μm in size. These conditions were replicated for both the WT Lp-PLA₂ and the apo-enzyme of the I120A/L123A/L124A lipoprotein binding. A single Lp-PLA₂ crystal, obtained from the WT apo screen, was picked, cryo-protected and flash frozen as described previously. The crystal was exposed to the beam four times, 30 min each, and did not diffract, as seen in Figure 4.1. Though this crystal was not suitable for structural determination, it gives an excellent starting point to screen around in order to determine conditions that produce diffraction quality crystals.

Crystals of the Lp-PLA₂ I120A/L123A/L124A lipoprotein binding mutant pre-mixed with saturating concentrations of the darapladib derivative SB-56 were observed after 4-5 weeks. The enzyme sample was 97% pure and concentrated to 6.2 mg/mL, in a 10 mM Tris Base buffer, pH 7.8, containing 0.01% w/v CHAPS, 4% v/v methanol. Two different well solutions resulted in the formation of protein crystals.

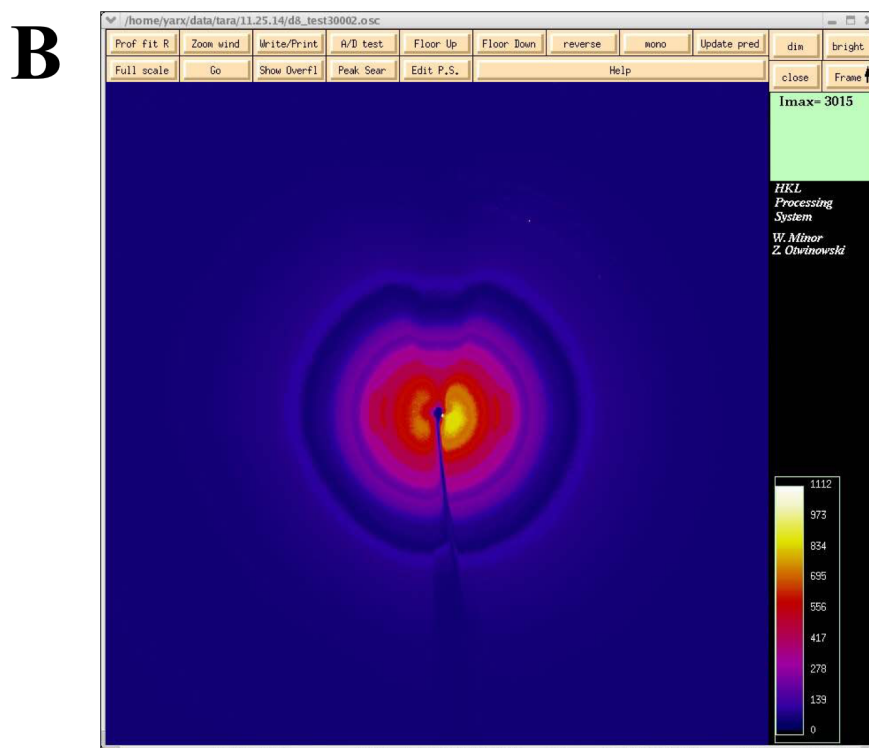
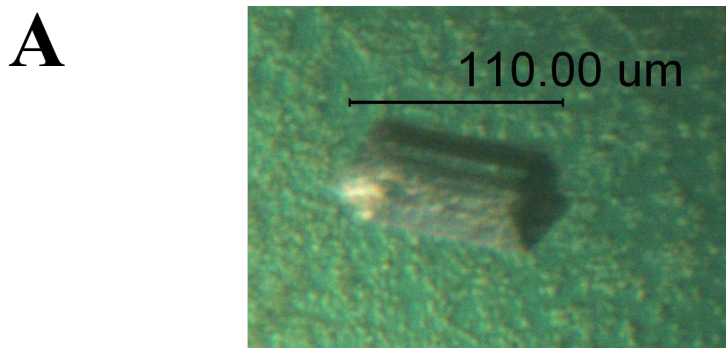


Figure 4.1: Lp-PLA₂ crystal diffraction. (A) WT apo-enzyme crystal. Protein was 6.5 mg/mL, 97% pure in a buffer of 10 mM Tris pH 7.8, 0.01% CHAPS, with a well solution of 2.0 M Ammonium Sulfate. (B) Diffraction of Lp-PLA₂ crystal from panel (A), there were no spots indicating that this is a protein crystal and not salt, however the crystal did not diffract and could not be indexed.

The first condition was the same as the apo-structure, 2.0 M ammonium sulfate. These crystals were long, thin monoclinic rods with the largest face measuring between 200 and 400 μm in size (Figure 4.2). The second crystallization condition, which yielded protein crystals, was 2.0 M ammonium sulfate and 5% isopropanol. These crystals were similarly shaped and measured between 100 and 150 μm (Figure 4.2). Both conditions were reproducible, however neither have been tested to determine diffraction.

Pre-mixing of both WT Lp-PLA₂ and the triple mutant with the carbamate inhibitor JMN21 resulted in crystal formation observed after 4-5 weeks. The enzyme samples used were 97% pure in a 10 mM Tris Base buffer, pH 7.8, containing 0.01% w/v CHAPS, 4% v/v DMSO. The WT Lp-PLA₂ enzyme sample was concentrated to 4.2 mg/mL while the I120A/L123A/L124A mutant sample was concentrated to 6.2 mg/mL. The I120A/L123A/L124A mutant inhibited with JMN21 formed crystals under the same conditions as this mutant inhibited with SB-56, as shown in Figure 4.3. The ammonium sulfate crystals of the triple mutant with JMN21 differed in shape from those inhibited with the darapladib inhibitor. The crystals grown in the ammonium sulfate and isopropanol were very similar to those previously shown with the SB-56 inhibitor.

A new condition was determined for the WT Lp-PLA₂ sample inhibited by JMN21, found using the Hampton Research A/S Grid Screen. The well solution was composed of 100 mM MES monohydrate pH 6.0, containing 2.4 M ammonium sulfate, and the crystals formed in a stick-like bundle (Figure 4.3). This was the first condition in which crystals formed in the presence of a buffered solution, and this condition was screened around with the aim of obtaining better-shaped crystals. Once

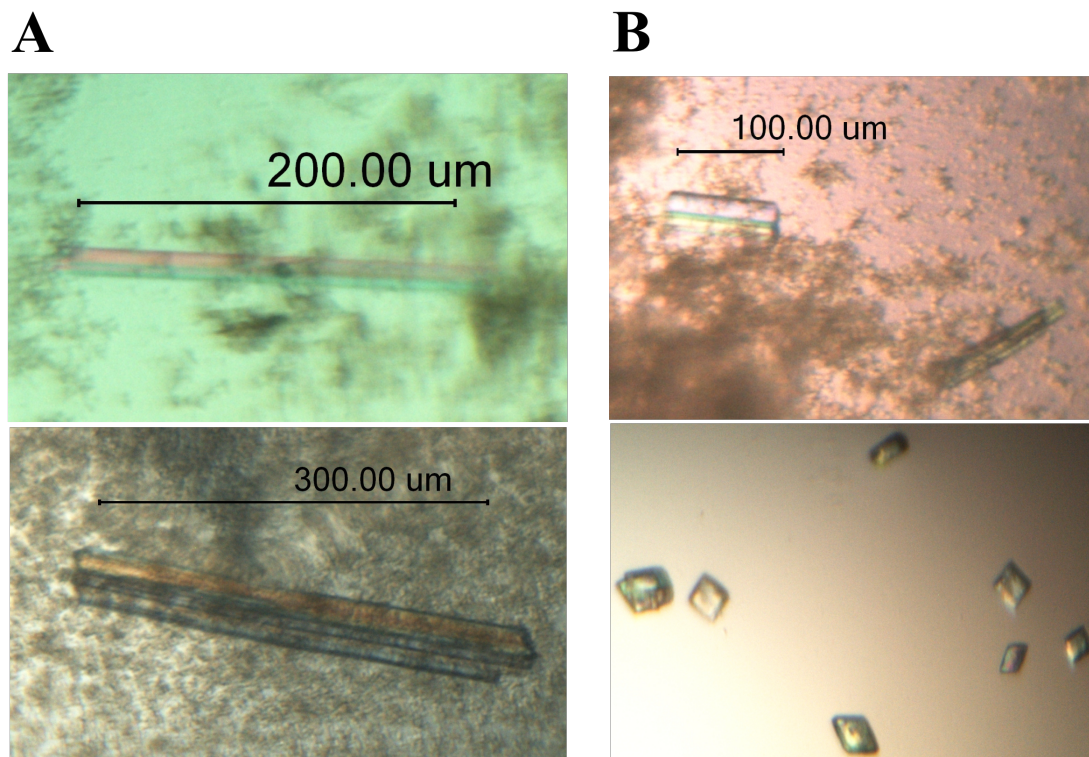


Figure 4.2: Crystals of Lp-PLA₂ inhibited with darapladib derivative SB-56. (A) Lipoprotein binding mutant I120A/L123A/L124A with the well solution of 2.0 M ammonium sulfate or (B) 2.0 M ammonium sulfate and 5% isopropanol. The bottom photo of (B) are crystals removed from the original drop and are therefore lacking amorphous precipitate seen in the other images

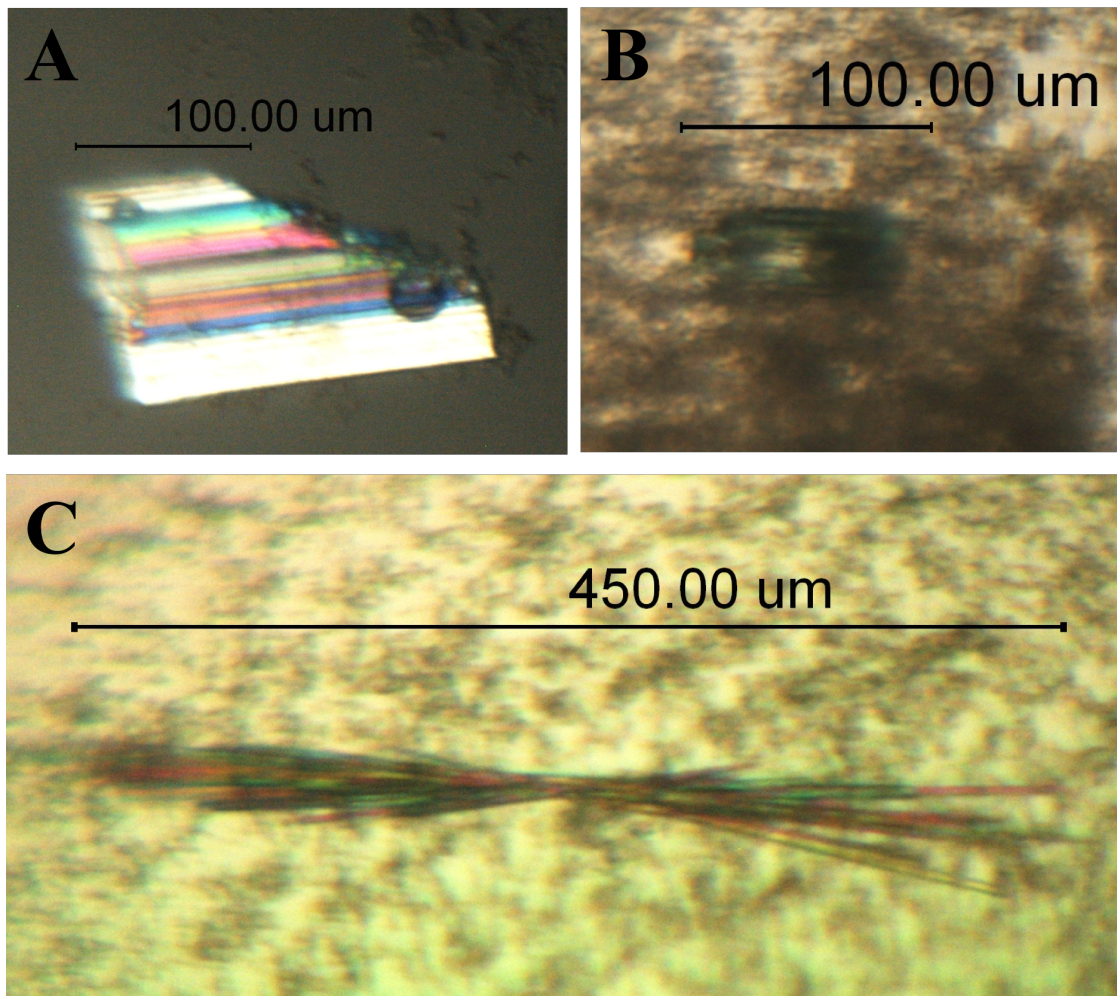


Figure 4.3: Crystals of Lp-PLA₂ inhibited with carbamate inhibitor JMN21. (A) Lp-PLA₂ lipoprotein binding mutant I120A/L123A/L124A with the well solution of 2.0 M ammonium sulfate or (B) 2.0 M ammonium sulfate and 5% isopropanol. (C) WT Lp-PLA₂ with a well solution of 100 mM MES monohydrate pH 6.0, containing 2.4 M ammonium sulfate.

again, the crystals of Lp-PLA₂ complexed with the carbamate inhibitor JMN21 have not yet been tested on our X-ray source, and their diffraction quality remains unknown.

4.3.2 Lp-PLA₂ complex models

Due to the lack of well diffracting crystals of Lp-PLA₂ complexed with the inhibitors SB-56 or JMN21, computational methods were employed in order to better understand their structure-function relationship. This was done using the high resolution crystal structure of ligand-free Lp-PLA₂ as well as the organophosphorus (OP) complexed LP-PLA₂ structures precisely determined in the lab as a guide, and the software AutoDockTools 1.4.5 and AutoDock 4.2 for the ligand docking [1,2,9].

In order to have successful docking of Lp-PLA₂ with the inhibitors darapladib and JMN21, as well as the substrate PAF, it was necessary to limit the number of rotatable bonds. The program allows for up to 32 torsions and the ligands on their own contain 14, 2, and 12, respectively. The side chains of those residues designated flexible also contain rotatable bonds, which are reported in Tables 4.1, 4.2 and 4.3. An increase in the amount of torsions has a direct impact on the free binding energies estimated by the AutoDock program. Though each combination of torsions was under the program limit of 32, any docking calculations performed with greater than 22 torsions resulted in free binding energy estimates greater than 10 Kcal mol⁻¹. For these reasons, the flexible ligand files were capped with a maximum of 10 torsions and the ligands were modified to contain a maximum of 12 torsions, as shown in Figure 4.4. This resulted in dockings with estimated free binding energies ranging from 0 to -10 Kcal mol⁻¹. The docked models of Lp-PLA₂ with each ligand, as well as the results of crystallization screening, will be discussed further in following sections.

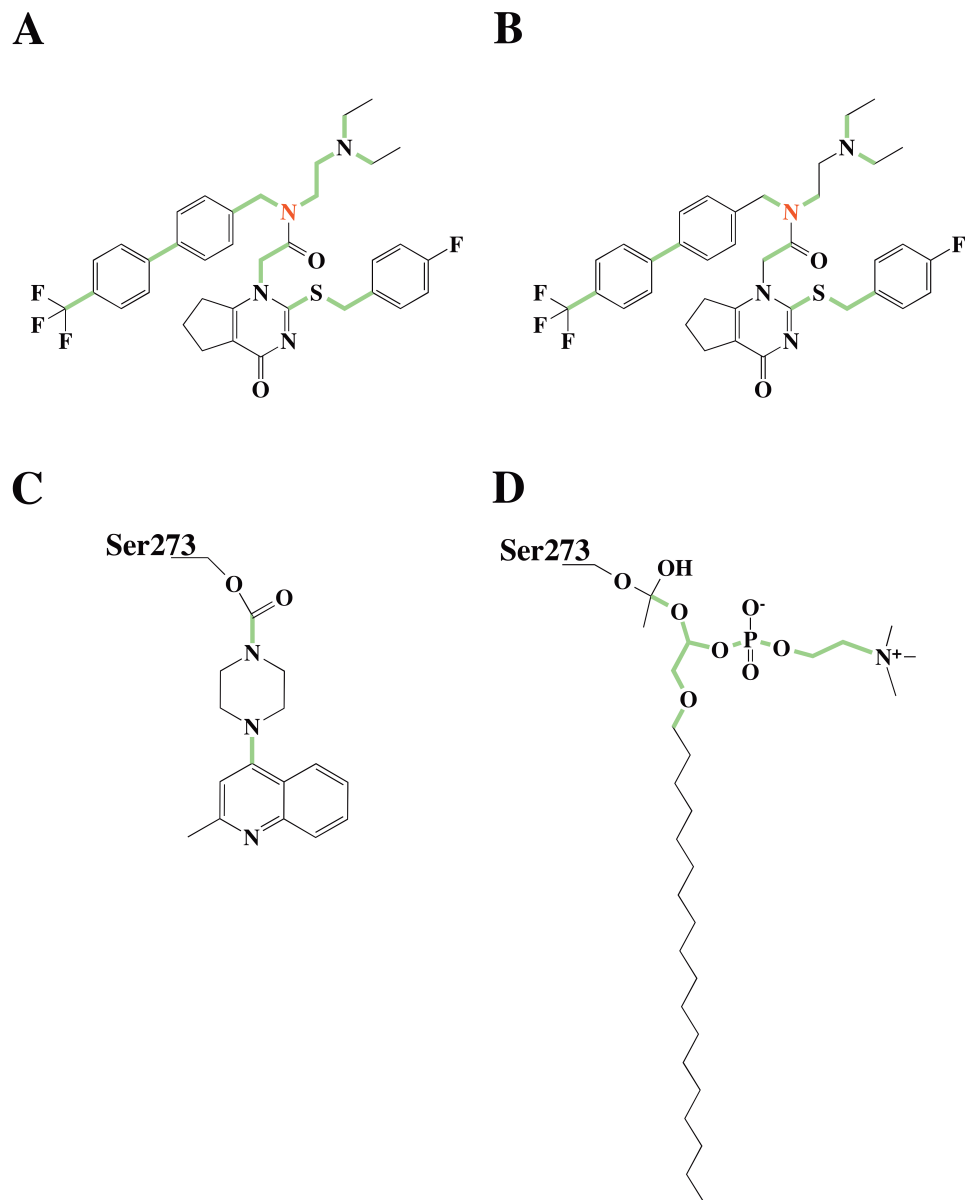


Figure 4.4: Ligands for AutoDock modeling. Rotatable bonds shown in green and bold, non-rotatable in black, and ligand root shown in red. (A) Darapladib with 14 torsions, as determined by AutoDockTools. (B) Darapladib with 10 torsions, as determined by AutoDockTools with the manual removal of 4 rotatable bonds. (C) JMN21 covalently bound to Ser273, containing 2 rotatable bonds (D) PAF intermediate covalently bound to Ser273 containing 11 torsions with the C₁₈ chain manually set to be non-rotatable

4.3.2.1 Lp-PLA₂-darapladib complex

The computational modeling of the Lp-PLA₂-darapladib complex was challenging for two reasons, the first being the large surface area for which the inhibitor is predicted to bind and the second is the number of rotatable bonds present in darapladib. The minimization of the surface area for the grid maps was not an option, therefore it was necessary to limit the number of rotatable bonds, as shown in Figure 4.4. Even with this minimization, there were still a large number of distinct conformations predicted in which 120-140 out of 200 dockings clustered within a 2 Å tolerance. This large number of distinct conformations was predicted using each of the three flexible residue files, shown in Table 4.1. It became necessary to perform a visual analysis of each binding prediction of those docked structures with free binding energies ranging from -10 to -5 Kcal mol⁻¹. The model of the Lp-PLA₂-darapladib complex in Figure 4.5 was selected due to its predicted interactions with the catalytic residues, positioning in the hydrophobic pocket, as well as its favorable free binding energy prediction.

The overall positioning of darapladib falls in the binding site pocket and stacks against the residues lining the hydrophobic pocket. The cyclopenta-pyrimidine ring moiety of darapladib projects backward into the core of the enzyme, and contains all predicted hydrogen bonds between the enzyme and darapladib. The model predicts three hydrogen bonding interactions as predicted by PyMOL, with the cyclopenta-pyrimidine ring moiety of darapladib [13]. The first hydrogen bond is between the OG atom of active site Ser273 and N4 atom of the cyclopenta-pyrimidine ring, thus inhibiting the catalytic activity of the enzyme. A second hydrogen bond is predicted from the model between the side chain nitrogen, ND1, of His351 and N4 of

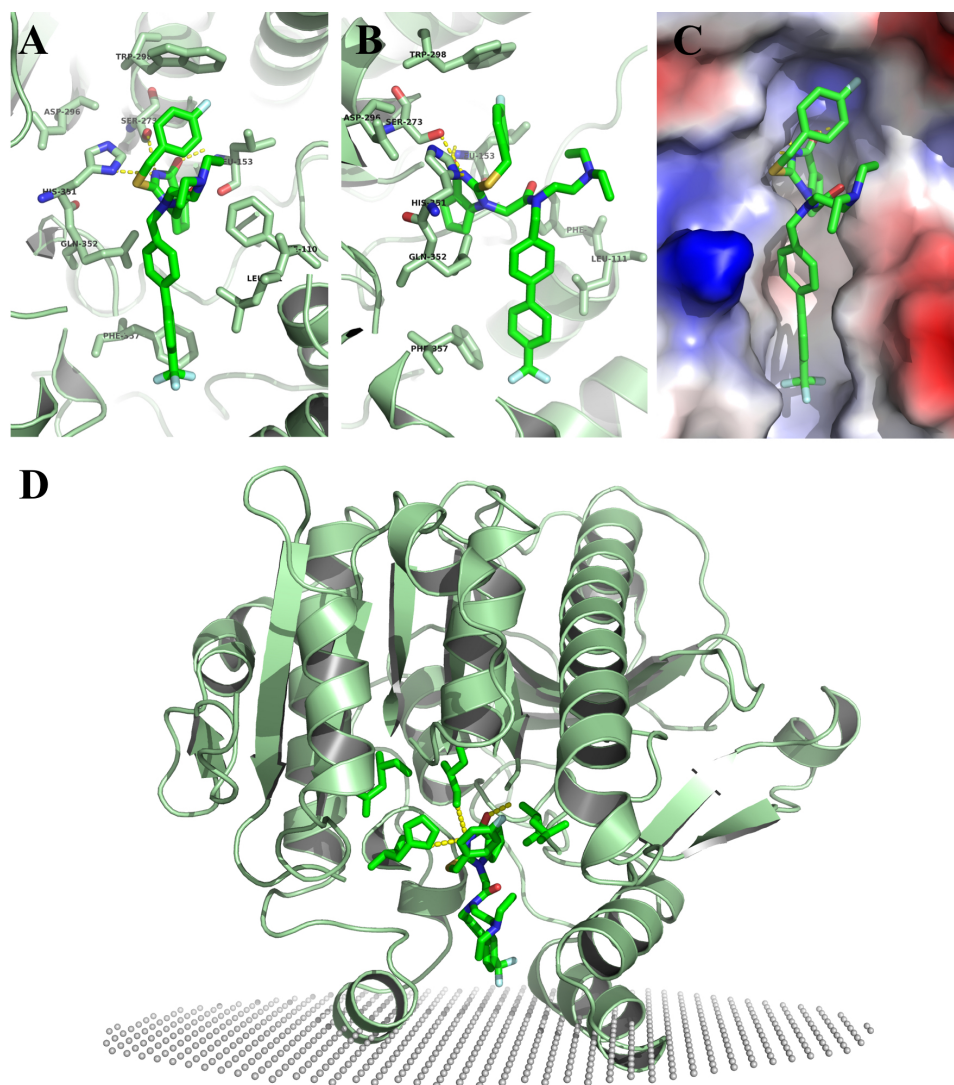


Figure 4.5: Lp-PLA₂ complexed with darapladib. (A) Darapladib, shown in bright green, and its interactions with Lp-PLA₂ active site. Hydrogen bonding interactions, shown as yellow dashes, with active site residues Ser273 and His351 as well as with residue Lys153. (B) 90° rotation around the Y-axis of Lp-PLA₂ from the image in (A) to better visualize the cyclopenta-pyrimidine ring moiety as well as the diethylpropan-amine moiety of darapladib. (C) Electrostatic surface of the hydrophobic pocket and positioning of darapladib and (D) OPM model of predicted darapladib interaction [4].

darapladib, the same nitrogen atom predicted to interact with Ser273. The final predicted interaction is between O2 of darapladib and the amide nitrogen of Leu153. This positioning of this moiety, and its predicted hydrogen bonds, prevents the necessary interactions between the active site residues for catalysis.

The hydrophobic interactions and π -stacking interactions of darapladib with Lp-PLA₂ were predicted using the Protein-Ligand Interaction Profiler online tool [14]. In addition to the hydrogen bonds on the cyclopenta-pyrimidine ring moiety, there is a predicted hydrophobic interaction between the cyclopentane ring and the side chain of Ala155. The fluorobenzyl sulfane moiety of darapladib is positioned under residue Trp298 and projects away from the core of the enzyme. There are hydrophobic interactions between this moiety and the side chains of residues Leu153 and Phe322, as well as two perpendicular π -stacking interactions with Trp298 between the aromatic ring centers. The small diethylpropan-amine moiety of darapladib is predicted to be located in the smaller *sn*-2 pocket of Lp-PLA₂. Finally, the trifluoromethyl-biphenyl moiety of darapladib lines the binding pocket and contains hydrophobic interactions with the side chain residues of Leu111, Gln352 and Leu371. In addition, there is a perpendicular π -stacking interaction between the terminal phenyl group and the aromatic center of Phe357.

After alignment of the Lp-PLA₂-darapladib model with the OPM plane, it is apparent that the inhibitor blocks substrates from entering the active site from the aqueous phase. Furthermore, all predicted interactions between Lp-PLA₂ and darapladib are non-covalent and provide further evidence that the inhibition is competitive and reversible.

4.3.2.2 Lp-PLA₂-JMN21 complex

There were two different approaches taken to model the covalently bound Lp-PLA₂-JMN21 complex, as described in the methods section. The first approach, in which covalent docking maps are created in the AutoDock program, was ultimately unsuccessful. The predicted binding models never contained a covalent bond between Ser273 and JMN21, even though the code for such a bond was written. It was necessary to superimpose the JMN21 complex onto the coordinates of Ser273 for each flexible ligand file. Visual inspection of these superimposed files was performed prior to running the docking calculations.

The models created which used only Ser273-JMN21 as the flexible residue file resulted in only one cluster containing all 100 docks. There was not enough flexibility in the residues to create distinct binding models, therefore it was necessary to increase the amount of torsions allowed for each docking calculation by adding additional amino acids to the flexible residue files. Using the Lp-PLA₂-OP complexes as a guide, the model of Lp-PLA₂-JMN21 complex was selected out of the most populated clusters with the lowest free energy of binding.

The final model shows that the carbamate inhibitor has a covalent bond at nucleophilic Ser273, as designed in Figure 4.6. There is a predicted hydrogen bonding interactions with side chain nitrogen of active site His351, NE2, as well as amide nitrogens on Leu153 and Phe274. The prediction of a hydrogen bond between the inhibitor and His351 maintains the residue in its protonated form. This form of His351 prevents the activation of a water molecule for nucleophilic attack and thus explains the stable inhibition of Lp-PLA₂ by this carbamate inhibitor. The interaction with Leu153 and Phe274 is slightly different than that of the OP complexes in that the

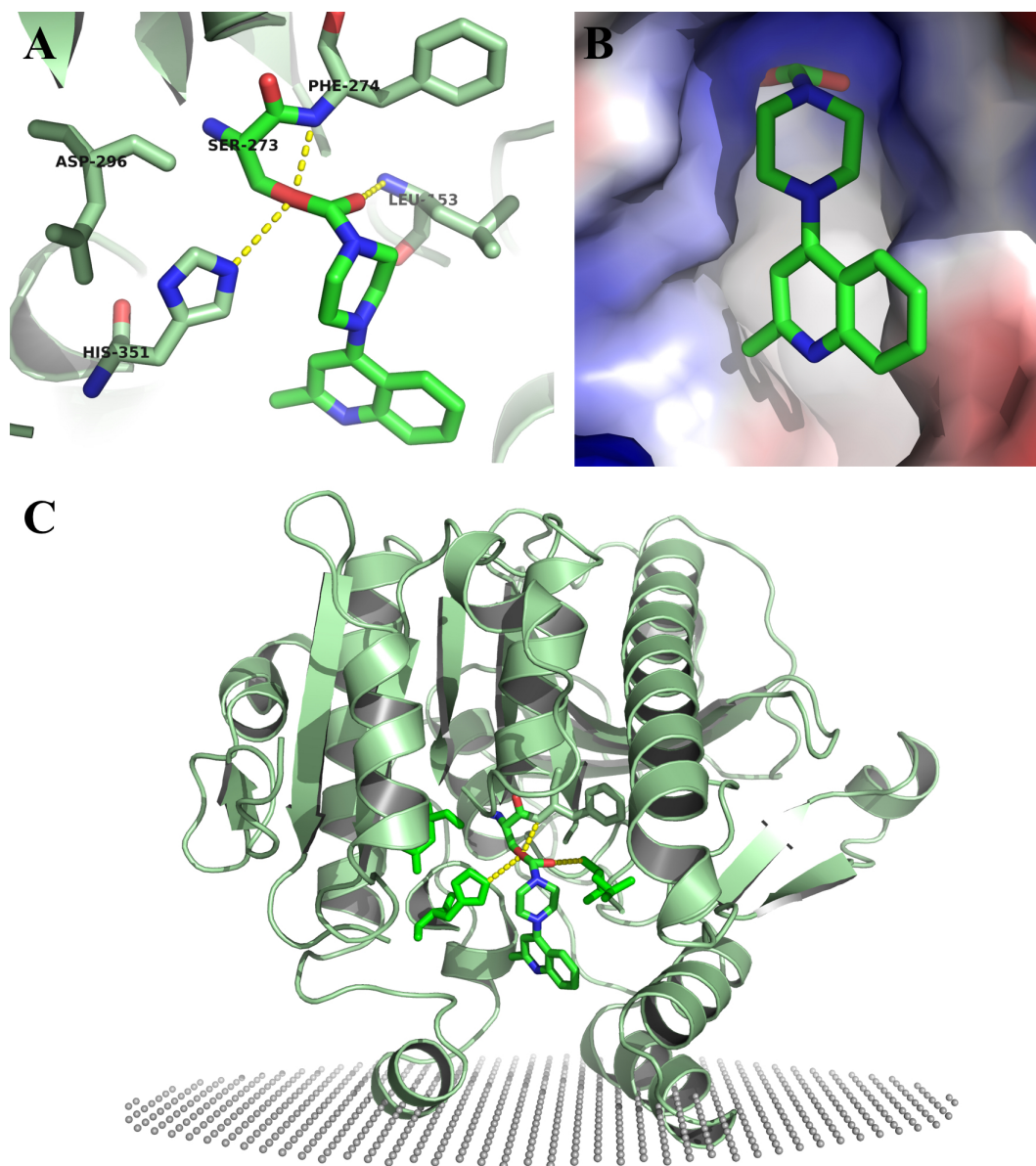


Figure 4.6: Lp-PLA₂ covalently complexed with JMN21. (A) JMN21, shown in bright green, and its interactions with Lp-PLA₂ active site. Hydrogen bonding interactions, shown as yellow dashes, with active site His351 as well as with residues Lys153 and Phe274. (B) Electrostatic surface of the hydrophobic pocket and positioning of JMN21 and (C) OPM model of predicted JMN21 interaction [4].

JMN21 compound is predicted to project out of the hydrophobic pocket. This projection of structure contrasts the tetrahedral intermediate mimics shown in the Lp-PLA₂-OP complexes.

4.3.2.3 Lp-PLA₂-PAF complex

A model of Lp-PLA₂ covalently complexed with its physiological substrate PAF was published in the initial crystal structure report for the enzyme [1]. This predicted binding interaction was created by substituting the paraoxon ligand from the structure with a speculative model of the tetrahedral intermediate of C₁₈-PAF. The modeling was performed by superimposing the coordinates of PAF on the nucleophilic Ser273, similar to the initial flexible ligand setup for the JMN21 docking. Using these superimposed coordinates of PAF on Ser273 as a starting point, modeling with the AutoDock program was performed in order to better validate the predicted binding interactions.

The modeling of Lp-PLA₂-PAF resulted in three distinct clusters, as shown in Figure 4.7, all with equal occupancy (50-60 conformations in each cluster, out of 200 total conformations) and similar predicted free binding energies. In each model, the short chain, representing the *sn*-2 chain of PAF, remains in a similar position, while the positioning of the C₁₈ chain varied. Using the predicted OPM model, which represents the interface between polar and nonpolar components of the membrane, it was apparent that the Lp-PLA₂-PAF docking model in Figure 4.7, panel C, is the most physiologically relevant. In this model, the long C₁₈ chain of the lyso-PAF moiety projects out of the active site and towards the solvent and polar portions of the membrane interface region. This is consistent with the hypothesis that the Lp-PLA₂ active site can bind substrates in the aqueous phase, as the long hydrophobic tail of

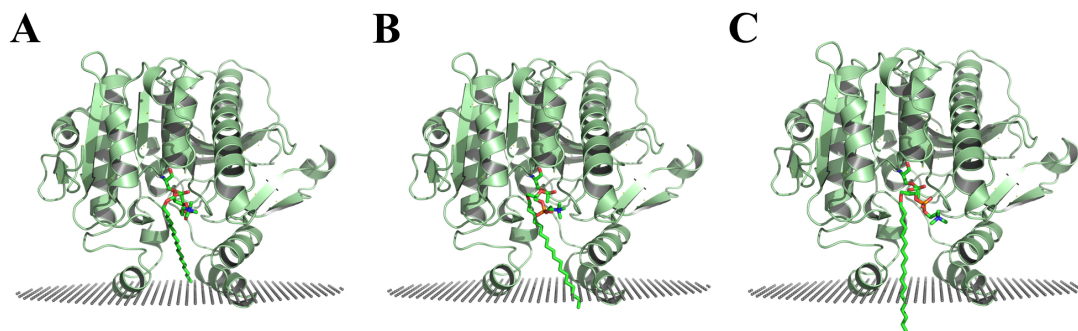


Figure 4.7: Predicted interactions of Lp-PLA₂ and PAF. In each figure, PAF is shown in bright green and the OPM predicted membrane interface in gray. The small *sn*-2 chain is similarly positioned in a small pocket. The C₁₈ chain of PAF is positioned (A) to the back, away from the interface (B) to the side near the α -helix predicted to bind the membrane, or (C) projecting down, towards the membrane interface, with predicted lipid interactions at the hydrophobic/hydrophilic interface.

PAF is partly imbedded in the interface between the hydrophobic and hydrophilic portions of the membrane.

The model of the Lp-PLA₂-PAF complex mimics the binding of a tetrahedral intermediate, similar to that reported of the OP complexes [1,2]. The shorter *sn*-2 chain of PAF, projects into a small pocket, near the hydrophobic core as shown in Figure 4.8. Based on the crystal structure, it was evident that this pocket is large enough to accommodate larger chains, however Lp-PLA₂ has a preference for short, polar, *sn*-2 chains. This preference is likely due to aqueous phase solubility and not related to the hydrophobic pocket size of Lp-PLA₂. This model of the Lp-PLA₂-PAF complex highlights the importance for *sn*-2 chains of oxidatively-fragmented phospholipids to flip away from the hydrophobic portion of the interface and allows them to be accessible to the active site residues.

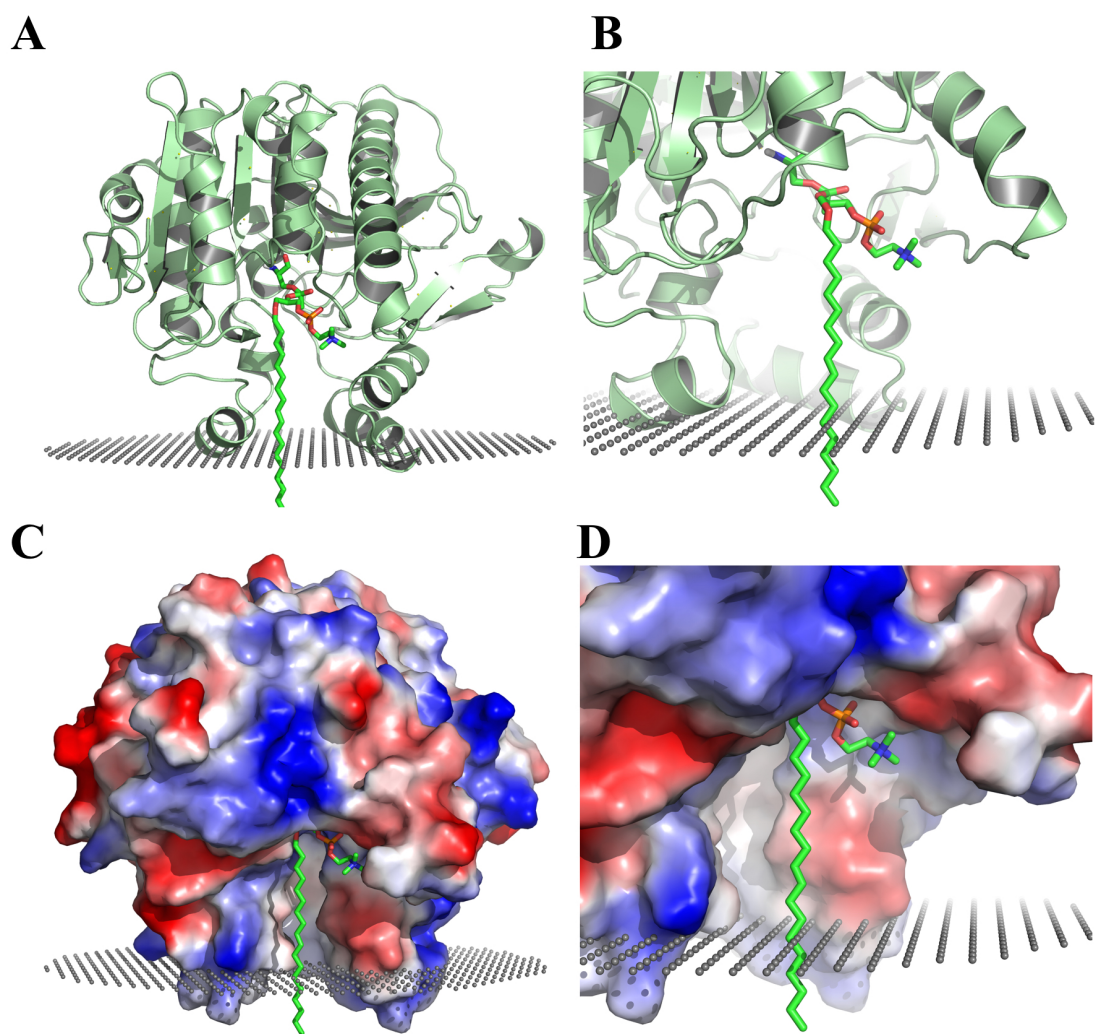


Figure 4.8: Lp-PLA₂ covalently complexed with PAF. (A) PAF, shown in bright green, shown as green ball and stick, at active site serine and its positioning in relationship to the hydrophobic/hydrophilic interface as predicted by the OPM method (B) Smaller, *sn*-2 chain of PAF and its positioning in the binding pocket (C) Electrostatic surface of the entire Lp-PLA₂-PAF interaction and (D) Electrostatic surface near small *sn*-2 chain of PAF

4.4 Conclusions

Highly purified and concentrated wild type Lp-PLA₂, as well as the lipoprotein binding mutant, I120A/L123A/L124A, were used for inhibitor complex crystallization screens. With the aim at determining the structure of Lp-PLA₂ complexed with the darapladib derivative, SB-56, or the carbamate inhibitor JMN21, two different approaches were taken. In the first, crystal screens were performed using apo-protein with the aim to soak in the inhibitor after crystals formed. Using the apo-enzyme, crystals formed when the well solution contained a high concentration of ammonium sulfate. When a single crystal was exposed to the x-ray, however, it did not diffract. Though this condition is not suitable for diffraction quality crystals, it is an excellent starting point to screen around.

The second approach at co-crystallization involves pre-mixing Lp-PLA₂ with inhibitors and then setting up the screen. The enzyme mixed with the darapladib inhibitor, SB-56, showed two conditions that resulted in protein crystals. The first condition was the same as that for the apo-enzyme, and the second also contained a high concentration of ammonium sulfate with the addition of isopropanol. Likewise, the carbamate inhibited Lp-PLA₂ produced crystals in these same conditions. In addition, it was shown that the enzyme inhibited by JMN21 produced needle-like crystals with the addition of a MES buffer at pH 6.0. Currently, all these conditions are being screened around in order to produce improved Lp-PLA₂ crystals that will diffract well enough for structural determination.

Due to the lack of co-crystal structures, computational methods were used to model the interaction of these inhibitors, as well as physiological substrate PAF, with Lp-PLA₂. The model of the Lp-PLA₂-darapladib complex consists of three hydrogen bond interactions at catalytic residues Ser273 and His351 as well as Leu153, thus

preventing the catalytic hydrolysis function of the enzyme. The inhibitor is predicted to lie in the hydrophobic pocket and prevent substrate from accessing the active site. The non-covalent interactions help to validate that darapladib is a reversible inhibitor.

In contrast, the carbamate inhibitor, JMN21, is covalently bound to the nucleophilic Ser273. The Lp-PLA₂-JMN21 model has three predicted hydrogen bonds with Leu153, Phe274 and His351. The hydrogen bond with His351 prevents the residue from deprotonating and therefore prevents the activation of a water molecule for nucleophilic attack. This interaction, in addition to the covalent bond to Ser273, helps explain the results presented in Chapter 3 in which recombinant Lp-PLA₂ inhibited with SB-56 showed a small amount of activity after a 60 day incubation while the enzyme inhibited with JMN21 remained completely inactivated.

Finally, a model of the physiological substrate, PAF, bound in the active site of the Lp-PLA₂ mimicking the tetrahedral intermediate of the esterolysis reaction was developed. The small *sn*-2 chain of PAF is positioned in a small active site pocket while the long C₁₈ chain of the substrate projects out of the active site and towards the interface region of the OPM lipoprotein binding model. This model also explains the mechanism of action of Lp-PLA₂ and oxidative fragmented phospholipids whose *sn*-2 chains are flipped up and away from the hydrophobic portion of the interface, making them accessible to the active site.

REFERENCES

1. Samanta, U. & Bahnson, B. J. Crystal structure of human plasma platelet-activating factor acetylhydrolase: structural implication to lipoprotein binding and catalysis. *J. Biol. Chem.* **283**, 31617–24 (2008).
2. Samanta, U., Kirby, S. D., Srinivasan, P., Cerasoli, D. M. & Bahnson, B. J. Crystal structures of human group-VIIA phospholipase A2 inhibited by organophosphorus nerve agents exhibit non-aged complexes. *Biochem. Pharmacol.* **78**, 420–9 (2009).
3. Lomize, M. A., Lomize, A. L., Pogozheva, I. D. & Mosberg, H. I. OPM: orientations of proteins in membranes database. *Bioinformatics* **22**, 623–5 (2006).
4. Lomize, A. L., Pogozheva, I. D., Lomize, M. A. & Mosberg, H. I. The role of hydrophobic interactions in positioning of peripheral proteins in membranes. *BMC Struct. Biol.* **7**, 44 (2007).
5. Min, J.-H. H. *et al.* Platelet-activating factor acetylhydrolases: Broad substrate specificity and lipoprotein binding does not modulate the catalytic properties of the plasma enzyme. *Biochemistry* **40**, 4539–4549 (2001).
6. Min, J.-H. *et al.* Membrane-Bound Plasma Platelet Activating Factor Acetylhydrolase Acts on Substrate in the Aqueous Phase. *Biochemistry* **38**, 12935–12942 (1999).
7. Gelb, M. H., Min, J.-H. & Jain, M. K. Do membrane-bound enzymes access their substrates from the membrane or aqueous phase: interfacial versus non-interfacial enzymes. *Biochim. Biophys. Acta - Mol. Cell Biol. Lipids* **1488**, 20–27 (2000).
8. Nagano, J. M. G., Hsu, K. L., Whitby, L. R., Niphakis, M. J., Speers, A. E., Brown, S. J., Spicer, T., Fernandez-Vega, V., Ferguson, J., Hodder, P., Srinivasan, P., Gonzalez, T. D., Rosen, H., Bahnson, B. J., and Cravatt, B. F. Selective inhibitors and tailored activity probes for lipoprotein-associated phospholipase A(2). *Bioorg. Med. Chem. Lett.* **23**, 839–43 (2013).
9. Morris, G. M. *et al.* AutoDock4 and AutoDockTools4: Automated docking with selective receptor flexibility. *J. Comput. Chem.* **30**, 2785–91 (2009).

10. Morris, G. M., Goodsell, D. S., Huey, R. & Olson, A. J. Distributed automated docking of flexible ligands to proteins: Parallel applications of AutoDock 2.4. *J. Comput. Aided. Mol. Des.* **10**, 293–304 (1996).
11. Sanner, M. Python: A programming language for software integration and development. *J. Mol. Graph. Model.* **17**, 57–61 (1999).
12. Sanner, M. F. A component-based software environment for visualizing large macromolecular assemblies. *Structure* **13**, 447–62 (2005).
13. DeLano, W. & Lam, J. PyMOL: A communications tool for computational models. *Abstr. Pap. Am. Chem. Soc.* **230**, U1371–U1372 (2005).
14. Salentin, S., Schreiber, S., Haupt, V. J., Adasme, M. F. & Schroeder, M. PLIP: fully automated protein–ligand interaction profiler. *Nucleic Acids Res.* **43**, W443–W447 (2015).

Chapter 5

THE ROLE OF LP-PLA₂ AND PAFAH-II IN PLATELETS

5.1 Introduction

Platelets are small anucleated cells derived from megakaryocytes that circulate freely in the blood. Upon vascular damage, platelets travel to the site of injury and form a barrier, known as a clot, to stop the bleeding. Activated platelets secrete agonists in order to recruit additional platelets to the damaged location. In addition to the agonists, activated platelets secrete inflammatory mediators and other vasoactive substances which promote hemostasis and tissue repair [1]. Platelets can become activated and in turn aggregate as a consequence of vascular disease. These aggregated platelets form a thrombosis, which leads to vascular occlusion and can ultimately result in myocardial infarction or stroke. In addition, activated platelets are involved in the modulation of the inflammatory response that promotes atherosclerosis [2]. The secretions of activated platelets have been implicated in these disease conditions.

The platelet secretions are known as the releasate, in which the contents of the platelets storage granules, α -granules, dense granules and lysosomes are released into the plasma. The proteins present in the storage granules are either endogenously synthesized in the megakaryocyte or the platelet and packaged into the granules by endocytosis from the plasma [3-5]. In addition, there are two distinct forms of membrane vesicles released upon platelet activation: microparticles and exosomes [6-8]. Many of the proteins identified in the releasate and associated with the membrane vesicles are known to have pro-inflammatory functions. In addition, platelets have

been identified as a component of atherosclerotic plaques and several known releasate enzymes have been shown to be present in the lesions [9,10].

As discussed in the introduction, Lp-PLA₂ and the enzyme PAFAH-II are 41% identical and function in a similar manner, catalyzing the hydrolysis of the *sn*-2 chain of PAF and oxidatively fragmented phospholipids. Unlike Lp-PLA₂, which circulates in plasma, PAFAH-II is primarily intracellular and distributed in the cytosol. In response to oxidative stress, PAFAH-II traffics to the membrane to prevent apoptosis [11]. Previous studies have shown that both Lp-PLA₂ and the homologous enzyme PAFAH-II are present in platelets, and that upon activation the releasate demonstrates PAF-acetylhydrolase activity [12-14]. In addition, studies have suggested that Lp-PLA₂ is associated with microparticles shedding during platelet activation and circulate with these microparticles in human plasma [14]. To this aim, we sought to identify the localization of Lp-PLA₂ and PAFAH-II after platelet activation with various platelet activation agonists in both human and mouse samples. This was assessed using Western blotting and a specific enzymatic assay that uses 2-thio-PAF as a substrate. The activated platelet samples were incubated with the specific inhibitors of Lp-PLA₂, discussed in detail in Chapters 3 and 4, and a specific inhibitor of PAFAH-II, AA39-2, which was also identified by a high throughput screen. The inhibited samples were assessed with the thio-PAF assay and the distribution of Lp-PLA₂ versus PAFAH-II released upon platelet activation was determined.

5.2 Materials and Methods

5.2.1 Materials

Sodium chloride, calcium chloride, sodium phosphate monobasic, sodium bicarbonate, calcium chloride, BSA (bovine serum albumin), EZ-Run Prestained-*Rec* protein ladder, glycerol, and Tris-HCl are from Fisher Scientific. Ellman's reagent (DTNB, 5,5'-Dithio-bis-(2-nitrobenzoic acid)) and enhanced chemiluminescence Western blotting kit are from Thermo Scientific. Magnesium chloride, glucose and Tween 20 are from Sigma-Aldrich. ADP (adenosine 5'-diphosphate sodium salt) was from Acros Organics and dry milk powder was purchased from Acme Supermarket. The Western blotting antibodies were purchased from three places, anti-PAFAH from Cayman Chemicals, anti-PAFAH-II was from Proteintech Group and anti-rabbit horseradish peroxidase was from Cell Signaling Technology. Magic Mark XP Western MW standard was purchased from Invitrogen. The ACD-A (Anticoagulant Citrate Dextrose Solution, Solution A), PGE₁ (Prostaglandin E1) and heparin were gifts from Dr. Ulhas Naik, formerly from the department of Biological Sciences, University of Delaware. The calcium ionophore platelet activator A23187 was a gift from Dr. Donna Woulfe from the department of Biological Sciences, University of Delaware.

5.2.2 Washing human platelets from whole blood

The human blood preparation was performed in the lab of Dr. Ulhas Naik at the Delaware Biotechnology Institute and approval for this work was obtained from the University of Delaware Institutional Review Board according to the Declaration of Helsinki. Prior to the blood collection, anti-coagulant, ACD-A, was warmed to 37 °C for 30 min in the collection tube in order to prevent the blood sample from clotting. The blood samples (50 mL) were obtained from healthy volunteers, free of any

medication, using a sterile technique. The collection tube was gently shaken during the draw to ensure mixing of ACD-A with the blood. Once the collection was complete, the tube was closed and inverted gently 3-4 times. The blood sample was split equally in two fresh tubes, using a sterile pipette, and centrifuged at 200 rcf for 10 min in order to separate the platelet rich plasma (PRP) from the red blood cell (RBC) suspension.

After centrifugation, the PRP was separated from the RBC suspension using transfer pipettes, avoiding pipetting RBCs in the buffy coat layer. To the PRP, PGE₁ was added to an appropriate concentration in order to prevent platelet activation. The PRP was then centrifuged at 800 rcf for 10 min.

The supernatant was decanted from the pellet, taking great care not to lose any platelets in the pellet. The pellet was then suspended using Tyrode's I, in a stepwise fashion to ensure a homogeneous solution. The Tyrode's stock buffer was prepared using 10 mM HEPES, pH 7.35, containing 150 mM NaCl, 2.5 mM KCl, 500 μM NaHPO₄, 12.5 mM NaHCO₃, 20 μM MgCl₂, and 10 mM glucose. To make Tyrode's I, the Tyrode's stock buffer was supplemented with 20 mM CaCl₂, 50 μM BSA, PGE₁ and heparin was added to prevent platelet activation. The suspension of platelets in Tyrode's I was incubated for 10 min at 37 °C and then centrifuged at 800 rcf for 10 min.

The supernatant was decanted and the pellet was resuspended using Tyrode's II in a stepwise manner to prevent platelet activation. Tyrode's II was made using the Tyrode's stock buffer and supplemented with 50 μM BSA and PGE₁. The suspension was incubated at 37 °C for 10 min and then centrifuged at 800 rcf for 10 min.

After the final centrifugation, the supernatant was decanted and the pellet resuspended using Tyrode's stock buffer, ensuring a homogenous solution to prevent platelet activation. This suspension was incubated for 30 min at 37 °C in order to deactivate the PGE₁. The platelets were counted using a hemocytometer and their concentration was adjusted using Tyrode's stock buffer.

5.2.3 Activating and isolating platelet components

Human platelet samples in Tyrode's stock buffer were treated with 100 μM ADP at room temperature, 22 °C for 30 min to ensure activation. The platelet samples from a wild type black mouse, gifted from the lab of Dr. Woulfe, were treated with 5 μM of the calcium ionophore A23187 for 30 min at room temperature.

Activated platelet samples, either mouse or human, were centrifuged at 6,000 rpm using a Sorvall Biofuge Pico microcentrifuge for 1 min to separate the platelet releasate from the membranous debris. The supernatant, containing the platelet releasate, was decanted from the pellet and stored at -80 °C.

The remaining pellet, containing the membranous portion of the platelets after activation, was resuspended with Tyrode's stock solution in order to wash the sample. The suspension was centrifuged at 6,000 rpm in the benchtop microcentrifuge for 5 min. The supernatant was discarded, and the pellet was resuspended with Tyrode's stock solution. This suspension, which contained the membranous portion of the activated platelets, was saved and stored at -80 °C.

5.2.4 Western blotting of platelet samples

The platelet samples were mixed with Laemmli sample buffer containing 20% v/v glycerol, 4% w/v SDS, bromophenol blue and the reducing agent 10% v/v β-

mercaptoethanol, and boiled for 10 min. The prepared samples, as well as Magic Mark XP Western MW standard and EZ-Run Prestained-*Rec* protein ladder, were separated by 12% or 15% sodium dodecyl sulfate-polyacrylamide gel electrophoresis (SDS-PAGE) at 200 V for 50 min. The platelet samples were then transferred to prepared polyvinylidene difluoride (PDV) membrane in a buffer of 25 mM Tris-HCl, pH 8.0, containing 100 mM glycine and 0.1% v/v SDS. The transfer was performed at 4 °C using an XCell-II blotting module from Invitrogen at 30 V for 90 min.

After the transfer, the blots were blocked for 2 h at room temperature while gently shaking, with 5% w/v dry milk in a Tris buffered saline with Tween 20 solution (TBS-T) of 20 mM Tris-HCl, pH 8.0, containing 140 mM NaCl and 0.1% Tween 20. After blocking, the membrane was washed with TBS-T 5 times for 10 min each at room temperature, gently shaking. The membrane was then incubated overnight, gently shaking at 4 °C, with primary antibody, anti-PAFAH or anti-PAFAH-II 1:1000, in a 1% w/v dry milk in TBS-T solution.

After overnight incubation with primary antibody, the blots were once again washed with TBS-T 5 times for 10 min each at room temperature, gently shaking. The blots were incubated at room temperature, gently shaking for 1 h with the secondary antibody, anti-rabbit horseradish peroxidase, as a 1:5000 dilution in 1% w/v dry milk in TBS-T solution. Following this incubation, the blots were washed with TBS-T 5 times for 10 min each at room temperature, gently shaking. The membrane was treated with enhanced chemilluminescence Western blotting substrate for 5 min, followed by exposure with the ImmunoChem 880 Imager from Alpha Innotech to visualize the bands.

5.2.5 Thio-PAF Assay

The activity of Lp-PLA₂ and PAFAH-II can be assessed using the physiologically relevant substrate, 2-thio-PAF (Cayman Chemical). Using thio-PAF as a substrate allows for detection of enzyme activity at low concentrations as well as in biological samples with multiple serine hydrolase enzymes. 2-thio-PAF mimics the structure of the enzyme's natural substrate, PAF, but contains a thio-ester bond attached to an acetyl group at the *sn*-2 position. The cleavage at the *sn*-2 position results in the formation of a free thiol, which then reacts with Ellman's reagent and the activity of the enzyme is determined, as shown in Figure 5.1. The assay was carried out in a 1 mL volume of 50 mM Tris, pH 7.5, containing 500 μM of Ellman's reagent (DTNB), and 2 μM 2-thio-PAF. The platelet sample along with the substrate, 2-thio-PAF, was incubated at room temperature in the Tris solution for a set period of time. The reaction was initiated with the addition of DTNB and the rate of formation of 5-thio-2-nitrobenzoic acid was measured at 412 nm to determine enzyme activity.

5.2.6 Treatment of platelets with inhibitors

The activated platelet releasate samples were aliquoted into 5 tubes of equal volume for both the human and mouse samples. The human aliquots ranged from 500 μL to 1 mL, depending upon their concentration, while the mouse tubes contained roughly 150 μL of platelet releasate suspension.

The protein samples were treated with 10 mM of a specific and potent inhibitor at room temperature and incubated for 2 h. The darapladib derivate, SB-56, and the carbamate inhibitor JMN21 were used to specifically inhibit Lp-PLA₂, while the inhibitor AA39-2 was used as a specific inhibitor of the intracellular PAFAH-II

(shown in Figure 5.2). The AA39-2 compound was developed using high throughput inhibitor screening for PAFAH-II, performed by the Molecular Libraries Screening Center Network at The Scripps Research Institute using the sample protocol described in Chapter 3 for the development of the Lp-PLA₂ inhibitor JMN21 and optimized in the lab of Dr. Ben Cravatt of The Scripps Research Institute [15]. In addition to the individually inhibited samples, an aliquot of the releasate was incubated with 10 mM of both JMN21 and AA39-2 in order to inhibit the hydrolase activity of both Lp-PLA₂ and PAFAH-II. A sample of releasate incubated with Tyrode's stock solution was used as a control.

After incubation, 50 to 100 μ L of each inhibited platelet releasate sample was aliquoted in microcentrifuge tubes and stored at -80 °C in order to prevent potential issues related to multiple exposures to freeze-thaw.

5.3 Results and Discussion

5.3.1 Localization of Lp-PLA₂ and PAFAH-II

Initially, human platelet activation was performed using the platelet agonist thrombin at a typical concentration of 0.5 U/mL. This procedure was altered to use the activator ADP due to the fact that thrombin, like Lp-PLA₂ and PAFAH-II, is a serine protease enzyme. In order to use the activity based protein profiling (ABPP) probes, (discussed in Chapter 3) activation with thrombin would be problematic as it would react with the probes. Furthermore, thrombin has a molecular weight of 36 kDa that is similar to the molecular weight of Lp-PLA₂ at 45 kDa. Therefore the band corresponding to thrombin would overshadow the bands representative of Lp-PLA₂ or

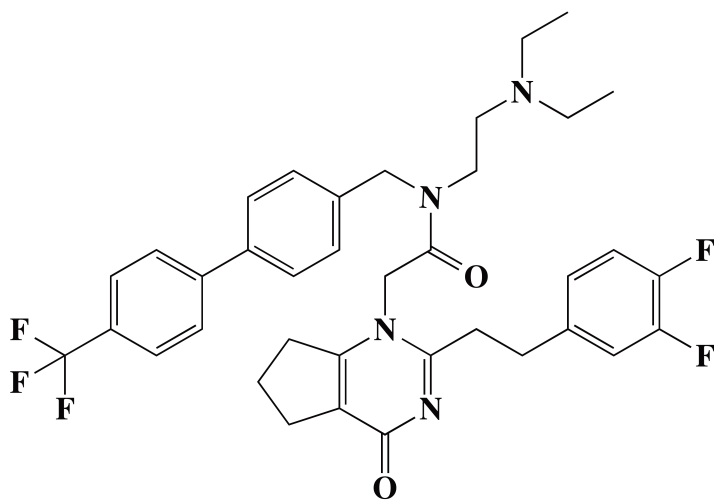
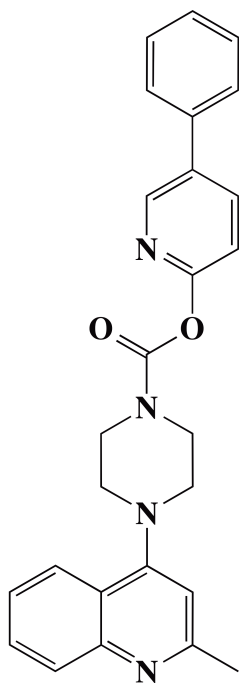
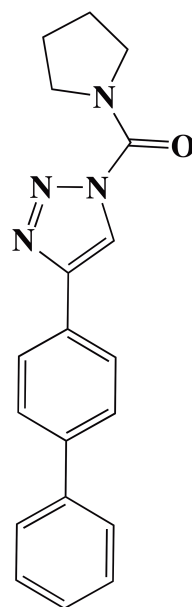
A**B****C**

Figure 5.2: Lp-PLA₂ and PAFAH-II specific inhibitors. Lp-PLA₂ inhibitors (A) Darapladib derivative SB-56, IC₅₀ 0.25 nm (B) Carbamate inhibitor JMN21, IC₅₀ 2.8 nm and PAFAH-II inhibitor (C) AA39-2, IC₅₀ 3.0 nm

the intracellular PAFAH-II as thrombin would be present at a significantly greater concentration. For these reasons, ADP was used as an agonist for platelet activation for these experiments. ADP is a weak activator of platelets that causes the release of the contents in the α -granules and dense granules. However ADP does not induce the release of the liposomal contents, nor does it stimulate the production of large amounts of membrane vesicles [5,7,16]. Previous reports indicate that Lp-PLA₂ is associated with platelet derived microparticles; therefore, activation with ADP can not be used to either confirm or refute this finding [14].

In order to activate the mouse platelet samples, the calcium ionophore A23187 was used as an agonist. In contrast to ADP, the Ca²⁺ ionophore is a strong activator and produces a large number of platelet derived microparticles [17]. Also, in contrast to ADP activation, it is important to note that any microparticles produced by the Ca²⁺ ionophore would be present in the releasate sample. Separation of microparticles from the soluble fraction requires ultracentrifugation and the releasate sample was centrifuged at a speed of 6,000 rpm.

5.3.1.1 Western blotting analysis

In order to determine where Lp-PLA₂ and PAFAH-II localizes in human platelets, Western blotting analysis was performed on the activated human platelet samples. When blotting against Lp-PLA₂ it was necessary to dilute the molecular weight marker, Magic Mark, in a 1:50 ratio due to the estimated low Lp-PLA₂ concentration. The EZ-Run marker was selected due to its prestained bands, which aid in visualization during transfer to the PDV membrane. The concentration of EZ-Run was not diluted, as the band was removed prior to developing the blot. The anti-PAFAH Western blot, of activated human platelet sample is shown in Figure 5.3.

Analysis of the Western blot revealed that Lp-PLA₂ is associated only with the releasate sample and does not appear in the membranous portion of the activated platelets. The Lp-PLA₂ present in the releasate is 45 kDa, indicative of a non-glycosylated enzyme, as previously reported [14]. The Lp-PLA₂ circulating in plasma associated with LDL and HDL is glycosylated. Therefore, we conclude that the Lp-PLA₂ present in the platelet releasate is not derived from platelet endocytosis of the plasma enzyme [18]. It is likely that the Lp-PLA₂ present in the platelets is generated during megakaryocyte differentiation [19].

In addition to the anti-PAFAH Western blots, the human samples were blotted against anti-PAFAH-II. Once again, the Magic Mark protein ladder was diluted in order to better visualize the PAFAH-II band. Similar to Lp-PLA₂, PAFAH-II is only present in the platelet releasate, as shown in Figure 5.3.

Western blots were only successfully performed using the human platelet samples, as the primary antibodies for anti-PAFAH and anti-PAFAH-II do not recognize the mouse Lp-PLA₂ and PAFAH-II enzymes.

5.3.1.2 Thio-PAF assay

In addition to Western blotting analysis of Lp-PLA₂ and PAFAH-II, Thio-PAF assays were performed to determine enzymatic activity in either the membranous portion or the platelet releasate for both the human and mouse samples. The human platelet sample concentrations were determined using a hemocytometer and platelet concentrations ranged from $1.5 - 2.0 \times 10^8 \text{ mL}^{-1}$. The concentration for the mouse sample was not determined.

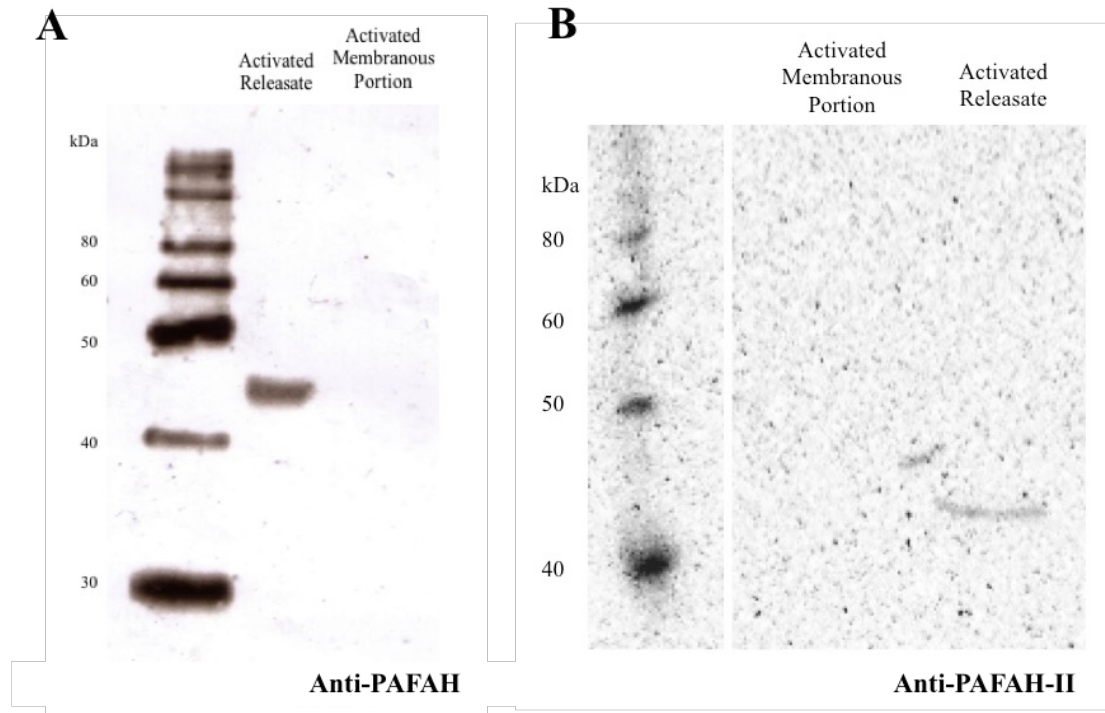


Figure 5.3: Activated human platelet Western blots. (A) Western blot showing the localization of human Lp-PLA₂ using Anti-PFAFH antibody. Lp-PLA₂ is only present in the releasate portion and does not associate with the membranous portion. The Lp-PLA₂ in platelets is 45 kDa, indicative of non-glycosylated sample. (B) Western blot showing the localization of PFAFH-II showing that the enzyme is only present in the releasate and not associated with the membranous portion.

5.3.1.2.1 Human platelet samples

For the human samples, 15 μL of either activated platelet membranous portion or releasate was incubated in the appropriate buffers with 2 μM 2-thio-PAF at room temperature for 20 min. The Ellman's reagent was added to this reaction mixture, and activity was monitored as described previously. The platelet sample was a mixture of many enzymes, so therefore it is possible to have turnover of DTNB due to free thiols in the solution. The free thiol turnover was determined through incubation of the platelet sample in appropriate buffer, with an equal volume of ethanol added to mimic the thio-PAF conditions without the substrate. The turnover of thio-PAF was determined after normalizing and setting the free thiol turnover to 1.

As expected, the membrane associated sample displayed no difference between the free thiol activity and thio-PAF activity. This further validates the Western blot, demonstrating no Lp-PLA₂ or PAFAH-II was present in the membranous portion of activated platelets. The thio-PAF turnover of the human releasate sample was significantly different than the free thiol turnover. This indicates the presence of Lp-PLA₂ and PAFAH-II in the human releasate sample, consistent with the Western blots. The relative thio-PAF activities of activated human platelet membranous portion and releasate are shown in Figure 5.4.

5.3.1.2.2 Mouse platelet samples

For the mouse samples, 5 μL of activated platelet membranous portion or releasate was incubated in the appropriate buffers with 2 μM 2-thio-PAF at room temperature for 10 min. As the mouse samples were activated with the Ca²⁺ ionophore A23187, a strong activator, a lower amount of sample was needed as well as a reduced

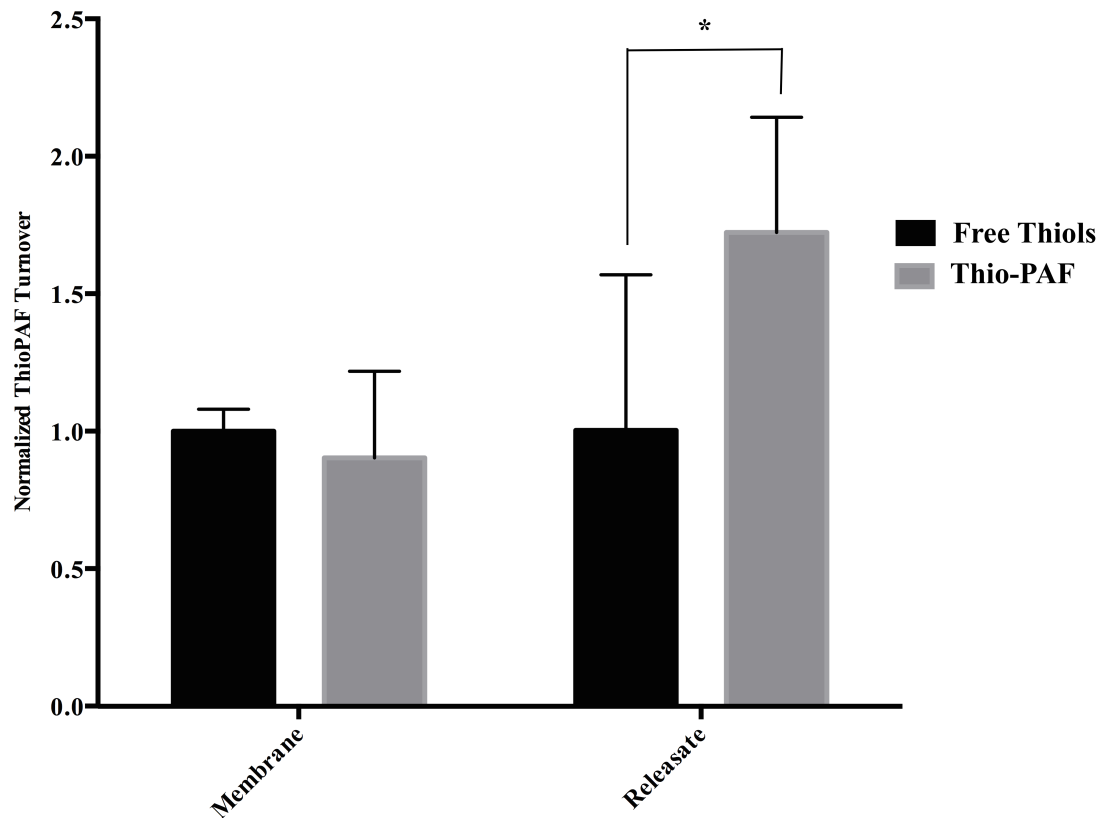


Figure 5.4: Human thio-PAF relative activity. On the left, it is shown that there is no difference in thio-PAF activity from that of the free thiols in solution, indicating that there is no Lp-PLA₂ or PAFAH-II present. The platelet releasate shows a significant difference in turnover between free thiols and thio-PAF, indicating that Lp-PLA₂ and/or PAFAH-II is present in the releasate. Membrane, n = 3, releasate, n = 6. Student's *t* test p value membrane = 0.327, releasate = 0.032.

incubation time. The reaction with Ellman's reagent was performed as previously described, and the turnover was normalized for free thiols in the same manner as the human platelet samples.

The activated mouse membranous portion demonstrated no difference in turnover between thio-PAF and free thiols, similar to that of the human membranous portion, as shown in Figure 5.5. This indicates that there is no Lp-PLA₂ or PAFAH-II associated with the membranous portion of activated mouse platelets. However, the mouse platelet releasate revealed a significant difference in thio-PAF activity compared to free thiols, indicating the presence of Lp-PLA₂ and/or PAFAH-II. This indicates that upon activation of mouse platelets, the Lp-PLA₂ and/or PAFAH-II is released. The relative thio-PAF activity response in the mouse releasate samples was greater than that in the human samples, indicative of the stronger activator used for the mouse platelet activation.

5.3.2 Effects of inhibitors on Lp-PLA₂ and PAFAH-II in platelets

The presence of Lp-PLA₂ and/or PAFAH-II in the releasate of both human and mouse samples was demonstrated using both Western blotting techniques and the enzyme specific thio-PAF assay. In order to determine the relative amount of Lp-PLA₂ and PAFAH-II in the releasate, I sought to determine if the potent inhibitors, darapladib derivative SB-56, JMN21, and AA39-2 can inhibit Lp-PLA₂ and/or PAFAH-II released from platelets in a specific manner. The systematic inhibition of either Lp-PLA₂ or PAFAH-II was used to characterize the relative activity of either enzyme in platelet releasate.

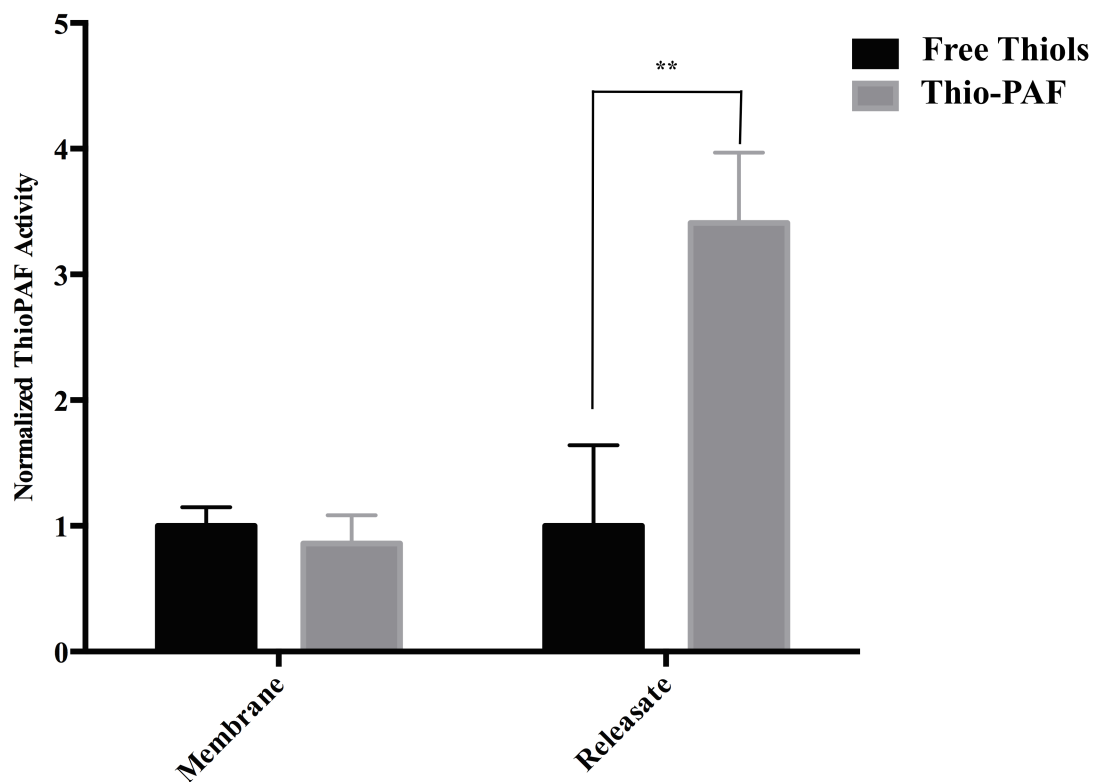


Figure 5.5: Mouse thio-PAF relative activity. There was no difference in turnover between free thiols and thio-PAF in the membranous portion of activated mouse platelets, indicating that neither Lp-PLA₂ nor PAFAH-II was present. There was a significant difference in the mouse releasate between free thiol turnover and Thio-PAF turnover. This revealed that upon activation, mouse platelets secrete Lp-PLA₂ and/or PAFAH-II. Membrane and releasate, n = 3. Student's *t* test p value membrane = 0.208, releasate = 0.002.

5.3.2.1 Human releasate samples

The human platelet releasate samples were inhibited as previously described. The thio-PAF assay was repeated using the Lp-PLA₂ inhibited preps, SB-56 and JMN21, the PAFAH-II inhibited sample with AA39-2, and the sample where both are inhibited with JMN21 and AA39-2. As a control, a sample without inhibitor was incubated with equivalent concentrations of the inhibitor stock solution cosolvents DMSO and methanol to mimic the storage conditions of the inhibitors. The free thiol turnover activity was subtracted from the data, and the results were normalized with releasate activity set to 1, presented in Figure 5.6.

Inhibition of Lp-PLA₂ in the human releasate resulted in a decrease in thio-PAF turnover with a statistically significant decrease in activity using the darapladib derivative, SB-56. In addition, the inhibition of PAFAH-II using the AA39-2 inhibitor resulted in a statistically significant decrease in thio-PAF turnover. These results indicate that activity from both Lp-PLA₂ and PAFAH-II contribute to the Thio-PAF activity in human platelet releasate. The combination of JMN21 and AA39-2, inhibiting both Lp-PLA₂ and PAFAH-II, yielded no difference in thio-PAF turnover compared to that of free thiols, thus completely eliminating thio-PAF turnover in the sample. This indicates that all thio-PAF hydrolysis, and in turn hydrolysis of the physiological substrate PAF at the *sn*-2 position, in human platelets is due to either Lp-PLA₂ or PAFAH-II.

5.3.2.2 Mouse releasate samples

The mouse releasate samples were inhibited and the thio-PAF assay was

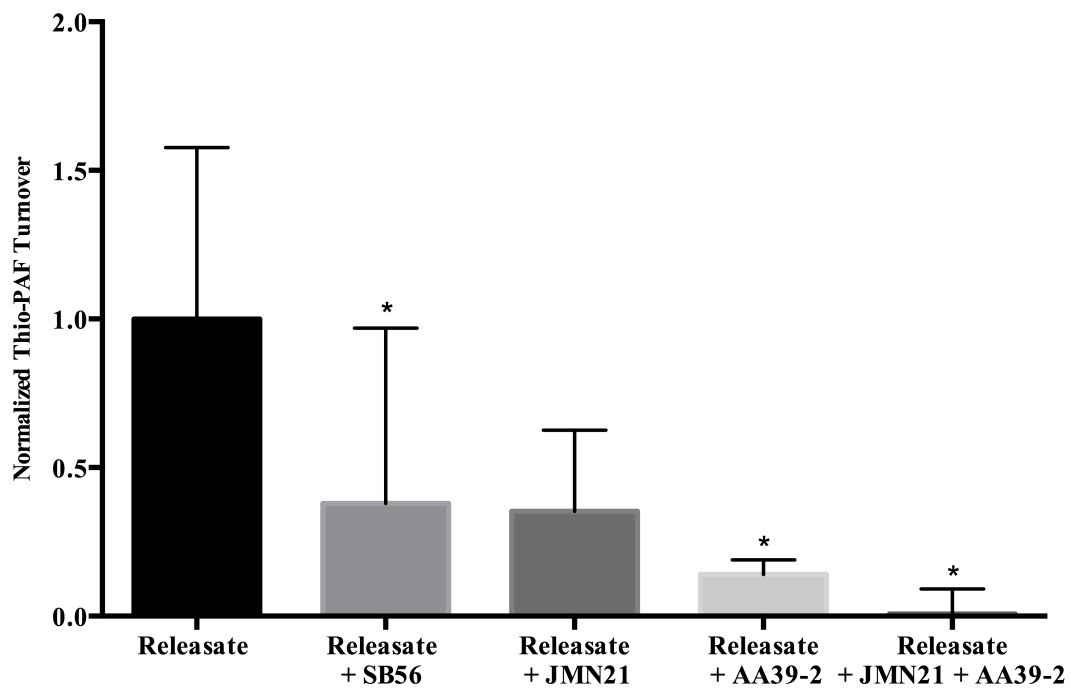


Figure 5.6: Human releasate treated with Lp-PLA₂ and PAFAH-II inhibitors. The Lp-PLA₂ inhibitors SB-56 and JMN21, as well as the PAFAH-II inhibitor AA39-2, decreased the thio-PAF turnover in the releasate samples. The inhibition of both Lp-PLA₂ and PAFAH-II completely eliminated thio-PAF turnover in platelet releasate. Releasate and SB-56, n = 6; JMN21, AA39-2 and JMN21+AA39-2 n = 3. Student's *t* test p value SB-56 = 0.048, JMN21 = 0.057, AA39-2 = 0.021, and JMN21+AA39-2 = 0.012.

carried out in the same manner previously described. The inhibited mouse releasate thio-PAF activity was normalized in the same way as the inhibited human releasate samples. The inhibition of Lp-PLA₂ with both the darapladib derivative SB-56, and the carbamate inhibitor JMN21 resulted in a statistically significant decrease in thio-PAF activity of mouse releasate. As with the human sample, inhibition of PAFAH-II with AA39-2 resulted in a statistically significant decrease of thio-PAF turnover. The inhibition of both Lp-PLA₂ and PAFAH-II resulted in the complete loss of thio-PAF activity. These results indicate that in mouse platelets, as in human, the only enzymes that hydrolyze PAF at the *sn*-2 position are Lp-PLA₂ and PAFAH-II.

It is important to note that for both mouse and human releasate, it was not possible to determine the percentage of thio-PAF turnover related to either Lp-PLA₂ or PAFAH-II. It may be possible to determine the ratio of PAF acetylhydrolase activity using a more sensitive assay with the radiolabeled substrate [³H]PAF. However, it is apparent from the thio-PAF assay that both Lp-PLA₂ and PAFAH-II contribute to the PAF acetylhydrolase activity in human and mouse platelet releasate.

5.4 Conclusions

The work presented here demonstrates successful isolation of human platelets from whole blood and activation of the platelet sample using the weak agonist ADP. In addition, isolated mouse platelets were activated with the Ca²⁺ ionophore A23187. Upon activation, the platelets released the contents of the α -granules, dense granules and lysosomes. The Ca²⁺ ionophore activated mouse samples also causes the

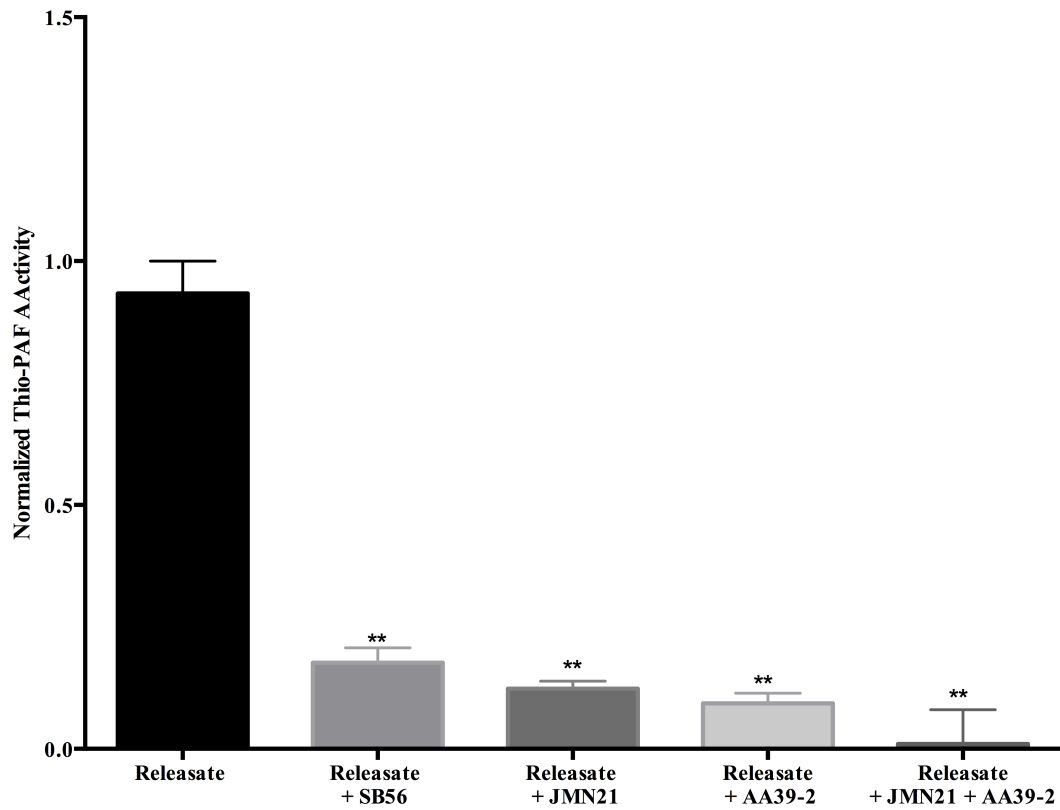


Figure 5.7: Mouse releasate treated with Lp-PLA₂ and PAFAH-II inhibitors. The Lp-PLA₂ inhibitors SB-56 and JMN21, as well as the PAFAH-II inhibitor AA39-2, show a statistically significant decrease in thio-PAF turnover in the releasate samples. The inhibition of both Lp-PLA₂ and PAFAH-II completely eliminated thio-PAF turnover. For all samples n = 3. Student's *t* test p value > 0.001 for all, as indicated with **

production of large amounts of platelet derived microparticles, a previously reported carrier of Lp-PLA₂ in humans [14]. The activated platelets were then isolated into two major components, the releasate and membranous portion, by centrifugation at 6,000 rpm. The releasate contains the enzymes secreted during platelet activation, as well as any platelet derived microparticles, while the membranous portion contains the remaining cellular debris that typically forms clots.

Using the human samples, Western blotting was performed against Lp-PLA₂ as well as the intracellular PAFAH-II in order to determine if the enzymes associated with the membrane or were secreted into the releasate upon platelet activation. The blot demonstrated that both Lp-PLA₂ and PAFAH-II were only associated with the releasate portion and no enzyme was associated with the membrane. The Western blot of releasate samples for Lp-PLA₂ revealed the enzyme to have a molecular weight of 45 kDa, indicating that the enzyme is non-glycosylated. The Lp-PLA₂ circulating in plasma associated with LDL and HDL is glycosylated; therefore, the enzyme present in platelets was not taken in from the plasma and likely was present during differentiation from megakaryocytes. The presence of Lp-PLA₂ and PAFAH-II in platelets may be important pathophysiologically, as their substrate PAF is also secreted upon platelet activation and predicted to be associated with platelet derived microparticles [20].

The human releasate and membrane samples were both tested using the thio-PAF assay, which demonstrated that only the releasate portion was able to hydrolyze thio-PAF. Taken together, these results indicate that there is no Lp-PLA₂ or PAFAH-II associated with the membrane fraction after platelet activation and are therefore

secreted upon platelet activation and circulate the bloodstream, possibly associated with platelet derived microparticles.

The human releasate samples were then treated with specific inhibitors against either Lp-PLA₂ (SB-56 and JMN12) or PAFAH-II (AA39-2), as well as inhibiting both enzymes (JMN21 and AA39-2), and the thio-PAF assays were repeated. The results demonstrated a significant decrease in activity when either Lp-PLA₂ or PAFAH-II was inhibited and a complete loss of activity when both enzymes were inhibited. This indicates that both Lp-PLA₂ and PAFAH-II are secreted upon platelet activation, and that they are the exclusive enzymes in platelets, which cleave PAF at the *sn*-2 position.

It has been previously reported that both Lp-PLA₂ and PAFAH-II are present in resting platelets and shown that Lp-PLA₂ is secreted upon platelet activation with the strong agonists; however, there was no evidence that PAFAH-II was secreted upon activation [14]. The Western blots, as well as the thio-PAF assay of inhibited releasate, clearly demonstrate that both Lp-PLA₂ and PAFAH-II are secreted from platelets upon activation.

These studies were additionally carried out in mouse platelets activated with the Ca²⁺ ionophore A23187, which induces platelet vesiculation and therefore creates large quantities of platelet derived microparticles. Western blotting using our human Lp-PLA₂ and PAFAH-II antibodies was unsuccessful for the mouse samples due to antibody specificity. Therefore, the thio-PAF assay was used exclusively to determine localization of Lp-PLA₂ and/or PAFAH-II in activated mouse platelets. It was determined that only mouse releasate turns over thio-PAF and therefore Lp-PLA₂ and/or PAFAH-II is secreted from the platelets upon activation.

The mouse releasate sample was inhibited and the thio-PAF assays were repeated. The mouse releasate, in which Lp-PLA₂ was inhibited by either SB-56 or JMN21, resulted in a statistically significant decrease in thio-PAF activity. Likewise, the PAFAH-II inhibited releasate demonstrated a significant reduction in thio-PAF turnover. The combined sample, in which both Lp-PLA₂ and PAFAH-II were inhibited, was unable to hydrolyze thio-PAF. Taken together, these results indicate that in mouse, as with human, Lp-PLA₂ and PAFAH-II are both secreted upon platelet activation. In addition, Lp-PLA₂ and PAFAH-II are the only enzymes secreted from platelets that hydrolyze PAF at the *sn*-2 position.

REFERENCES

1. Hynes, R. O. Integrins: Versatility, modulation, and signaling in cell adhesion. *Cell* **69**, 11–25 (1992).
2. Ross, R. Mechanisms of disease - Atherosclerosis - An inflammatory disease. *N. Engl. J. Med.* **340**, 115–126 (1999).
3. George, J. N. Platelet immunoglobulin G: its significance for the evaluation of thrombocytopenia and for understanding the origin of alpha-granule proteins. *Blood* **76**, 859–70 (1990).
4. Lindemann, S. *et al.* Activated platelets mediate inflammatory signaling by regulated interleukin 1beta synthesis. *J. Cell Biol.* **154**, 485–90 (2001).
5. Coppinger, J. A. & Maguire, P. B. Insights into the platelet releasate. *Curr. Pharm. Des.* **13**, 2640–6 (2007).
6. Wiedmer, T., Shattil, S. J., Cunningham, M. & Sims, P. J. Role of calcium and calpain in complement-induced vesiculation of the platelet plasma membrane and in the exposure of the platelet factor Va receptor. *Biochemistry* **29**, 623–632 (1990).
7. Heijnen, H., Schiel, A., Fijnheer, R., Geuze, H. & Sixma, J. Activated platelets release two types of membrane vesicles: Microvesicles by surface shedding and exosomes derived from exocytosis of multivesicular bodies and alpha-granules. *Blood* **94**, 3791–3799 (1999).
8. Freyssinet, J.-M. & Toti, F. Formation of procoagulant microparticles and properties. *Thromb. Res.* **125 Suppl** , S46–8 (2010).
9. Huo, Y. *et al.* Circulating activated platelets exacerbate atherosclerosis in mice deficient in apolipoprotein E. *Nat. Med.* **9**, 61–7 (2003).
10. Coppinger, J. A. *et al.* Characterization of the proteins released from activated platelets leads to localization of novel platelet proteins in human atherosclerotic lesions. *Blood* **103**, 2096–104 (2004).

11. Thevenin, a F., Monillas, E. S., Winget, J. M., Czymbek, K. & Bahnson, B. J. Trafficking of platelet-activating factor acetylhydrolase type II in response to oxidative stress. *Biochemistry* **50**, 8417–8426 (2011).
12. Korth, R., Bidault, J., Palmantier, R., Benveniste, J. & Ninio, E. Human Platelets Release a Paf-Acether: Acetylhydrolase Similar to that in Plasma. *Lipids* **28**, 193–199 (1993).
13. Rice, S. *et al.* Expression, purification and characterization of a human serine-dependent phospholipase A(2) with high specificity for oxidized phospholipids and platelet activating factor. *Biochem. J.* **330**, 1309–1315 (1998).
14. Mitsios, J. V, Vini, M. P., Stengel, D., Ninio, E. & Tselepis, A. D. Human platelets secrete the plasma type of platelet-activating factor acetylhydrolase primarily associated with microparticles. *Arterioscler. Thromb. Vasc. Biol.* **26**, 1907–13 (2006).
15. Adibekian, A. *et al.* Optimization and characterization of a triazole urea inhibitor for platelet-activating factor acetylhydrolase type 2 (PAFAH2) - PubMed - NCBI. (2013). at <<http://www.ncbi.nlm.nih.gov/books/NBK133429/>>
16. Barry, O. & FitzGerald, G. Mechanisms of cellular activation by platelet microparticles. *Thromb. Haemost.* **82**, 794–800 (1999).
17. White, J. G., Rao, G. H. & Gerrard, J. M. Effects of the ionophore A23187 on blood platelets I. Influence on aggregation and secretion. *Am. J. Pathol.* **77**, 135–49 (1974).
18. Elstad, M. R., Stafforini, D. M., McIntyre, T. M., Prescott, S. M. & Zimmerman, G. A. Platelet-activating factor acetylhydrolase increases during macrophage differentiation. A novel mechanism that regulates accumulation of platelet-activating factor. *J. Biol. Chem.* **264**, 8467–70 (1989).
19. Foulks, J. M. *et al.* PAF-acetylhydrolase expressed during megakaryocyte differentiation inactivates PAF-like lipids. *Blood* **113**, 6699–706 (2009).
20. Iwamoto, S., Kawasaki, T., Kambayashi, J., Ariyoshi, H. & Monden, M. Platelet Microparticles: A Carrier of Platelet-Activating Factor? *Biochem. Biophys. Res. Commun.* **218**, 940–944 (1996).

Chapter 6

CONCLUSIONS AND FUTURE DIRECTIONS

The work presented here contributes to a better understanding of the enzyme Lp-PLA₂. An expression and purification procedure was optimized for an Lp-PLA₂ construct (residues 49-423) using a pGEX-6P-1 vector. In addition to the wild-type Lp-PLA₂, two site-directed mutants were made with the goal of disrupting the membrane binding of the enzyme resulting in higher yields of pure enzyme. The I120A/L123A/L124A and Y205A mutant constructs were expressed and purified in the same manner as the wild type Lp-PLA₂. A comparison of the activity between the wild type and mutants using a PNPA assay demonstrated no significant difference in the K_{cat} value between the lipoprotein binding mutants and wild type, however there was a decrease in the K_M for the mutants. It would be interesting to repeat the kinetic assays using a physiological relevant substrate, such as radiolabeled [³H]PAF, in order to determine if the decrease in K_M is due to the mutations made or just a consequence of using the general substrate PNPA.

A high throughput inhibitor screen was carried out in collaboration with the Molecular Libraries Screening Center Network at The Scripps Research Institute Florida and the lab of Prof. Ben Cravatt from The Scripps Research Institute La Jolla. A variety of new compounds that displayed inhibition of Lp-PLA₂ were identified and interactions with serine hydrolases were characterized. The most prominent inhibitor leads were determined to be from a class of compounds known as carbamates. These compounds have been shown to demonstrate selectivity with serine hydrolases *in vivo*

and inhibit the enzymes through a reaction with nucleophilic serine, resulting in a covalent bond at the active site. The top hits from the screen were optimized in the lab of our collaborator, Dr. Ben Cravatt of The Skaggs Institute for Chemical Biology at The Scripps Research Institute, and the potency and selectivity of the new compounds were analyzed. It was determined that the optimized inhibitor, JMN4, demonstrated both increased potency and selectivity for Lp-PLA₂ *in vitro* compared to the lead compounds from the screening. The optimized inhibitor was then studied in comparison to the GlaxoSmithKline inhibitor darapladib. Through a variety of activity-based protein profiling experiments, it was determined that JMN4 was as selective of an inhibitor *in vitro* and *in situ* as darapladib.

A similar carbamate inhibitor, JMN21, was sent to our lab for further analysis with the ultimate goal of co-crystallization. Using the PNPA assay, it was shown that initial inhibition of recombinant Lp-PLA₂ with either the carbamate inhibitor JMN21 or darapladib derivatives SB-56 or SB-59 was identical. However, after 60 days, the catalytic activity of the darapladib inhibited compounds returned while the JMN21 inhibited Lp-PLA₂ remained inactive. This plays to the nature of darapladib binding Lp-PLA₂ in a reversible manner and JMN21 binding covalently at the nucleophilic Ser273. In addition, the CD spectra of Lp-PLA₂, and the inhibited Lp-PLA₂ complexes with either SB-56 or JMN21 did not show any apparent differences, confirming loss of activity was only due to inhibition at the active site.

Initial attempts at crystallization of Lp-PLA₂ complexed with the darapladib derivative SB-56 and carbamate inhibitor JMN21 were promising. However, despite further screening, the best crystals formed to this point do not diffract well enough to enable structural determination. For this reason, computational methods were used to

model the interaction of these inhibitors, as well as the physiological substrate PAF, using the program AutoDock4.2.

The model of the Lp-PLA₂-darapladib complex consists of three hydrogen bond interactions at catalytic residues Ser273 and His351 as well as Leu153, thus preventing the catalytic hydrolysis function of the enzyme. The inhibitor is predicted to lie in the hydrophobic pocket and prevent substrate from accessing the active site. In contrast, the carbamate inhibitor, JMN21, is covalently bound to the nucleophilic Ser273 and has three predicted hydrogen bonds with Leu153, Phe274 and His351. The hydrogen bond with His351 prevents the residue from deprotonating and therefore prevents the activation of a water molecule for nucleophilic attack. The predicted interactions between Lp-PLA₂ and its inhibitors validate the results of the PNPA assay after 60 days of incubation with either inhibitor.

A model of the physiological substrate PAF bound in the active site of the Lp-PLA₂ was also developed. The ligand is situated in the active site mimicking the tetrahedral intermediate of the esterolysis reaction. The small *sn*-2 chain of PAF is positioned in a small active site pocket, while the long C₁₈ chain of the substrate projects out of the active site and towards the interface region of the OPM lipoprotein binding model. This model provides insight into the mechanism of action of Lp-PLA₂ and oxidative fragmented phospholipids whose *sn*-2 chains are flipped up and away from the hydrophobic portion of the interface, making them accessible to the active site.

It has been reported that carbamate inhibitors can specifically inhibit a serine hydrolase target *in vitro* and *in situ* with only slight modifications to the moieties around the carbonyl [1]. While the models presented here represent the inhibition of

Lp-PLA₂ by JMN21, it does not account for the specificity the enzyme has for this inhibitor. In the model, a portion of the compound has already been lost due to the semi-catalytic nature of the enzyme on the carbamate inhibitor. It is probable, however, that the entire inhibitor compound plays a role in its specificity *in vitro* and *in situ*. We propose that there is a biphasic inhibition mechanism, in which an initial binding interaction occurs between Lp-PLA₂ and JMN21, followed by the catalytic release of a portion of the inhibitor, which results in a covalently inhibited enzyme. Future work to test this biphasic binding mechanism hypothesis could be probed by surface plasmon resonance (SPR) [2]. In addition, derivatives of JMN21 can be synthesized and any binding changes as a result of the modifications to the compound can provide clues on the nature of this interaction. For example, if a derivative of JMN21 no longer demonstrated biphasic binding, the change in the moiety might also remove the inhibitor's specificity for Lp-PLA₂ *in vivo* or *in situ*, which could also be tested.

It has been previously reported that resting platelets contain both Lp-PLA₂ and PAFAH-II. It has also been identified that upon activation, Lp-PLA₂ is secreted and circulates in the plasma associated with platelet derived microparticles [3]. The work here represents an analysis of human and mouse activated platelets and the role Lp-PLA₂ and PAFAH-II play in these cells. It was demonstrated that upon activation with either weak or strong agonists, Lp-PLA₂ and PAFAH-II are secreted from human and mouse platelets. The inhibitor compounds developed from high throughout screening were used with the aim to determine activity of the releasate related to either Lp-PLA₂ or PAFAH-II [4,5]. Though it was not possible to determine the percent activity related to each specific enzyme, it was evident that both Lp-PLA₂ and PAFAH-II are

present in the releasate. In addition, it was determined that the homologous enzymes Lp-PLA₂ and PAFAH-II are the only enzymes secreted from platelets that can cleave PAF at the *sn*-2 position.

The enzyme Lp-PLA₂ has been reported to aid in the progression of atherosclerosis. As a PAF-acetylhydrolase, the homologous enzyme, PAFAH-II can hydrolyze PAF and oxidatively fragmented phospholipids in the same manner as Lp-PLA₂. However, until now there has been no evidence to suggest that PAFAH-II has direct links to the progression of atherosclerosis as it is primarily found intracellularly. Other work in the Bahnson lab has found that upon activation from oxidative stress, PAFAH-II becomes a monomer and binds the outer leaflet membranes of the Golgi and endoplasmic reticulum in order to prevent apoptosis [6,7]. In addition to this prior work, the work presented in Chapter 5 of this thesis now suggests PAFAH-II may also play an important role at the site of platelet activation physiologically.

The proteins and enzymes released from platelets upon activation play a large role in platelet adhesion and contribute to the development of atherosclerosis. Several known proteins in the platelet releasate have been found in atherosclerotic lesions [8]. One specific enzyme secreted upon activation is Platelet Factor 4 (PF4), which is known to bind LDL. This enzyme has been shown to contribute to oxidized LDL uptake into the macrophage-derived foam cells, and has been shown to be co-localized with LDL in atherosclerotic plaques [9].

The identification of Lp-PLA₂, known to play a role in atherosclerosis, as well as the homologous enzyme PAFAH-II in platelet releasate serves as a starting point to understand the role these enzymes play in atherosclerotic plaques. It is likely that targeting both Lp-PLA₂ and PAFAH-II with specific inhibitors will be necessary to

provide full protection from coronary heart disease. Prior studies by GlaxoSmithKline (O'Donoghue, *et al* and White, *et al.*) and others have focused only on inhibition of Lp-PLA₂ [10-14]. There are many studies that can be done in order to examine this relationship, but the next step would be determining if the inhibitors have any effect on platelet activation. After this is determined, specific studies can be designed to study the interaction of Lp-PLA₂ and/or PAFAH-II and platelet derived microparticles. From initial studies performed here with mouse platelets, it may be beneficial to translate this work into animal models (*e.g.* mouse) and study the effects of inhibiting both Lp-PLA₂ and PAFAH-II on atherosclerosis.

REFERENCES

1. Alexander, J. P. & Cravatt, B. F. Mechanism of carbamate inactivation of FAAH: implications for the design of covalent inhibitors and in vivo functional probes for enzymes. *Chem. Biol.* **12**, 1179–87 (2005).
2. Shinohara, Y. *et al.* Kinetic measurement of the interaction between an oligosaccharide and lectins by a biosensor based on surface plasmon resonance. *Eur. J. Biochem.* **223**, 189–194 (1994).
3. Mitsios, J. V, Vini, M. P., Stengel, D., Ninio, E. & Tselepis, A. D. Human platelets secrete the plasma type of platelet-activating factor acetylhydrolase primarily associated with microparticles. *Arterioscler. Thromb. Vasc. Biol.* **26**, 1907–13 (2006).
4. Nagano, J. M. G., Hsu, K. L., Whitby, L. R., Niphakis, M. J., Speers, A. E., Brown, S. J., Spicer, T., Fernandez-Vega, V., Ferguson, J., Hodder, P., Srinivasan, P., Gonzalez, T. D., Rosen, H., Bahnson, B. J., and Cravatt, B. F. Selective inhibitors and tailored activity probes for lipoprotein-associated phospholipase A(2). *Bioorg. Med. Chem. Lett.* **23**, 839–43 (2013).
5. Adibekian, A. *et al.* Click-generated triazole ureas as ultrapotent in vivo-active serine hydrolase inhibitors. *Nat. Chem. Biol.* **7**, 469–478 (2011).
6. Thevenin, a F., Monillas, E. S., Winget, J. M., Czymmek, K. & Bahnson, B. J. Trafficking of platelet-activating factor acetylhydrolase type II in response to oxidative stress. *Biochemistry* **50**, 8417–8426 (2011).
7. Monillas, E. S., Caplan, J. L., Thévenin, A. F. & Bahnson, B. J. Oligomeric state regulated trafficking of human platelet-activating factor acetylhydrolase type-II. *Biochim. Biophys. Acta* **1854**, 469–75 (2015).
8. Coppinger, J. A. *et al.* Characterization of the proteins released from activated platelets leads to localization of novel platelet proteins in human atherosclerotic lesions. *Blood* **103**, 2096–104 (2004).
9. Nassar, T. *et al.* Platelet Factor 4 Enhances the Binding of Oxidized Low-density Lipoprotein to Vascular Wall Cells. *J. Biol. Chem.* **278**, 6187–6193 (2002).

10. O'Donoghue, M. L. *et al.* Study design and rationale for the Stabilization of pLaques usIng Darapladib-Thrombolysis in Myocardial Infarction (SOLID-TIMI 52) trial in patients after an acute coronary syndrome. *Am. Heart J.* **162**, 613–619.e1 (2011).
11. O'Donoghue, M. L. *et al.* Effect of darapladib on major coronary events after an acute coronary syndrome: the SOLID-TIMI 52 randomized clinical trial. *JAMA* **312**, 1006–15 (2014).
12. White, H. *et al.* Study design and rationale for the clinical outcomes of the STABILITY Trial (STabilization of Atherosclerotic plaque By Initiation of darapLadIb TherapY) comparing darapladib versus placebo in patients with coronary heart disease. *Am. Heart J.* **160**, 655–61 (2010).
13. White, H. D. *et al.* Darapladib for preventing ischemic events in stable coronary heart disease. *N. Engl. J. Med.* **370**, 1702–11 (2014).
14. Fenning, R. S. *et al.* Atherosclerotic plaque inflammation varies between vascular sites and correlates with response to inhibition of lipoprotein-associated phospholipase A2. *J. Am. Heart Assoc.* **4**, (2015).

Appendix A

METHYLTRANSFERASE ENZYMES MtaABC

In conjunction with University of Delaware Department of Chemical and Biomedical Engineering, research was done on the methanol:coenzyme M methyltransferases enzyme complex MtaABC on the ARPA-E funded project 0881-1528 (and incorporating 0881-1550) with the ultimate goal of demonstrating reversibility of the enzyme system. Work on this project was done in collaboration with fellow graduate student Meghan Klems.

A.1 Introduction

The methanogenic archaeon, *Methanosarcina barkeri*, can be sustained using methanol as a sole carbon source with methanol metabolism initiated by the formation of methylated coenzyme M [1,2]. The methanol:coenzyme M methyltransferases complex (MtaABC) that catalyze this reaction is composed of three protein subunits MtaA, MtaB and MtaC that are derived from the gene *mtaABC* in *M. barkeri*. The genes *mtaBC* are naturally expressed on the same operon and the enzymes function as a heterodimer with MtaB (50 kDa) and MtaC (27 kDa) tightly bound to a corrinoid prosthetic group. The function of this heterodimer is to catalyze the transfer of CH₃ from methanol onto the corrinoid. After this transfer, the monomeric, zinc protein, MtaA (35 kDa) will catalyze the transfer of the methyl group on to coenzyme M (Figure A.1) [1,3-5].

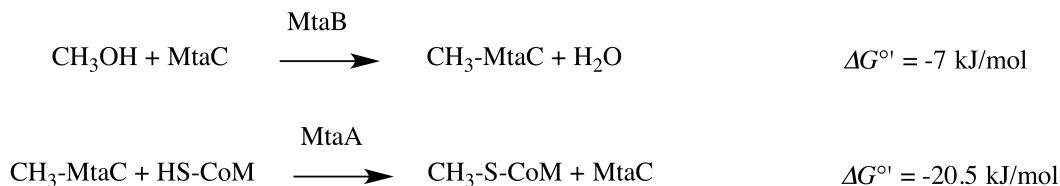


Figure A.1: Methanol metabolism in *M. barkeri* with enzymes MtaABC

Previous work by the Thauer group has demonstrated the ability to express the genes for *mtaA* and *mtaBC* in *E. coli*. Their work was initiated with genomic DNA extraction from *M. barkeri*, cloned into an *E. coli* expression vector, and subsequently expressed anaerobically [6,7]. Purification of MtaA was done anaerobically using affinity chromatography and the activity of the recombinant enzyme was assayed. The activity assay exploits the ability of MtaA to transfer the methyl group off of methylcobalamin onto coenzyme M in the absence of the MtaBC complex [6,8]. The enzymes MtaB and MtaC were also purified anaerobically using size exclusion chromatography and assays were developed to assess the recombinant enzymes catalytic activity [7]. Although the crystal structures of MtaA and the MtaBC complex have been determined, there is no structure of all three subunits together in a single complex [9,10].

A.2 Materials and Methods

A.2.1 Materials

Synthesized genes were purchased from GenScript. The pET-16b vector was from EMD Millipore. *XhoI*, *BamHI*, *NcoI* and T4 DNA ligase were purchased from New England Biolabs. Sodium 2-mercaptoethanesulfonate (coenzyme-M) was from Fluka analytical. 5-5'-dithiobis-(2-nitrobenzoic acid) (DTNB or Ellman's reagent) was

purchased from Thermo Scientific. Ampicillin, ATP, MgCl₂, imidazole, lysozyme, and methylcobalamin were from Sigma-Aldrich. Isopropyl β-D-1-thiogalactopyranoside (IPTG) was from Goldbio.com. Luria-Bertani media (LB), LB agar, agarose, sodium phosphate dibasic anhydrate, sodium phosphate monobasic monohydrate, methanol, 3-(4-morpholino)propane sulfonic acid (MOPS), KOH, NaCl, pepstatin, mineral oil, and ethylene diamine tetraacetic acid (EDTA) were purchased from Fisher Scientific.

A.2.2 Gene synthesis and subcloning of MtaA and MtaBC

The protein sequences of MtaA and MtaBC were designed to mimic the natural enzyme found in *Methanosarcina barkeri* strain fusaro (EMBL X91893 and Y08310, respectively) but the cDNA was optimized for an *E. coli* expression system. MtaA is expressed from one operon while MtaBC is naturally transcribed as a single mRNA transcript from same operon. Therefore, we aimed to express MtaA in one plasmid with MtaBC co-expressing in a second. The *M. barkeri* sequence for MtaA contained 20 rare codons for *E. coli* expression, including 10 rare arginines, and MtaBC contained 29 rare codons making codon-optimized gene synthesis the preferred approach for expressing these enzyme subunits.

MtaA was optimized to remove the rare codons and designed with the restriction enzyme sequences of *XhoI*, 5' – CTCGAG – 3', at the N-terminus and *BamHI*, 5' – GGATCC – 3', at the C-terminus for cloning into the pET-16B expression vector. MtaBC was optimized to remove rare codons and oriented as it is naturally expressed with the MtaC transcript first followed by MtaB. After the stop codon for MtaC, an *E. coli* ribosome binding site, 5' – TTAAGAAAGGAGATATACC – 3' (RBS underlined), was engineered as well as a His-tag with a serine linker, 5' –

ATGCATCATCATCATCATCATCATCATCATCACAGCAGCAGC – 3' (serine linker underlined), to the N-terminus of MtaB. The entire MtaBC gene was designed with the restriction enzyme *NcoI*, 5' – CCATGG – 3', at the N-terminus and *BamHI* at the C-terminus for cloning into the pET-16B expression vector (Figure A.2).

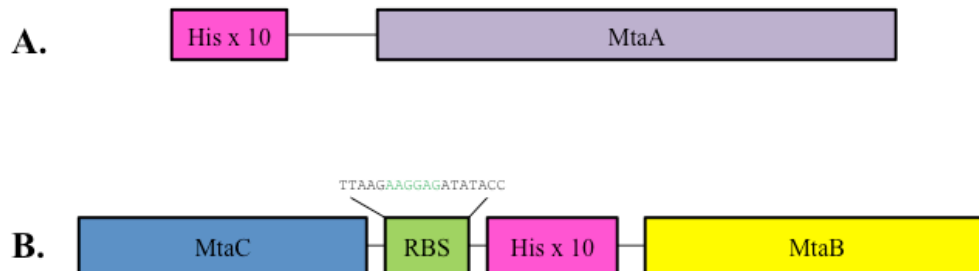


Figure A.2: MtaABC transcripts. (A) Cartoon of MtaA transcript; His-Tag is from the pET-16B vector. (B) Cartoon of the MtaBC transcript.

The genes for MtaA and MtaBC were received from GeneScript in pUC57 plasmids. The MtaA pUC57 and pET-16B were digested with *XhoI* and *BamHI* at 37 °C for 2 h and gel purified. Their concentrations were assessed using the nanodrop and then ligated with T7 ligase over night at 14 °C at a ratio of 10:1 insert to vector. The ligated MtaA in pET-16B was transformed into *E. coli* DH5 α cells and plated on LB agar plates with 100 μ g/mL ampicillin and grown overnight at 37 °C. Several colonies were picked and grown individually overnight in 5 mL of LB with 100 μ g/mL ampicillin at 37 °C. The following morning, the DNA was isolated using the QIAprep spin miniprep kit and each colony was sent for sequencing at GeneWiz. The successful ligation of MtaA into pET-16B was confirmed and a glycerol stock of the

construct in DH5 α cells was made and stored at -80 °C. The MtaBC pUC57 construct and pET-16B vector were digested with *NcoI* and *BamHI* and ligated using the same method as MtaA. Successful ligation of MtaBC in pET-16B was also confirmed by sequencing.

A.2.3 Expression of recombinant MtaA in *E. coli*

The MtaA pET-16B expression construct was transformed into *E. coli* BL21 cells and plated on LB agar plates with 100 $\mu\text{g}/\text{mL}$ ampicillin and grown overnight at 37 °C. A single colony was grown in 5 mL of LB with 100 $\mu\text{g}/\text{mL}$ ampicillin at 37 °C overnight and the following morning was made into a glycerol stock to be stored at -80 °C for starter cultures. For expression, a starter culture was made using a scrape of the glycerol stock and was grown overnight in 200 mL of LB with 100 $\mu\text{g}/\text{mL}$ ampicillin at 37 °C. In the morning, 20 mL of the overnight growth was inoculated into 1 L of fresh LB containing 100 $\mu\text{g}/\text{mL}$ ampicillin and grown at 30 °C until it reached an $\text{OD}_{600} \sim 0.7$. The culture was then induced with 0.5 mM IPTG and expressed overnight at 16 °C. The cells were harvested by centrifugation at 8,000 rpm (Sorvall SLA-3000) for 10 min at 4 °C and pellets were stored at -80 °C until purification.

A.2.4 Purification of recombinant MtaA

The purification protocol was developed based on the previously published methodology of the Thauer group [6]. The cell pellet was thawed at room temperature and suspended (average 0.10 g wet weight of cells per 1 mL buffer) in lysis buffer consisting of 50 mM sodium phosphate, pH 7.8 containing 300 mM NaCl, 1 μM pepstatin and 1.5 mg/mL lysozyme. The resuspended cells were lysed by sonication

for 2 min twice with 5 min rest in between each sonication. The suspension was then clarified by centrifugation twice at 13,000 rpm (Sorvall SS-34) for 20 min at 4 °C. The supernatant was applied to a column containing Ni-NTA resin equilibrated with a binding buffer of 120 mM sodium phosphate, pH 7.8, containing 300 mM NaCl and rocked for 1 h at 4 °C to insuring binding of MtaA to the resin. Following the incubation on the Ni-NTA resin, the column was washed with a series of buffers of 50 mM sodium phosphate, pH 6.0, containing 300 mM NaCl and incrementally increasing concentrations of imidazole (0 mM, 10 mM, 25 mM, 50 mM, and 60 mM) of 5 column volumes each to remove the non-specifically bound proteins. The His-MtaA fusion protein was then eluted from the resin by incubating 30 mL of 50 mM sodium phosphate, pH 6.0, containing 300 mM NaCl and 500 mM imidazole. The eluted protein was then dialyzed overnight at 4 °C against 50 mM MOPS/KOH pH 7.2 to equilibrate it with the buffers for further purification using the anion exchange column Q-sepharose. The next day, the dialyzed sample was loaded using FPLC onto a Q-sepharose column equilibrated with the low salt buffer of 50 mM MOPS/KOH, pH 7.2. The resin was washed with 20 mL at a 1.5 mL/min flow rate of low salt buffer. A gradient was then introduced with a high salt buffer of 50 mM MOPS/KOH, pH 7.2 containing 200 M NaCl, ranging from 0% - 100% high salt buffer over 75 mL at a 1 mL/min flow rate. Finally the Q-sepharose column was washed with the high salt buffer over 20 mL at a flow rate of 1.5 mL/min to remove all bound proteins. Fractions from the gradient were collected and the fusion protein of MtaA was determined to elute between 200 and 300 mM NaCl. These fractions were pooled, concentrated and dialyzed against 50 mM MOPS/KOH pH 7.2 at 4 °C overnight and stored at 4 °C.

A.2.5 Methylcobalamin assay of MtaA

Activity of MtaA was assessed using a modified assay based on the previously published work of Harms and Thauer [6]. The assay measures the demethylation of methylcobalamin in a coenzyme M dependent manner by the enzyme MtaA. The assay was performed with 1 mL reaction volume containing 6 mM substrate, methylcobalamin, in 50 mM MOPS/KOH, pH 7.2, and 10 – 15 µg of MtaA with a layer of mineral oil on top of the cuvette to minimize oxygen transfer. The reaction was initiated with the addition of 10 mM coenzyme M and the formation of cobalamin was monitored as an increase in absorbance at 310 nm.

A.2.6 DTNB combined assays

A.2.6.1 Forward reaction

The activity of MtaABC in the forward direction was assessed using a DTNB assay measuring the decrease of free thiols present in coenzyme M as a result of the MtaABC dependent methylation of coenzyme M. The assay was performed in a discontinuous fashion, as a continuous DTNB assay can only be used to monitor an increase in free thiols. The 1 mL reaction mixture was warmed at 37 °C with a mineral oil overlay and in 50 mM MOPS/KOH, pH 7.2, containing ~ 1 mg of each subunit of MtaABC, 200 µM ATP, 10 mM MgCl₂, and 50 mM coenzyme M. The reaction was initiated with the addition of 100 µL of methanol. At various time points, 10 µL of the reaction sample was removed and added to a cuvette to a total volume of 1 mL with 100 mM Tris, pH 7.5, containing 1 mM DTNB, and the change in absorbance was monitored at 412 nm.

A.2.6.2 Reverse Reaction

The activity of the reverse reaction was assessed using a continuous DTNB assay monitoring the formation of free thiols as a result of the MtaABC demethylation of methyl-coenzyme M. The reaction was assayed in a total volume of 1 mL of 100 mM Tris, pH 7.5, containing ~ 1 mg of each subunit of MtaABC, 200 μ M ATP, 10 mM MgCl₂, and 1 mM DTNB. The reaction was initiated with the addition of methyl-coenzyme M and the change in absorbance was monitored at 412 nm.

A.3 Results and Discussion

A.3.1 Expression and purification of recombinant MtaA

MtaA is naturally found in an anaerobic environment; however all expression, purification and assays were done under aerobic conditions. Care was taken to minimize oxygen transfer during enzymatic assays and will be discussed further in the following sections, however no attempts to minimize oxygenation were made for MtaA expression and purification. MtaA was expressed aerobically in *E. coli* (strain BL21) using a His-tag for purification. Several expression trials were attempted, including varying the temperature for both growth and expression and IPTG concentration to determine the best method to obtain high levels of soluble protein. It was found that the construct optimally grew at 30 °C and expressed with 0.5 mM IPTG overnight at 16 °C. However, it was ultimately determined that while each colony from the initial BL21 transformation would express at similar levels under these conditions, they did not all carry the same levels of activity which will be discussed further in the next section.

Initial purification attempts of MtaA used a Ni-Sepharose resin. However, a great many impurities remained so the resin was then switched to a Ni-NTA resin for

His-tag affinity chromatography. This result gave increased the purity of MtaA to 60% and the total protein yield to 0.25 mg/L of culture. The enzyme's presence was confirmed by anti-His western blot with a prominent band at the expected molecular weight of 38 kDa (Figure A.3).

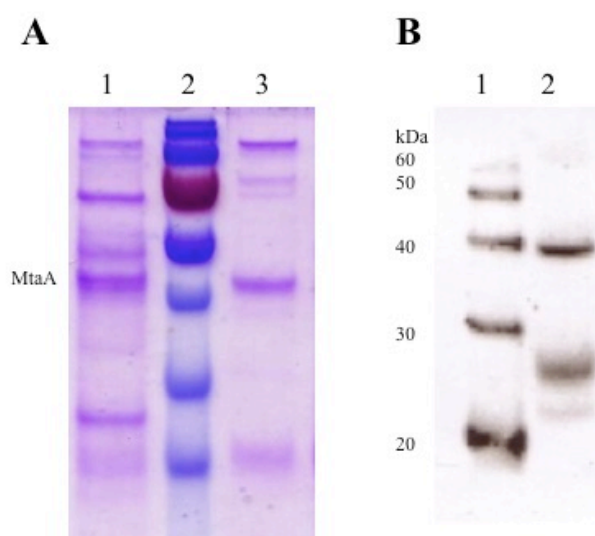


Figure A.3: Expression and purification of MtaA (A) SDS PAGE Analysis: Lane 1. MtaA Ni-Sepharose, 40% pure, 2. Protein marker, 3. MtaA Ni-NTA, 60% pure (B) Anti-His Western Blot: Lane 1. Protein marker, 2. MtaA

A.3.2 Characterization of purified MtaA

The purified MtaA samples were characterized by SDS PAGE in order to estimate purity using the ImageJ64 software and the enzyme concentration was determined using a bicinchoninic acid (BCA) assay. The activities of the samples were assessed using the methylcobalamin assay as described previously. It was found that the activity of MtaA varied greatly depending upon the original BL21 colony used for the expression. It was determined that colony 2 produced the highest levels of activity and therefore all further experimentation with MtaA used colony 2 (Figure A.4).

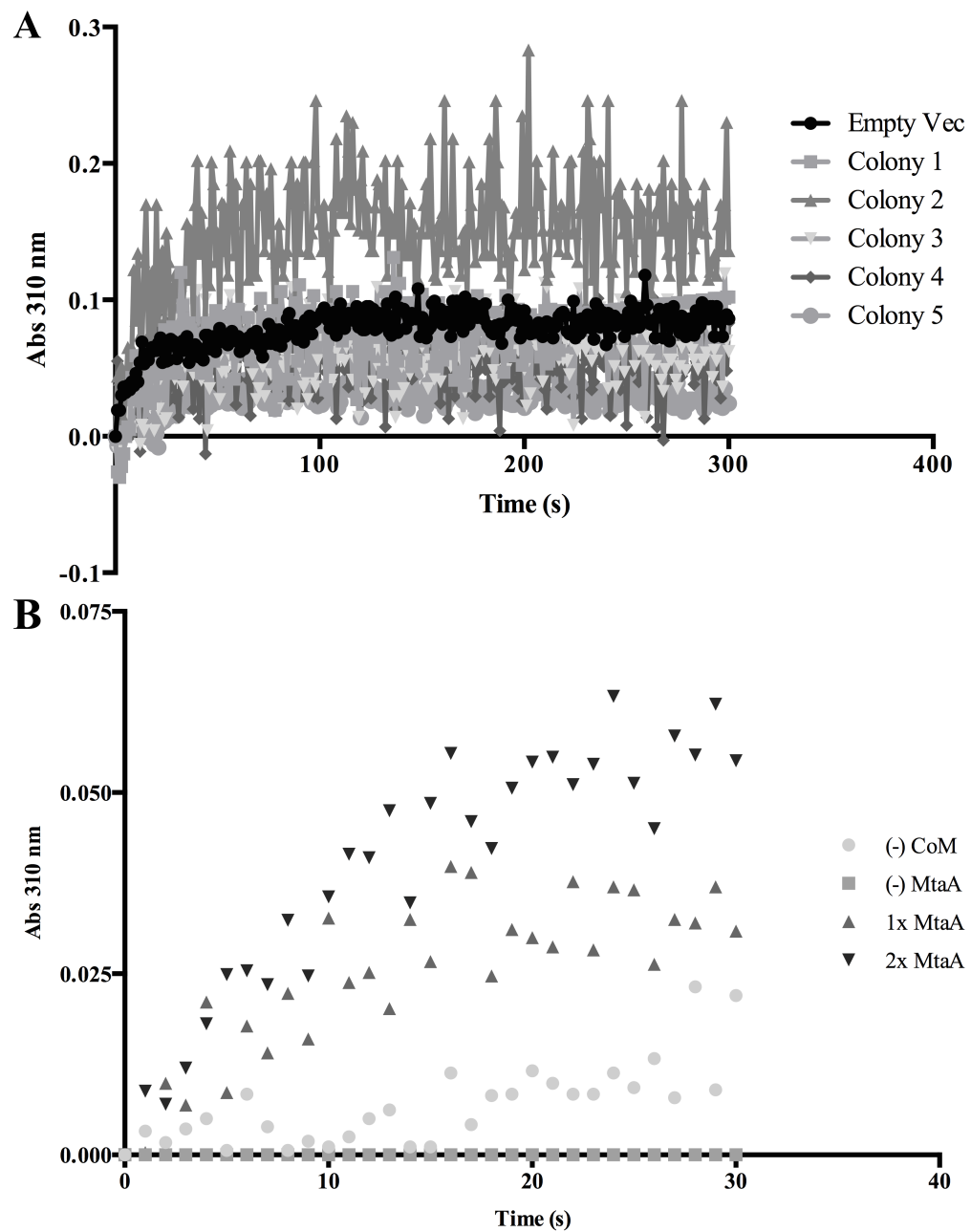


Figure A.4: Activity of MtaA. (A) Activity of MtaA lysate from several small scale expressions of various colonies; blank was lacking the required substrate, coenzyme M. (B) Activity of purifying MtaA from colony 2, shown above to be most active. Two blanks were used, the first without the required substrate, CoM, and the second without enzyme. The initial amount of MtaA used was 15 μg (1x MtaA) and was then increased to 30 μg (2x MtaA) with proportional increases in activity.

A.3.3 Combined MtaABC assays

With the ultimate goal of reversing the MtaABC pathway for the production of methanol from methylated coenzyme M, we first needed to produce the methylated CoM via the MtaABC reaction in the forward direction. To this aim, the active and pure MtaA was combined with active MtaBC from Meghan Klems and carried out as described in the Materials and Methods section. As expected, a decrease in free thiols was observed as CoM-SH was converted to CoM-S-CH₃ and could no longer react with DTNB (Figure A. 5).

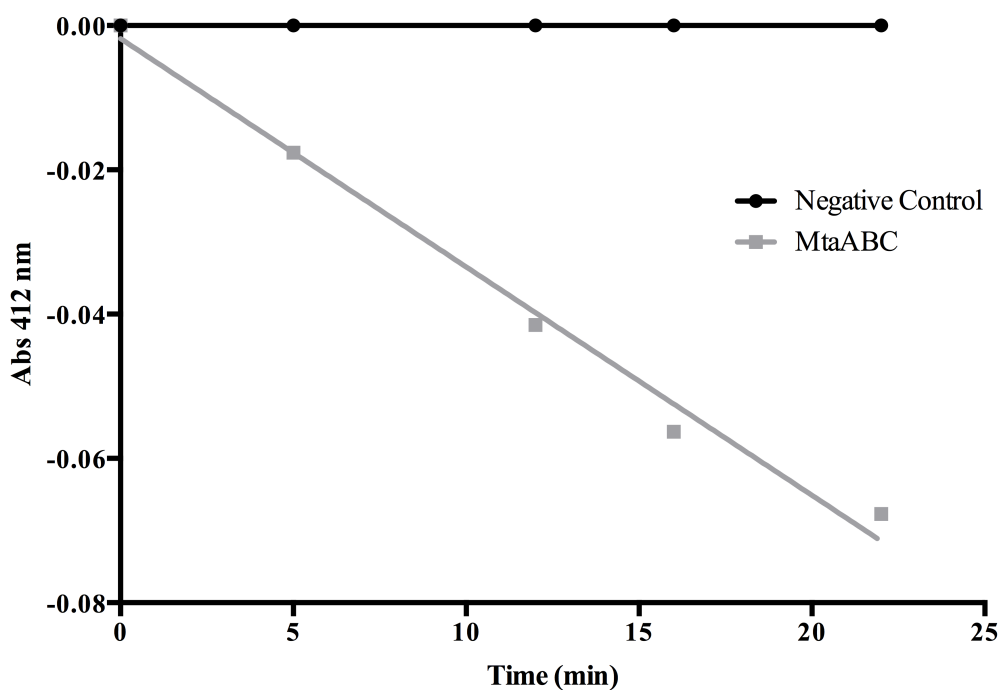


Figure A.5: MtaABC Forward Reaction. DTNB assay following the decrease in absorbance as a result of the MtaABC dependent methylation of coenzyme M and subsequent reduction of free thiols present.

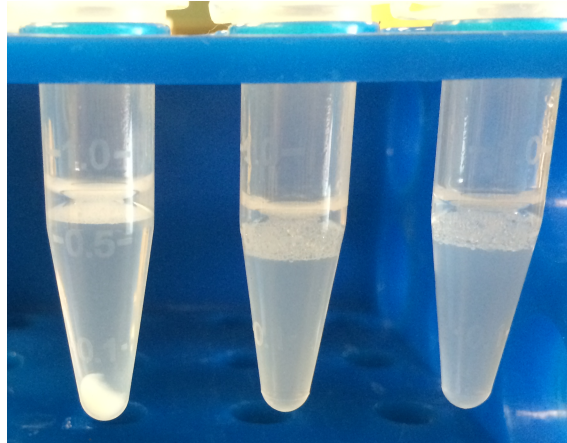
As the forward MtaABC reaction was proceeding, a white precipitate formed at the bottom of the tube, which was not present in any of the control experiments. We deduced that this precipitate formed in the forward reaction was the product, methylated CoM. This precipitate was then pelleted, washed thoroughly and suspended for use as a substrate in the reverse reaction, which was assayed as previously described. In the assay we were able to detect an increase in free thiols as a result of $\text{CH}_3\text{-SH-CoM}$ being converted back to SH-CoM and the subsequent production of methanol (Figure A.6).

A.3.4 Conclusions

With the overall goal of demonstrating reversibility of the MtaABC reaction pathway, it was first necessary to design the MtaA and MtaBC genes in a manner that would result in successful expression in an *E. coli* system. The synthesized genes were cloned into *E. coli* expression vectors and trials were performed to determine the optimal expression protocol. For the MtaA enzyme, a purification scheme was developed resulting in about 60% pure protein. After each purification, MtaA was assessed for enzymatic activity using a methylcobalamin assay, which measures the demethylation of methylcobalamin in a coenzyme M dependent manner by MtaA.

Once the activity of the singular component of MtaA was confirmed, this enzyme was combined with pure and active MtaBC to demonstrate the enzymatic activity in the forward direction. Upon reaction of MtaABC with methanol and CoM, a distinct precipitate would form, which was deduced to be the product, methylated CoM. The product was isolated from the reaction mixture and used as a reactant in order to demonstrate the reversibility of MtaABC. The reversibility of the enzyme

A. 1 2 3



B.

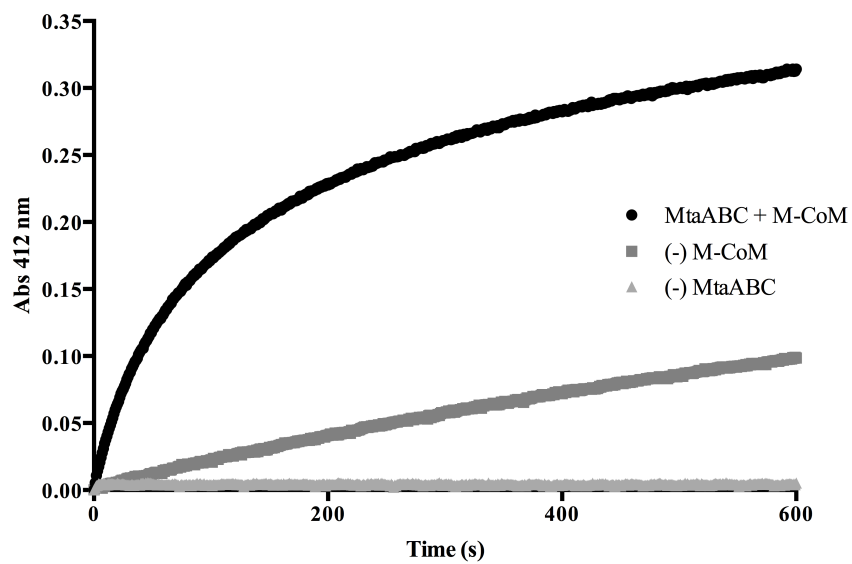


Figure A.6: MtaABC Reverse Reaction. (A) Precipitate formed from the forward reaction. Tube 1. MtaABC reaction with precipitate, 2. Negative control, no methanol, 3. Negative control, no coenzyme M. (B) MtaABC Reverse Reaction. DTNB Assay of the shows an increase in absorbance due to the MtaABC dependent demethylation of methylated CoM and subsequent increase in free thiols present in solution.

system was confirmed by the enzymatic DTNB assay, where an increase in free thiols was observed as MtaABC reduced CH₃-SH-CoM back to the original SH-CoM, and in theory, resulted in the production of methanol.

These experiments demonstrated successful expression and purification of the enzymes MtaABC in an *E. coli* system, giving rise in active enzymes. These individually active enzymes were combined and demonstrated cooperative enzymatic activity in both the forward and reverse directions, thus reaching the endpoint goals of this portion of the ARPA-E funded project.

REFERENCES

1. Wassenaar, R. W., Daas, P. J., Geerts, W. J., Keltjens, J. T. & van der Drift, C. Involvement of methyltransferase-activating protein and methyltransferase 2 isoenzyme II in methylamine:coenzyme M methyltransferase reactions in *Methanosarcina barkeri* Fusaro. *J. Bacteriol.* **178**, 6937–44 (1996).
2. Shapiro, S. & Wolfe, R. S. Methyl-coenzyme M, an intermediate in methanogenic dissimilation of C1 compounds by *Methanosarcina barkeri*. *J. Bacteriol.* **141**, 728–34 (1980).
3. Van der Meijden, P. *et al.* Activation and inactivation of methanol: 2-mercaptoethanesulfonic acid methyltransferase from *Methanosarcina barkeri*. *J. Bacteriol.* **153**, 6–11 (1983).
4. Van der Meijden, P. *et al.* Methyltransferases involved in methanol conversion by *Methanosarcina barkeri*. *Arch. Microbiol.* **134**, 238–42 (1983).
5. Krüer, M., Haumann, M., Meyer-Klaucke, W., Thauer, R. K. & Dau, H. The role of zinc in the methylation of the coenzyme-M thiol group in methanol:coenzyme M methyltransferase from *Methanosarcina barkeri*. *Eur. J. Biochem.* **269**, 2117–2123 (2002).
6. Harms, U. & Thauer, R. K. Methylcobalamin:coenzyme M Methyltransferase Isoenzymes MtaA and MtbA from *Methanosarcina barkeri*. Cloning, Sequencing and Differential Transcription of the Encoding Genes, and Functional Overexpression of the mtaA Gene in *Escherichia coli*. *Eur. J. Biochem.* **235**, 653–659 (1996).
7. Sauer, K., Harms, U. & Thauer, R. K. Methanol: coenzyme M Methyltransferase from *Methanosarcina Barkeri*. Purification, Properties and Encoding Genes of the Corrinoid Protein MT1. *Eur. J. Biochem.* **243**, 670–677 (1997).
8. Daas, P. J., Gerrits, K. A., Keltjens, J. T., van der Drift, C. & Vogels, G. D. Involvement of an activation protein in the methanol:2-mercaptoethanesulfonic acid methyltransferase reaction in *Methanosarcina barkeri*. *J. Bacteriol.* **175**, 1278–83 (1993).

9. Hoepfner, A. *et al.* Structure of the corrinoid:coenzyme M methyltransferase MtaA from *Methanosarcina mazei*. *Acta Crystallogr. D. Biol. Crystallogr.* **68**, 1549–57 (2012).
10. Hagemeyer, C. H., Krer, M., Thauer, R. K., Warkentin, E. & Ermler, U. Insight into the mechanism of biological methanol activation based on the crystal structure of the methanol-cobalamin methyltransferase complex. *Proc. Natl. Acad. Sci. U. S. A.* **103**, 18917–18922 (2006).

Appendix B
REPRINT PERMISSIONS

**NATURE PUBLISHING GROUP LICENSE
TERMS AND CONDITIONS**

Jul 02, 2015

This is a License Agreement between Tara D Gonzalez ("You") and Nature Publishing Group ("Nature Publishing Group") provided by Copyright Clearance Center ("CCC"). The license consists of your order details, the terms and conditions provided by Nature Publishing Group, and the payment terms and conditions

All payments must be made in full to CCC. For payment instructions, please see information listed at the bottom of this form.

License Number	3660900766750
License date	Jul 02, 2015
Licensed content publisher	Nature Publishing Group
Licensed content publication	Nature
Licensed content title	Inflammation in atherosclerosis
Licensed content author	Peter Libby
Licensed content date	Dec 19, 2002
Volume number	420
Issue number	6917
Type of Use	reuse in a dissertation / thesis
Requestor type	academic/educational
Format	print and electronic
Portion	figures/tables/illustrations

Number of figures/tables/illustrations	1
High-res required	no
Figures	Figure 1
Author of this NPG article	no
Your reference number	None
Title of your thesis / dissertation	LIPOPROTEIN-ASSOCIATED PHOSPHOLIPASE A2: UTILIZING POTENT AND SPECIFIC INHIBITORS TO PROBE THE STRUCTURE FUNCTION RELATIONSHIP
Expected completion date	Jul 2015
Estimated size (number of pages)	150
Total	0.00 USD
Terms and Conditions	

Terms and Conditions for Permissions

Nature Publishing Group hereby grants you a non-exclusive license to reproduce this material for this purpose, and for no other use, subject to the conditions below:

1. NPG warrants that it has, to the best of its knowledge, the rights to license reuse of this material. However, you should ensure that the material you are requesting is original to Nature Publishing Group and does not carry the copyright of another entity (as credited in the published version). If the credit line on any part of the material you have requested indicates that it was reprinted or adapted by NPG with permission from another source, then you should also seek permission from that source to reuse the material.
2. Permission granted free of charge for material in print is also usually granted for any electronic version of that work, provided that the material is incidental to the work as a whole and that the electronic version is essentially equivalent to, or substitutes for, the print version. Where print permission has been granted for a fee, separate permission must be obtained for any additional, electronic re-use (unless, as in the case of a full paper, this has already been accounted for during your initial request in the calculation of a print run). NB: In all cases, web-based use of full-text articles must be authorized separately through the 'Use on a Web Site' option when requesting permission.
3. Permission granted for a first edition does not apply to second and subsequent editions and for editions in other languages (except for signatories to the STM Permissions Guidelines, or where the first edition permission was granted for free).
4. Nature Publishing Group's permission must be acknowledged next to the figure, table or abstract in print. In electronic form, this acknowledgement must be visible at the same time as the figure/table/abstract, and must be hyperlinked to the journal's homepage.
5. The credit line should read:
Reprinted by permission from Macmillan Publishers Ltd: [JOURNAL NAME] (reference citation), copyright (year of publication)
For AOP papers, the credit line should read:
Reprinted by permission from Macmillan Publishers Ltd: [JOURNAL NAME], advance online publication, day month year (doi: 10.1038/sj.[JOURNAL ACRONYM].XXXXX)

Note: For republication from the *British Journal of Cancer*, the following credit lines apply.

Reprinted by permission from Macmillan Publishers Ltd on behalf of Cancer Research UK: [JOURNAL NAME] (reference citation), copyright (year of publication) For AOP papers, the credit line should read: Reprinted by permission from Macmillan Publishers Ltd on behalf of Cancer Research UK: [JOURNAL NAME], advance online publication, day month year (doi: 10.1038/sj.[JOURNAL ACRONYM].XXXXX)

6. Adaptations of single figures do not require NPG approval. However, the adaptation should be credited as follows:

Adapted by permission from Macmillan Publishers Ltd: [JOURNAL NAME] (reference citation), copyright (year of publication)

Note: For adaptation from the *British Journal of Cancer*, the following credit line applies.

Adapted by permission from Macmillan Publishers Ltd on behalf of Cancer Research UK: [JOURNAL NAME] (reference citation), copyright (year of publication)

7. Translations of 401 words up to a whole article require NPG approval. Please visit <http://www.macmillanmedicalcommunications.com> for more information. Translations of up to a 400 words do not require NPG approval. The translation should be credited as follows:

Translated by permission from Macmillan Publishers Ltd: [JOURNAL NAME] (reference citation), copyright (year of publication).

Note: For translation from the *British Journal of Cancer*, the following credit line applies.

Translated by permission from Macmillan Publishers Ltd on behalf of Cancer Research UK: [JOURNAL NAME] (reference citation), copyright (year of publication)

We are certain that all parties will benefit from this agreement and wish you the best in the use of this material. Thank you.

Special Terms:

v1.1

Questions? customercare@copyright.com or +1-855-239-3415 (toll free in the US) or +1-978-646-2777.

**ELSEVIER LICENSE
TERMS AND CONDITIONS**

Jun 22, 2015

This is a License Agreement between Tara D Gonzalez ("You") and Elsevier ("Elsevier") provided by Copyright Clearance Center ("CCC"). The license consists of your order details, the terms and conditions provided by Elsevier, and the payment terms and conditions.

All payments must be made in full to CCC. For payment instructions, please see information listed at the bottom of this form.

Supplier	Elsevier Limited The Boulevard, Langford Lane Kidlington, Oxford, OX5 1GB, UK
Registered Company Number	1982084
Customer name	Tara D Gonzalez
Customer address	University of Delaware NEWARK, DE 19716
License number	3622060860441
License date	May 04, 2015
Licensed content publisher	Elsevier
Licensed content publication	Bioorganic & Medicinal Chemistry Letters
Licensed content title	Selective inhibitors and tailored activity probes for lipoprotein-associated phospholipase A2
Licensed content author	Joseph M.G. Nagano, Ku-Lung Hsu, Landon R. Whitby, Micah J. Niphakis, Anna E. Speers, Steven J. Brown, Timothy Spicer, Virmeliz Fernandez-Vega, Jill Ferguson, Peter Hodder, Prabhavathi Srinivasan, Tara D. Gonzalez, Hugh Rosen, Brian J. Bahnson, Benjamin F. Cravatt
Licensed content date	1 February 2013
Licensed content volume number	23
Licensed content issue number	3
Number of pages	5
Start Page	839
End Page	843

Type of Use	reuse in a thesis/dissertation
Intended publisher of new work	other
Portion	figures/tables/illustrations
Number of figures/tables/illustrations	4
Format	both print and electronic
Are you the author of this Elsevier article?	Yes
Will you be translating?	No
Order reference number	3615540369057
Original figure numbers	1,2,3,4
Title of your thesis/dissertation	LIPOPROTEIN-ASSOCIATED PHOSPHOLIPASE A2: UTILIZING POTENT AND SPECIFIC INHIBITORS TO PROBE THE STRUCTURE FUNCTION RELATIONSHIP
Expected completion date	Jul 2015
Estimated size (number of pages)	150
Elsevier VAT number	GB 494 6272 12
Permissions price	0.00 USD
VAT/Local Sales Tax	0.00 USD / 0.00 GBP
Total	0.00 USD
Terms and Conditions	

INTRODUCTION

1. The publisher for this copyrighted material is Elsevier. By clicking "accept" in connection with completing this licensing transaction, you agree that the following terms and conditions apply to this transaction (along with the Billing and Payment terms and conditions established by Copyright Clearance Center, Inc. ("CCC"), at the time that you opened your Rightslink account and that are available at any time at <http://myaccount.copyright.com>).

GENERAL TERMS

2. Elsevier hereby grants you permission to reproduce the aforementioned material subject to the terms and conditions indicated.

3. Acknowledgement: If any part of the material to be used (for example, figures) has appeared in our publication with credit or acknowledgement to another source, permission must also be sought from that source. If such permission is not obtained then that material may not be included in your publication/copies. Suitable acknowledgement to the source must be made, either as a footnote or in a reference list at the end of your publication, as follows:

"Reprinted from Publication title, Vol /edition number, Author(s), Title of article / title of chapter, Pages No., Copyright (Year), with permission from Elsevier [OR APPLICABLE SOCIETY COPYRIGHT OWNER]." Also Lancet special credit - "Reprinted from The Lancet, Vol. number, Author(s), Title of article, Pages No., Copyright (Year), with permission from Elsevier."

4. Reproduction of this material is confined to the purpose and/or media for which permission is hereby given.

5. Altering/Modifying Material: Not Permitted. However figures and illustrations may be altered/adapted minimally to serve your work. Any other abbreviations, additions, deletions and/or any other alterations shall be made only with prior written authorization of Elsevier Ltd. (Please contact Elsevier at permissions@elsevier.com)

6. If the permission fee for the requested use of our material is waived in this instance, please be advised that your future requests for Elsevier materials may attract a fee.

7. Reservation of Rights: Publisher reserves all rights not specifically granted in the combination of (i) the license details provided by you and accepted in the course of this licensing transaction, (ii) these terms and conditions and (iii) CCC's Billing and Payment terms and conditions.

8. License Contingent Upon Payment: While you may exercise the rights licensed immediately upon issuance of the license at the end of the licensing process for the transaction, provided that you have disclosed complete and accurate details of your proposed use, no license is finally effective unless and until full payment is received from you (either by publisher or by CCC) as provided in CCC's Billing and Payment terms and conditions. If full payment is not received on a timely basis, then any license preliminarily granted shall be deemed automatically revoked and shall be void as if never granted. Further, in the event that you breach any of these terms and conditions or any of CCC's Billing and Payment terms and conditions, the license is automatically revoked and shall be void as if never granted. Use of materials as described in a revoked license, as well as any use of the materials beyond the scope of an unrevoked license, may constitute copyright infringement and publisher reserves the right to take any and all action to protect its copyright in the materials.

9. Warranties: Publisher makes no representations or warranties with respect to the licensed material.

10. Indemnity: You hereby indemnify and agree to hold harmless publisher and CCC, and their respective officers, directors, employees and agents, from and against any and all claims arising out of your use of the licensed material other than as specifically authorized pursuant to this license.

11. No Transfer of License: This license is personal to you and may not be sublicensed, assigned, or transferred by you to any other person without publisher's written permission.

12. No Amendment Except in Writing: This license may not be amended except in a writing signed by both parties (or, in the case of publisher, by CCC on publisher's behalf).

13. Objection to Contrary Terms: Publisher hereby objects to any terms contained in any purchase order, acknowledgment, check endorsement or other writing prepared by you, which terms are inconsistent with these terms and conditions or CCC's Billing and Payment terms and conditions. These terms and conditions, together with CCC's Billing and Payment terms and conditions (which are incorporated herein), comprise the entire agreement between you and publisher (and CCC)

concerning this licensing transaction. In the event of any conflict between your obligations established by these terms and conditions and those established by CCC's Billing and Payment terms and conditions, these terms and conditions shall control.

14. **Revocation:** Elsevier or Copyright Clearance Center may deny the permissions described in this License at their sole discretion, for any reason or no reason, with a full refund payable to you. Notice of such denial will be made using the contact information provided by you. Failure to receive such notice will not alter or invalidate the denial. In no event will Elsevier or Copyright Clearance Center be responsible or liable for any costs, expenses or damage incurred by you as a result of a denial of your permission request, other than a refund of the amount(s) paid by you to Elsevier and/or Copyright Clearance Center for denied permissions.

LIMITED LICENSE

The following terms and conditions apply only to specific license types:

15. **Translation:** This permission is granted for non-exclusive world **English** rights only unless your license was granted for translation rights. If you licensed translation rights you may only translate this content into the languages you requested. A professional translator must perform all translations and reproduce the content word for word preserving the integrity of the article. If this license is to re-use 1 or 2 figures then permission is granted for non-exclusive world rights in all languages.

16. **Posting licensed content on any Website:** The following terms and conditions apply as follows: Licensing material from an Elsevier journal: All content posted to the web site must maintain the copyright information line on the bottom of each image; A hyper-text must be included to the Homepage of the journal from which you are licensing at <http://www.sciencedirect.com/science/journal/xxxxx> or the Elsevier homepage for books at <http://www.elsevier.com>; Central Storage: This license does not include permission for a scanned version of the material to be stored in a central repository such as that provided by Heron/XanEdu.

Licensing material from an Elsevier book: A hyper-text link must be included to the Elsevier homepage at <http://www.elsevier.com> . All content posted to the web site must maintain the copyright information line on the bottom of each image.

Posting licensed content on Electronic reserve: In addition to the above the following clauses are applicable: The web site must be password-protected and made available only to bona fide students registered on a relevant course. This permission is granted for 1 year only. You may obtain a new license for future website posting.

17. **For journal authors:** the following clauses are applicable in addition to the above:

Preprints:

A preprint is an author's own write-up of research results and analysis, it has not been peer-reviewed, nor has it had any other value added to it by a publisher (such as formatting, copyright, technical enhancement etc.).

Authors can share their preprints anywhere at any time. Preprints should not be added to or enhanced

in any way in order to appear more like, or to substitute for, the final versions of articles however authors can update their preprints on arXiv or RePEc with their Accepted Author Manuscript (see below).

If accepted for publication, we encourage authors to link from the preprint to their formal publication via its DOI. Millions of researchers have access to the formal publications on ScienceDirect, and so links will help users to find, access, cite and use the best available version. Please note that Cell Press, The Lancet and some society-owned have different preprint policies. Information on these policies is available on the journal homepage.

Accepted Author Manuscripts: An accepted author manuscript is the manuscript of an article that has been accepted for publication and which typically includes author-incorporated changes suggested during submission, peer review and editor-author communications.

Authors can share their accepted author manuscript:

- - immediately
 - via their non-commercial person homepage or blog
 - by updating a preprint in arXiv or RePEc with the accepted manuscript
 - via their research institute or institutional repository for internal institutional uses or as part of an invitation-only research collaboration work-group
 - directly by providing copies to their students or to research collaborators for their personal use
 - for private scholarly sharing as part of an invitation-only work group on commercial sites with which Elsevier has an agreement
- - after the embargo period
 - via non-commercial hosting platforms such as their institutional repository
 - via commercial sites with which Elsevier has an agreement

In all cases accepted manuscripts should:

- - link to the formal publication via its DOI
- - bear a CC-BY-NC-ND license - this is easy to do
- - if aggregated with other manuscripts, for example in a repository or other site, be shared in alignment with our hosting policy not be added to or enhanced in any way to appear more like, or to substitute for, the published journal article.

Published journal article (JPA): A published journal article (PJA) is the definitive final record of published research that appears or will appear in the journal and embodies all value-adding publishing activities including peer review co-ordination, copy-editing, formatting, (if relevant) pagination and online enrichment.

Policies for sharing publishing journal articles differ for subscription and gold open access articles:

Subscription Articles: If you are an author, please share a link to your article rather than the full-text. Millions of researchers have access to the formal publications on ScienceDirect, and so links

will help your users to find, access, cite, and use the best available version.

Theses and dissertations which contain embedded PJAs as part of the formal submission can be posted publicly by the awarding institution with DOI links back to the formal publications on ScienceDirect.

If you are affiliated with a library that subscribes to ScienceDirect you have additional private sharing rights for others' research accessed under that agreement. This includes use for classroom teaching and internal training at the institution (including use in course packs and courseware programs), and inclusion of the article for grant funding purposes.

Gold Open Access Articles: May be shared according to the author-selected end-user license and should contain a [CrossMark logo](#), the end user license, and a DOI link to the formal publication on ScienceDirect.

Please refer to Elsevier's [posting policy](#) for further information.

18. **For book authors** the following clauses are applicable in addition to the above: Authors are permitted to place a brief summary of their work online only. You are not allowed to download and post the published electronic version of your chapter, nor may you scan the printed edition to create an electronic version. **Posting to a repository:** Authors are permitted to post a summary of their chapter only in their institution's repository.

19. **Thesis/Dissertation:** If your license is for use in a thesis/dissertation your thesis may be submitted to your institution in either print or electronic form. Should your thesis be published commercially, please reapply for permission. These requirements include permission for the Library and Archives of Canada to supply single copies, on demand, of the complete thesis and include permission for Proquest/UMI to supply single copies, on demand, of the complete thesis. Should your thesis be published commercially, please reapply for permission. Theses and dissertations which contain embedded PJAs as part of the formal submission can be posted publicly by the awarding institution with DOI links back to the formal publications on ScienceDirect.

Elsevier Open Access Terms and Conditions

You can publish open access with Elsevier in hundreds of open access journals or in nearly 2000 established subscription journals that support open access publishing. Permitted third party re-use of these open access articles is defined by the author's choice of Creative Commons user license. See our [open access license policy](#) for more information.

Terms & Conditions applicable to all Open Access articles published with Elsevier:

Any reuse of the article must not represent the author as endorsing the adaptation of the article nor should the article be modified in such a way as to damage the author's honour or reputation. If any changes have been made, such changes must be clearly indicated.

The author(s) must be appropriately credited and we ask that you include the end user license and a DOI link to the formal publication on ScienceDirect.

If any part of the material to be used (for example, figures) has appeared in our publication with credit or acknowledgement to another source it is the responsibility of the user to ensure their reuse complies with the terms and conditions determined by the rights holder.

Additional Terms & Conditions applicable to each Creative Commons user license:

CC BY: The CC-BY license allows users to copy, to create extracts, abstracts and new works from the Article, to alter and revise the Article and to make commercial use of the Article (including reuse and/or resale of the Article by commercial entities), provided the user gives appropriate credit (with a link to the formal publication through the relevant DOI), provides a link to the license, indicates if changes were made and the licensor is not represented as endorsing the use made of the work. The full details of the license are available at <http://creativecommons.org/licenses/by/4.0>.

CC BY NC SA: The CC BY-NC-SA license allows users to copy, to create extracts, abstracts and new works from the Article, to alter and revise the Article, provided this is not done for commercial purposes, and that the user gives appropriate credit (with a link to the formal publication through the relevant DOI), provides a link to the license, indicates if changes were made and the licensor is not represented as endorsing the use made of the work. Further, any new works must be made available on the same conditions. The full details of the license are available at <http://creativecommons.org/licenses/by-nc-sa/4.0>.

CC BY NC ND: The CC BY-NC-ND license allows users to copy and distribute the Article, provided this is not done for commercial purposes and further does not permit distribution of the Article if it is changed or edited in any way, and provided the user gives appropriate credit (with a link to the formal publication through the relevant DOI), provides a link to the license, and that the licensor is not represented as endorsing the use made of the work. The full details of the license are available at <http://creativecommons.org/licenses/by-nc-nd/4.0>. Any commercial reuse of Open Access articles published with a CC BY NC SA or CC BY NC ND license requires permission from Elsevier and will be subject to a fee.

Commercial reuse includes:

- - Associating advertising with the full text of the Article
- - Charging fees for document delivery or access
- - Article aggregation
- - Systematic distribution via e-mail lists or share buttons

Posting or linking by commercial companies for use by customers of those companies.

20. Other Conditions:

v1.7

Questions? customercare@copyright.com or +1-855-239-3415 (toll free in the US) or +1-978-646-2777.